Synthesis and Surface Functionalization of Group 14 Nanomaterials

by

Ziqi Li

A thesis submitted in partial fulfillment of the requirements for the degree of

Master of Science

Department of Chemistry
University of Alberta

Abstract

Nanomaterials based upon Group 14 elements (i.e., silicon and germanium) are drawing a great deal of attention from researchers since they are biocompatible and exhibit unique optical and electronic properties. Surface functionalization, which is one of the most critical aspects of nanomaterial design, can modify nanomaterials' electronic, optical, and physical property, possibly laying a path to designer materials. In this thesis, we are dedicated to investigating on the surface chemistry regarding three materials: synthesized Si nanocrystals (NCs), polygermane (PGs) and Ge nanosheets (GeNSs) and try to change some of their properties (i.e., solubility or resistance to oxidation).

In Chapter 2, we designed dissipative self-assembly of functionalized SiNCs driven by the kinetics of a dissipative reaction chemical cycle, which was developed based upon the work of Grotsch et al. This study examines how aspartic acid and derivatives of succinic acid can independently functionalize SiNCs and produce two different types of precursors for the dissipative reaction cycle. A series of experiments successfully prepared the functionalized SiNCs and discovered the combined effects of the acids and SiNCs. Through analyzing the combined effects, dicarboxylic acids such as aspartic and succinic acid showcase assembly properties while SiNCs demonstrate the property of luminescence. It is worth noting that the functionalized SiNCs can retain its characteristic photoluminescence for months. On the condition of adding EDC to functionalized SiNCs, the aspartic acid terminated SiNCs failed to show dissipative

self-assembly, whereas the succinic acid terminated SiNCs reacted partially as expected.

In Chapter 3, we carried out the thiolation on the hydride-terminated PGs and GeNSs to produce Ge–S bonding by simply heating the reaction with thiols and disulfides. After the completion of the reaction, the Ge–H bonds were consumed, and C–H and C–S vibration modes were observed in FTIR spectra. In the end, a series of characterizations were carried out to confirm the thiol-termination.

Preface

This thesis is an original work by Ziqi Li. The research was conducted under the supervision of Professor Jonathan G. C. Veinot at the Department of Chemistry, University of Alberta. No part of this thesis has been published previously.

In Chapter 2, This is an Alberta/Technical University of Munich International Graduate School for Hybrid Functional Materials (ATUMS) project between the Technical University of Munich (TUM) and the University of Alberta (UA). I was responsible for designing the precursor, carrying out material characterization and analyzing the data. Dr. Muhammad Amirul Islam and Dr. Christopher Jay Robidillo developed the method of preparing water-soluble SiNCs via mixed ligands. Laura Tebcharani (TUM) explored the dissipative self-assemble chemical reaction cycle and optimized the reaction conditions. Professor Job Boekhoven and Professor Jonathan G. C. Veinot supervised the project and were involved with the concept formation.

In Chapter 3, Dr. Haoyang Yu developed the method of preparing polygermane, he was also involved with the concept formation. I was responsible for designing the project, performing the experiments, carrying out material characterization, analyzing data and writing the materials. Chuyi Ni assisted in the precursor synthesis, data acquisition and analysis. Professor Jonathan G. C. Veinot supervised the project and was involved with the thesis composition.

Acknowledgments

It is with great pleasure that I thank and acknowledge the people who have contributed to my thesis throughout my master studies. I have had the good fortune to work with so many talented people at the University of Alberta.

First, I would like to thank my supervisor, Dr. Jonathan G. C. Veinot, for being an enthusiastic scientist, and for offering me the opportunity to work on such interesting and exciting projects. His persistence in research has inspired me to continue my education. I will always be grateful for the opportunity you offered me so that I can work in this amazing team.

I would like to thank Dr. Michael Serpe and Dr. Julianne Gibbs-Davis for serving on my committee and for being encouraging and supportive.

I would like to thank the members of the Veinot team from 2019 onwards. First and foremost, I would like to express my deepest appreciation to Leah Veinot for her understanding and patience with each student in the ATUMS program. I am so grateful to be part of the ATUMS program, which helps me to start my collaborations. I would also like to thank all the past and present group members Dr. Haoyang (Emmette) Yu, Dr. Christopher Jay Robidillo, Dr. Alyxandra N. Thiessen, Md Asjad Hossain, Dr. Jonathan Hiltz, Dr. Nduka Ikpo, Sarah Milliken, Yingjie (Jay) He, I Teng (Emily) Cheong, Kevin O'Connor, Riley Hooper, Chuyi (Martin) Ni, Jonathan Trach, Leanne Milburn and many others for their help and support throughout this process. Chuyi (Martin) Ni deserves a special thank you for being open to scientific discussions and working with me together.

I would like to thank my ATUMS collaborator Laura Tebcharani for your input and contribution throughout the most stressful times of our project. This work would not have been possible without your help. I would like to thank Professor Job Boekhoven for his support throughout the ATUMS program.

I would like to acknowledge academic and technical support from Wayne Moffat (Analytical Services), Dr. Haoyang Yu (TEM), and Dmitri Karpuzov (XPS). I appreciate all your cooperation and assistance. I am deeply grateful to Dr. Anna Jordan

for the editing and proofreading as the thesis looks a lot better now. It would not look nearly as well put together without your valuable contribution.

I would like to thank my flatmates and friends Yvonne, Kaining, Kai and Timothy for their help and company whilst in Edmonton. A special thanks to Yvonne for being a great mate during hard times. I wish to thank Willis and Sherry back in Ontario, for their affection and support over the years. The weekly phone calls were our only connections in the past two years when I studied in Alberta, but the talk with you always makes me feel warm and encouraging.

Most importantly, I would like to thank my family back in China, who have been supportive from afar both financially and emotionally and have done their best to cheer me up when I have struggled through a world, which is quite foreign to them.

Table of Contents

List of Figures

List of Tables

List of Schemes

List of Symbols and Abbreviations

Å	Angstrom
Asp-SiNCs	Aspartic acid functionalized silicon nanocrystals
N_A	Avogadro number
E_g	Band gap
BE	Binding energy
CB	Conduction band
c-Ge	Crystalline germanium
CHT	Cyclohexanethiol
Da	Dalton(s)
d	Day(s)
°C	Degree Celsius
DI water	Deionized water
DOS	Density of state
ODS	Di-*n*-octadecyl disulfide
d	Diameter
ε	Dielectric constant of the bulk semiconductor materials
DRA	Diffuse Reflective Analysis
DDT	Dodecanethiol
DLS	Dynamic light scattering
m_e	Effective mass of the electron in the CB
m_h	Effective mass of the hole in the VB
eV	Electronvolt
e	Elementary charge of an electron
ΔE	Excitation energy
F	Faraday
FTIR	Fourier-Transform Infrared Spectroscopy
FWHM	Full-width-at-half-maximum
GeNSs	Germanane
$(Ge_6H_6)_n$	Germanane
g	Gram(s)
HDT	Hexadecanethiol
HT	Hexanethiol
HAADF-STEM	High-angle annular dark-field scanning transmission electron microscopy
HRTEM	High-resolution transmission electron microscopy
h	Hour(s)
H-GeNS(s)	Hydride-terminated germanium nanosheet(s)
H-SiNC(s)	Hydride-terminated silicon nanocrystal(s)
HBr	Hydrobromic acid
HCl	Hydrochloric acid
HF	Hydrofluoric acid
HSQ	Hydrogen silsesquioxane

IR	Infrared
μL	Microliter(s)
mL	Millilitre(s)
mmol	Millimole(s)
mW	Milliwatt(s)
min	Minute(s)
M (L)	Molar mass of ligand
M (Si)	Molar mass of Si
MBE	Molecular beam epitaxy
EDC	N-(3-Dimethylaminopropyl)-N′-ethylcarbodiimide hydrochloride
NHS	N-Hydroxysuccinimide
Sulfo-NHS	N-hydroxysulfosuccinimide
nm	Namometers
NCs	Nanocrystals
NMR	Nuclear magnetic resonance
OT	Octanethiol
PGs	Oligo/polygermanes
1D	One-dimension
ppm	Parts per millions
PL	Photoluminescence
PL max	Photoluminescence emission maximum
h	Plank's constant
PEG	Polyethylene glycol
QD	Quantum dot
R	Radius
rpm	Revolutions per minute
ROP	Ring-opening polymerization
RT	Room temperature
sec	Second(s)
$(Si_6H_6)_n$	Silicane
$SiNC/SiO_2$	Silicon nanocrystals embedded in a silica matrix
kV	Kilovolt(s)
Suc-SiNCs	Succinic acid functionalized silicon nanocrystals
THF	Tetrahydrofuran
TGA	Thermogravimetric analysis
3D	Three-dimension
N (L)	Total number of ligands per NC surface
N (Si)	Total number of silicon atoms per NC
TEM	Transmission electron microscopy
BCF	Tris(penta-fluorophenyl)borane
ACF	Tris(pentafluorophenyl)alane
2D	Two-dimension
UHV	Ultrahigh vacuum
UV	Ultraviolet
VB	Valence band

vdw	Van der Waals
cm^{-1}	Wavenumber(s)
XRD	X-ray diffraction
XPS	X-ray Photoelectron Spectroscopy
XP	X-ray photoemission
0D	Zero-dimensional

Chapter 1: Nanomaterials

Introduction to Nanomaterials

At an annual meeting of the American Physical Society in 1959, a lecture entitled 'There's Plenty of Room at the Bottom' was presented by Richard Feynman. In this presentation, Feynman described the possibility of manipulating and controlling individual atoms and molecules as a powerful aspect of synthetic chemistry.[1] Fast forward to 2021, many of these futuristic ideas proposed in the late 1950s are becoming a reality. It is fair to say Feynman's ideas lay the foundation for the field of nanoscience and nanotechnology.[2]

The 'nano' prefix is derived from the Greek word for 'dwarf'; now it refers to an order of magnitude (i.e., billionth of a meter, or 10^{-9} m).[3] The modern definition for nanotechnology is "*science, engineering, and technology conducted at the nanoscale, about 1 to 100 nanometers;*"[4] Such size regime is highlighted in Figure 1-1. To understand nanoscale materials further, it is useful to compare these nanoscale materials with the diameter of a single carbon (C) atom (which is about 0.16 mm) and other common materials (Figure 1-1). As a result of their small sizes, the surface-to-volume ratios of nanoscale materials are very high. Hence, surface effects play important roles in defining their material properties.

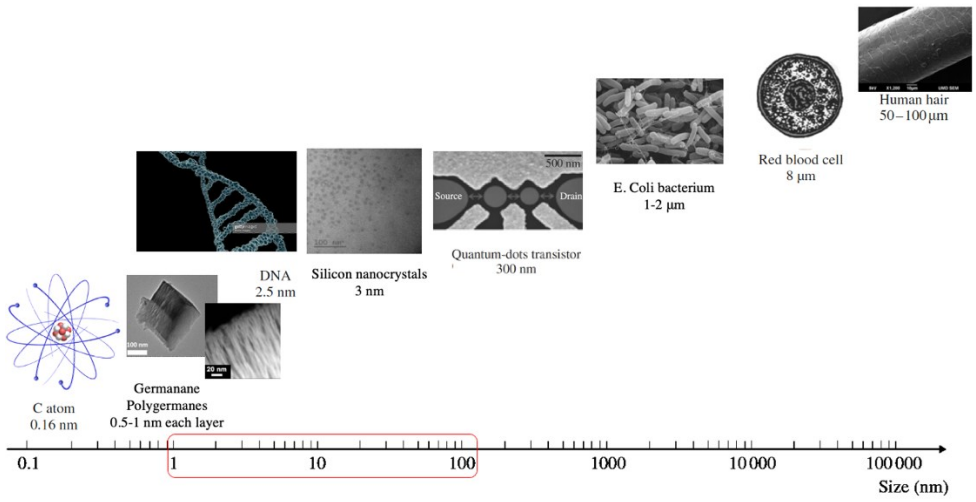

Figure 1-1. A pictorial representation of the relative size of germanane (Ge), polygermane, silicon (Si) nanocrystals, and other objects. Some images were obtained from literature sources.[5,6]

Often, nanomaterials are categorized based on the number of dimensions in which they are confined (Figure 1-2).[7] First and foremost, nanomaterials with all three external dimensions (i.e., length × width × height) in the range of 1 to 100 nm are considered to be zero-dimensional (0D). Examples include quantum dots, metal nanoparticles, and fullerene (C_{60}) (Figure 1-2 d). One-dimensional (1D) nanomaterials are materials with two external dimensions in the nanoscale regime (Figure 1-2 c); such as nanotubes, nanorods, and quantum wires. Different from 1D nanomaterials, 2D nanomaterials only have one external dimension in the nanoscale regime (Figure 1-2 b); examples include nano-thin films, nano-sheets, quantum wells, and nano-plates.

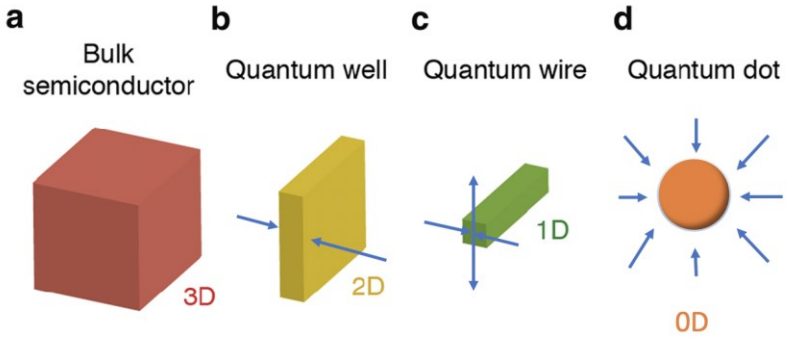

Figure 1-2. A pictorial representation of (a) 3D nanomaterials, such as bulk semiconductors, (b) 2D materials, such as quantum wells, (c) 1D materials, such as quantum wires, and (d) 0D materials, such as quantum dots. The blue arrows represent the dimensions, where electron motion is confined.

Due to the quantized dimensions (nano-scale size), nanomaterials are different from traditional bulk systems in terms of their mechanical (i.e., superplasticity, exceptional hardness, and toughness), chemical (i.e., high catalytic activity, poor stability), optical (i.e., fluorescence), and magnetic properties (i.e., superparamagnetism).[8] Similar to other nanomaterials, semiconductor nanomaterials (e.g., nanoparticles/quantum dots of cadmium selenide (CdSe), indium phosphide (InP), Si, Ge) are very promising for a variety of applications due to their size-dependent tunable optical properties (i.e., photoluminescence, photostability), electronic properties (i.e., band gap), as well as surface functionalities.[9] Semiconductor nanomaterials usually contain inorganic cores or backbones. Each of them is coated with a layer of organic ligand molecules. This hybrid inorganic-organic nature adds to their versatility and allows the combining of optoelectronic properties of the core and backbone with straightforward surface manipulation.[10]

1.1 Quantum Dots and Quantum Confinement Effects

Quantum dots (QDs) are semiconductor nanoparticles usually in the size range of 2–10 nm, which were discovered by Brus and Ekimov and many other researchers in the early 1980-1990s.[11–17] QDs are particularly attractive among all semiconductor nanomaterials because they have discrete energy levels, which make their properties extremely unique.[10,18,19]

When a quantum dot is impinged by a photon that has an energy equal to or greater than the energy difference between the valence band (VB) and conduction band (CB) (i.e., band gap (E_g)) of the QD, an electron is promoted from the VB to the CB leaving a hole in the VB. This process leads to the formation of an exciton (i.e., an electron-hole pair bound by Coulomb interaction). The property of the exciton is dictated by its Bohr radius, and its wave function is determined by the spatial confinement. As a result, when the dimensions of the semiconductor nanoparticles are approximately those of the exciton Bohr radius in the bulk material, energy separation occurs between each state in the density of state (DOS), increasing the band gap. This causes a blue shift in the material photoluminescent maximum. This phenomenon is called quantum confinement (Figure 1-3),[20] which is described by Equation 1-1:[21]

$$E_{g,QD} = E_{g,b} + \left(\frac{h^2}{8R^2}\right)\left(\frac{1}{m_e} + \frac{1}{m_h}\right) - \left(\frac{1.8e^2}{4\pi\varepsilon_0\varepsilon R}\right) \qquad (1\text{-}1)$$

where $E_{g,QD}$ and $E_{g,b}$ are the band gaps of the QDs and bulk semiconductor material, respectively, R is the radius of the QD, m_e and m_h are the effective masses of the electron in the CB and the hole in the VB, respectively, h is Plank's constant, e is the elementary charge of an electron, and ε is the dielectric constant of the bulk semiconductor material. Based on Equation 1-1, the size of QDs determines their DOS and band gap. The QDs of CdSe is an ideal example; Figure 1-3 shows their size-dependent photoluminescence emission colors.[10,22]

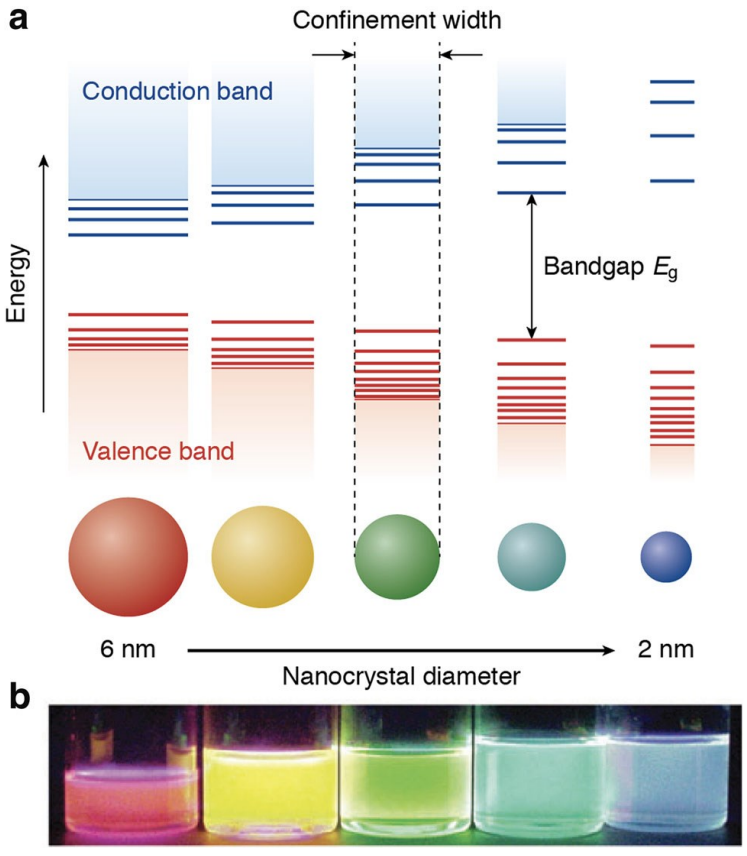

Figure 1-3. (a) Scheme of quantum confinement effect: the band gap (E_g) of the QDs decreases with the increasing size, and vice versa. The discrete energy level becomes closer at the band-edges. (b) Photo of CdSe QDs in the size range from 6 nm to 2 nm (photoluminescence from red to blue), taken under excitation with UV. [Reprinted and adapted with permission from The Royal Society of Chemistry.][10]

1.2 Composition Effects: Core-shell Nanostructures

As mentioned previously, QDs have been studied since the 1980s. Initially, researchers only focused on homogeneous colloidal semiconductor QDs. Later, they found that heterogeneous composite QDs have better efficiency. In the early 1990s, researchers prepared QDs consisting of concentric multilayers (i.e., core and shell) to improve/design material properties.[23,24]

It is possible to engineer these core/shell structures by defining the materials. They often are classified into three types, based upon the band alignment of the different layers (Figure 1-4). In Type I, the VB and CB of the core are located in the band gap of the shell, thus, both electrons and holes are confined within the particle core.[25,26] The emission energy of this type of QDs is determined only by the core instead of the shell. In the Inverse Type I system, the band gap of the shell is narrower than that of the core, which allows the electron and hole to be delocalized into the shell.[27]As a result, photoemission is tuned by defining the thickness. In Type II QDs, the energy of the CB and VB of the shell is lower than that of the CB and VB of the core.[28] The overlap between the VB and CB of the core/shell materials allows the spatial separation of electron and hole into the core and shell.[18]

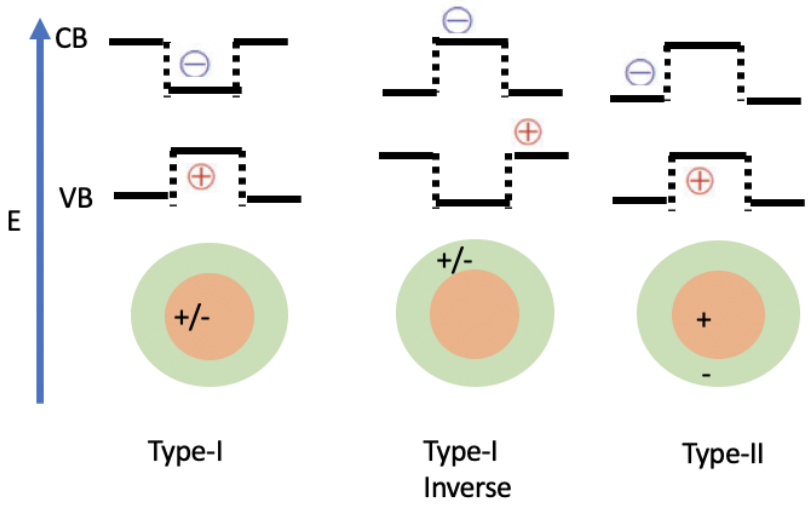

Figure 1-4. An illustration of band edge alignment in Type I, Type I inverse, and Type II of core/shell QDs.[29]

1.3 Synthesis of Si Quantum Dots

Although the fundamental principles that dictate the properties of QDs are well developed, many of the corresponding materials rely on rare elements (e.g., In, Se) or toxic heavy metals (e.g., Pb, Hg). These aspects alone can limit the scope of QDs in many applications, such as bio-imaging or drug delivery.[30,31] In this regard, a more abundant and non-toxic semiconductor element emerges. Silicon (Si) is the second most abundant element, making up about 28% of the Earth's crust by mass, and not toxic. Si QDs display photoluminescence (PL) in the visible region, which can be used for the next-generation light source.[32–36] Thus, it is important to find a scalable, controllable, and cost-effective method to prepare Si QDs. To control the PL wavelength, researchers have developed many synthetic methods, including electrochemical etching,[37–41] reduction reaction,[42–45] nonthermal plasma,[46–48] synthetic laser ablation,[49] and thermal pyrolysis.[50–59] Among all methods, thermal pyrolysis, or the thermally-inducing disproportionation of hydrogen silsesquioxane (HSQ) are the most frequently used methods for preparing high-quality Si QDs. Veinot et al. successfully synthesized size-tunable Si QDs with controlled PL wavelength by changing the thermal processing conditions (i.e., temperature and dwelling time) under an atmosphere of 5% H_2 and 95% Ar (Figure 1-5).[50] The silicon nanocrystals, which are quantum dots, are liberated via HF etching.

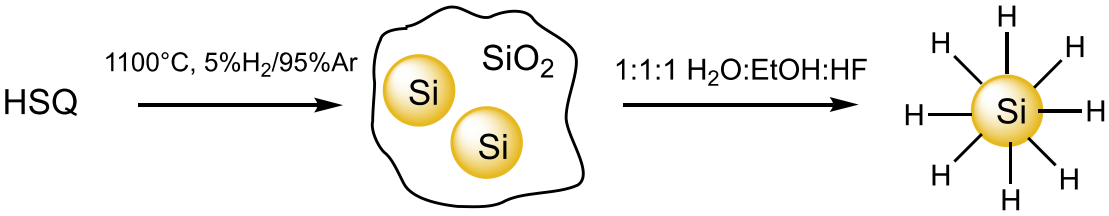

Figure 1-5. Preparation of hydride-terminated Si QDs via reductive thermal processing of hydrogen silsesquioxane (HSQ) as a precursor.

1.4 Synthesis of 2D Ge Nanomaterials

As for two-dimensional nanomaterials, graphene is one of the most widely recognized 2D nanomaterials. It can be described as a one-atom-thick sheet, in which carbon atoms are arranged in a familiar hexagonal configuration (sp^2 hybridization). Graphene was

discovered by Geim and Novoselov in 2004.[60–62] After graphite is exfoliated to form nanosheets, all the atoms within the sheets are exposed to the surroundings, which provide unique properties/characteristics that include high thermal and electrical conductivity,[63] the quantum Hall effect,[60] and ballistic carrier transport.[64] Given the vast promise offered by graphene,[65–68] it is essential to explore other Group 14 elements and their corresponding 2D nanomaterials. Many theoretical and experimental studies of 2D nanomaterials comprised of the heavy Group 14 elements have been reported, such as silicene, germanene, and stanene.[69]

Preparation of 2D nanomaterials based upon the heavy Group 14 elements can be achieved by "bottom-up" or "top-down" techniques.[69] Bottom-up approaches typically employ ultrahigh vacuum (UHV) deposition and use molecular beam epitaxy (MBE) to deposit layers on the well-organized metallic substrates.[19] These procedures can provide silicon (i.e., silicene), germanium (i.e., germanene), and tin (i.e., stanene) analogs of graphene. The preparation and properties have been reviewed elsewhere, and the readers are directed to the selected reviews for a more comprehensive description.[69] Silicene has been prepared on a variety of substrates, including Ag (111) (Figures 1-6 a, c),[70] ZrB_2 (0001),[71] and Ir (111) surfaces.[72]

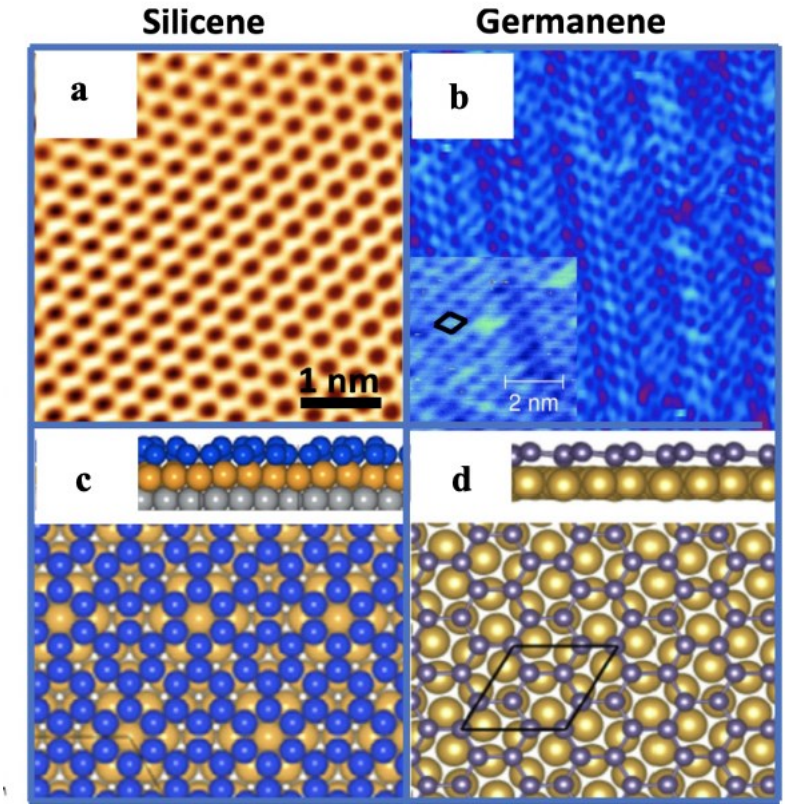

Figure 1-6. Scanning tunneling microscopy (STM) scan of (a) silicene on Ag (111)[70] and (c) a corresponding model structure[73] and (b) germanene on Au (111) substrate and (d) a corresponding model structure.[74] [(a, c) Reprinted and adapted with permission from Copyright 2012 IOP Publishing Ltd. (b, d) Reprinted and adapted with permission from Copyright 2014 IOP Publishing Ltd.]

Different from graphene, silicene is in a flat Si single layer (mixed sp^2/sp^3-hybridization) with a hexagonal arrangement, having great potential for application in devices[75] because of its high thermal conductivity, large anisotropic elastic deformation under strain, and high carrier mobility.[75] Furthermore, silicene has a high surface chemical activity, which facilitates tunable electronic states (from indirect 2.9 eV to a direct band gap of 2.1–2.5 eV)[76,77] via functionalization, including hydrogenation, halogenation, oxidation, and metal atom adsorption (Figure 1-7).[78–82]

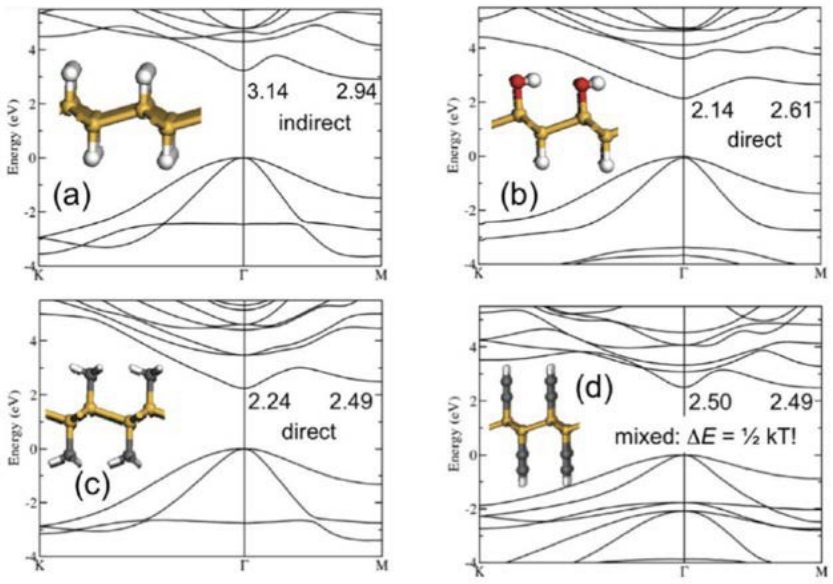

Figure 1-7. Calculated band structures of the functionalized silicene: (a) hydrogen, (b) mixed hydrogen and hydroxyl (OH), (c) methyl CH_3, and (d) acetylene C = CH functionalized silicene.[83] [Reprinted and adapted with permission from Copyright 2013 American Chemical Society.]

From the work related to silicene, several research groups described the preparation of germanene on Au(111)[74] and Pt(111) substrates (Figure 1-6 b, d).[84] Recently, researchers studied the top germanene layer, which possesses a honeycomb structure similar to that of silicone. Germanene also is a promising candidate for many optoelectronic applications because it has a high spin-orbital gap (23.9 meV) and a high charge carrier mobility.[85] Functionalization of germanene cannot only impart stability and photoreactivity but also can tailor material band structure or electronic properties.[86–88]

Stanene also has been prepared on Bi_3Te_3(111) substrates, whose structures are almost the same as germanene.[89] It also has some remarkable features, such as a large spin-orbital gap, magnetoresistance, thermoelectricity, topological superconductivity, and the quantum spin Hall behavior.[90] Thus, stanene can be used as a topological insulator.

Another approach to obtaining 2D materials of the heavy Group 14 elements is the deintercalation of Zintl phases that contain layers of the target element within their bulk structure. Deintercalation of intermetallic precursors provides an intriguing strategy for synthesizing Group 14 nanosystems.[19] Zintl phases were named after the

German chemist Eduard Zintl, who investigated them in the 1930s.[91–94] A Zintl phase is regarded as a chemical compound composed of an electropositive alkali or alkaline-earth metal cation "A" and electronegative group elements "M" (i.e., p-block metals of Groups 13, 14, and 15). Their structures include formal electron transfer from A to M and the anionic substructure of M atoms satisfying the octet rule.[91,94–96] These ideas were developed further to become the Zintl rule or Zintl-Klemm concept, which can be used as a guideline for making new compounds and materials. The Zintl-Klemm concept was extended by Klemm and Laves and has been developed into a versatile and general concept.[94,95]

As in the case for CaM_2 (M = Si or Ge), the bonded layers of Group 14 elements are anionic, and they are separated and charge-balanced by metal cations (e.g., Ca or Eu).[69] Materials prepared in this way contain the Group 14 elemental atoms arranged in hexagonal arrays in 2D layers of 6-membered rings (i.e., "chair" confirmations). The remaining bonding site on the Group 14 element is filled with a heteroatom (Figure 1-8).[19]

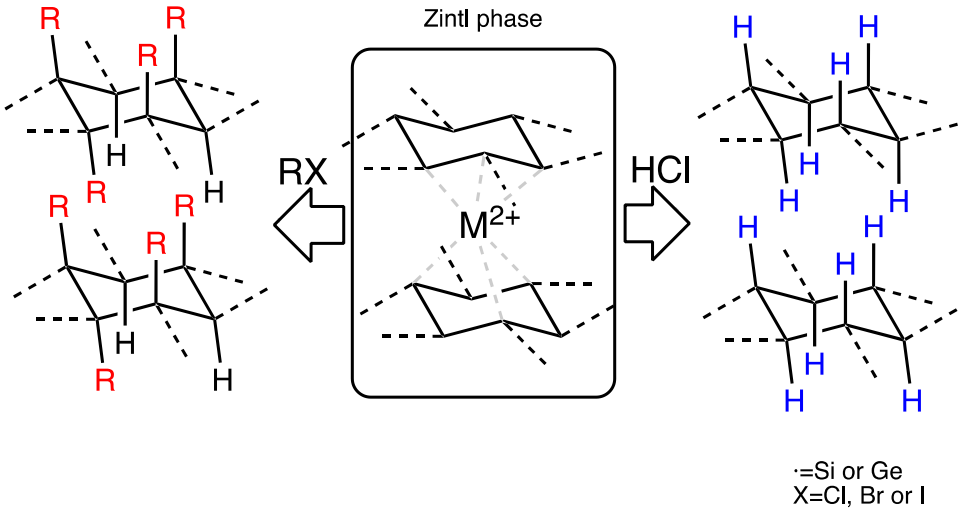

Figure 1-8. Schematic deintercalation of metal silicides or germanides using HCl or with RX (i.e., methyl iodide) to provide different functionalized silicene and germanene.

These layers are liberated from the corresponding Zintl phase upon exposure to a strong acid (i.e., HCl, HBr, etc.), which selectively removes metal atoms, preserves the stacked layers, and balances the charge with protons, leading to Si–H and Ge–H

that exhibit hydridic character.[97] These 2D materials are referred to as silicane (i.e., $(Si_6H_6)_n$) and germanane (i.e., $(Ge_6H_6)_n$).

Deintercalation and exfoliation of Zintl phases were investigated first in the 1860s by Wohler et al. [98] and in the 1920s by Kautsky et al.[99] These studies used exfoliated $CaSi_2$ to prepare a stable siloxane sheet polymer in ice-cold aqueous HCl, and the products were termed "polysiloxane sheets". The structures and properties of these materials were investigated subsequently by Weiss et al.[100] and Dahn et al. (Figure 1-9).[101] Weiss et al. reported that the structure of the polymer sheet was a puckered 2D layer, which was stabilized through the heteroatoms (i.e., hydrogen or hydroxide) group termination pointing out of the sheet plane.[100] The findings were confirmed by Dahn et al.[101] Different from the previous study, HCl was used in methanol or ethanol instead of water to prepare the alkoxide-terminated siloxenes ($Si_6H_3(OCH_3)_3$ or $Si_6H_3(OC_2H_5)_3$). Dahn et al. also performed the reaction at a lower temperature (i.e., below -30 °C) to obtain non-oxidized silicon sheets, $(Si_6H_6)_n$, that were structurally similar to $Si_6H_3(RO)_3$. However, Yamanaka et al. found that this reaction also formed $Si_6H_3OH_3$ as a by-product. [102]

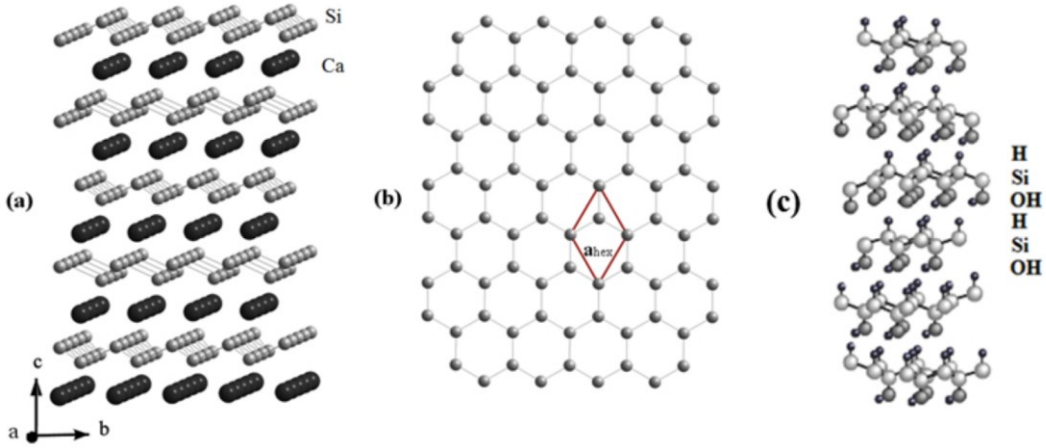

Figure 1-9. (a) Structures of $CaSi_2$, where the dark gray spheres represent Ca and the light gray spheres represent Si. (b) Silicon sheet crystalline structures. (c) Weiss siloxene.[103] [Reprinted and adapted with permission from Copyright 2014 Journal of Physics: Conference Series]

Deintercalation of $CaSi_2$ provides partially OH-terminated $SiH_x(OH)_{1-x}$, presumably because the Si–O bond (800 kJ/mol) is stronger than the Si–H bond

(300 kJ/mol).[104] Surface functionalization can be achieved by hydrosilylation, the addition of an unsaturated bond into the silicon-hydride (Si–H) group. Nakano et al. functionalized SiH with hexene via Pt-catalyzed hydrosilylation to prepare a stable suspension in an organic solvent.[105] The formation of the Si–C bond on the Si_6H_6 surface also can be achieved by using Grignard reagents. Sugiyama et al. reported the synthesis of phenyl-terminated organosilicon sheets using phenyl magnesium bromide [PhMgBr].[106] Si_6H_6 also can be functionalized upon reaction with other nucleophiles like amines (Figure 1-10).[107] More details can be found in Section 1.8.3.

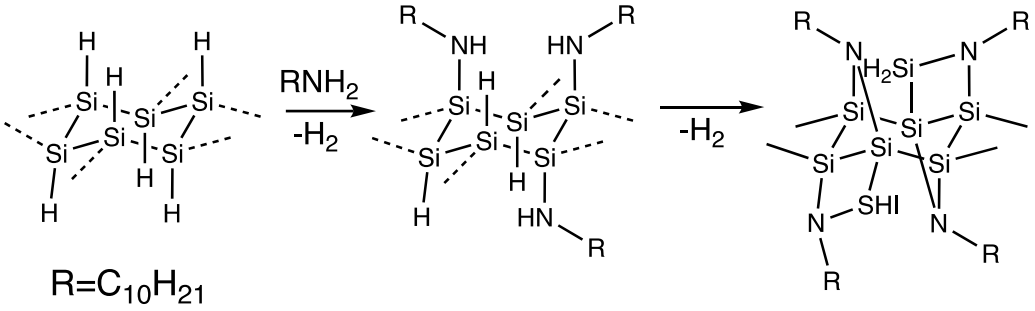

Figure 1-10. Functionalized Si_6H_6 with decylamine.[107]

Unlike the case for silicane, when working with germanane, issues arising from oxide formation are addressed partly by the more comparable Ge–O (660 kJ/mol) and Ge–H (320 kJ/mol) bond strengths[104] and the more dissolvable native germanium oxides in aqueous HCl. Such solubility provides a "built-in" purification.[108] Vogg et al. used reactive deposition epitaxy to grow $Ca(Si_{1-x}Ge_x)_2$ alloys on the Si (111)/(110) substrate and successfully grew high-quality pure $CaGe_2$ on the Ge (111) substrate.[109–113] The alloys were deintercalated by HCl, producing layered polygermanosilynes or polygermanes. They also determined the relationship between Ge content x and oxidation ability (or distribution of –OH). If $x < 0.5$, the –OH remained constant.; if $x > 0.5$, the –OH decreased to zero (pure germanene).[112] The Ge content also can influence the electric properties; for example, pure GeH (100% Ge) has a band gap of 1.3 eV, while it is 2.4 eV for SiH (0% Ge).[111–113]

Jiang et al. expanded the deintercalation of calcium digermanide ($CaGe_2$) by using aqueous acid (i.e., HCl) at -40 °C (Equation 1-2) or methyl halide (i.e., CH3I) at

room temperature to prepare germanane and methyl-terminated germanane (Equation 1-3).[76,83,114]

$$3n\ CaGe_2 + 6n\ HCl \rightarrow (Ge_6H_6)_n + 3n\ CaCl_2 \quad (1\text{-}2)$$

$$3n\ CaGe_2 + 6n\ CH_3I \rightarrow (Ge_6(CH_3)_6)_n + 3n\ CaI_2 \quad (1\text{-}3)$$

Nicholas et al. showed that there were two forms: $EuGe_2$ (trigonal) and α-$CaGe_2$ (rhombohedral), which could be transformed into different types (1T-Ge_6H_6, 2H-Ge_6H_6, or 6R-Ge_6H_6) with various band gaps (1.59, 1.45, and 1.63 eV).[116] Nakamura and Nakano determined the condition of liquid-phase exfoliation of Ge_6H_6 by sonication in a different solvent;[115] more details can be found in Section 1.7.

Jiang et al. determined a buckled honeycomb structure of the resulting compounds, with germanium atoms covalently bonded in 6-membered rings and bonded covalently terminated with –H or –CH_3, above and below the sheet (Figure 1-11).[19,76,116,117]

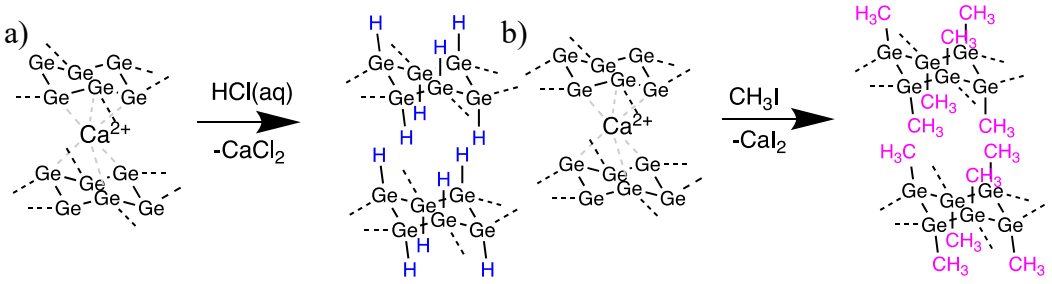

Figure 1-11. a) Deintercalation of $CaGe_2$ (left) into hydrogen-terminated germanane (right) b) $CaGe_2$ (left) into and methyl-terminated germanane (right).[83,116]

Hydrogen-terminated germanane has a band gap of ≈1.6 eV, with electron mobility up to 18 000 $cm^2\ V^{-1}\ s^{-1}$, which is five-fold bigger than that of the bulk (3900 cm^2/Vs).[118] It is highly resistant to oxidation (slowly oxidized in the air over 5 months) and thermally stable to 75 °C.[119,120] Compared to Ge_6H_6 (0.55 nm), methyl terminated germanane (0.86 nm) is larger, with a direct band gap that is bigger by ~0.1 eV to ≈1.7 eV and a significantly higher thermal stability up to 250 °C. It shows remarkable photocatalytic activities, photoluminescence properties, and band edge fluorescence.[64,116,121] The formation of methyl terminated germanane will produce CaI_2 as a by-product, which would form a protective layer on the surface of $CaGe_2$, thus

preventing it from further reaction. Therefore, hydrogen-terminated germanane serves as a better starting material for functionalization than methyl terminated ones. Jiang et al. functionalized germanenes with 10 different ligands and compared their electronic structures and property difference; more details are discussed in Section 1.8.3.

Following Jiang's method, Yu et al. recently functionalized the freestanding hydrogen-terminated germanane by a radical-initiated/thermal-induced hydrogermylation reaction to form a C–Ge bond,[122] and a heteronuclear dehydrocoupling reaction to form a Si–Ge bond (Figure 1-12).[123] More details are discussed in Section 1.8.3.

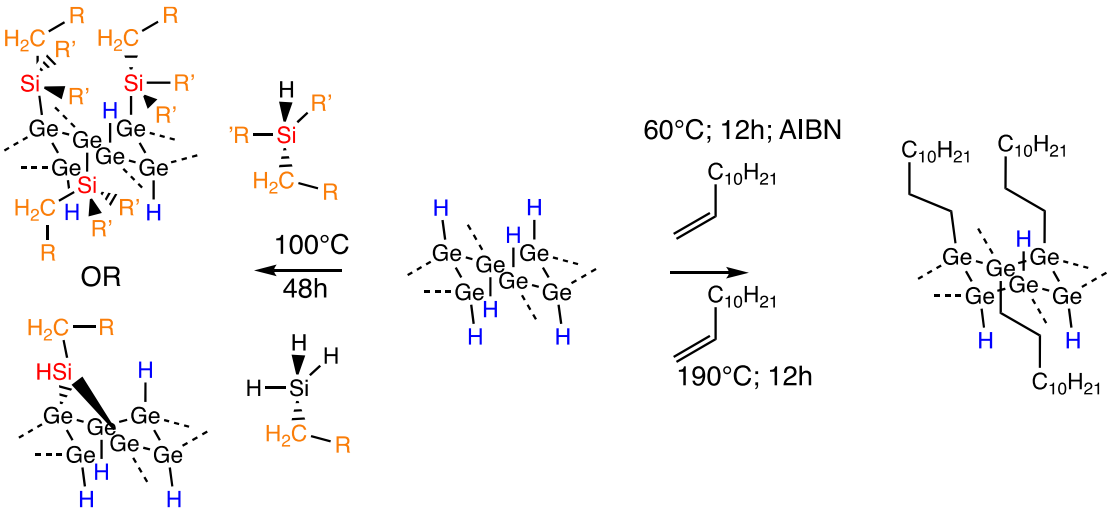

Figure 1-12. Radical-initiated/thermal-induced hydrogermylation reaction of Si–Ge bond formation and heteronuclear dehydrocoupling reaction of C–Ge bond formation to functionalize the freestanding hydrogen-terminated germanane surface, where R = $–CH_2–C_6F_{13}$, R' = CH_3.[122,123]

1.5 Preparation of Oligo- and Poly-germanes

To date, much research has been carried out on 2D nanostructures. Significant progress has been made about different kinds of one-dimensional (1D) nanostructures in the past years;[124] these include polymers, small molecules, and inorganic species.[125] Among those, we only focus on 1D polymer nanostructures since they can be prepared by all Group 14 elements with the general formula $(ER_2)_n$, where E = C, Si, Ge, or Sn. A polymer is a substance or material composed of very large molecules, which consist of repeating units connected by covalent bonds (i.e., DNA is made from A, T, C, G). Each

$(ER_2)_n$ is in a linear chain of E–E single covalent bonds (ignore cross-linking or side chains here) with σ bond electron delocalization (σ-delocalization), which can be defined as the delocalized electrons across the entire backbone.

The σ-delocalization can influence the molecular conformations, which will affect material properties further according to Michl et al.[126–128] Conformationally constrained oligosilanes were prepared by Tsuji and Tamao to investigate the relationship between conformation and σ-bond electron delocalization.[126,129–133] They found that the optical properties of polymeric 1D nanomaterials were mainly dependent on the chain length, substituents, backbone conformation, and some secondary structures. For example, the band (λ_{max}) position and absorptivity of polysilanes increase regularly with the increase of Si–Si chain length.[128,134]

The first polysilane, named poly(diphenylsilane), was synthesized with an alkali metal by Kipping and Sands in 1921 (Wurtz-type coupling reaction).[135] However, the Kipping approach has some limitations since it requires drastic reaction conditions.[136] Thus, more alternative synthesis methods have been developed, including (a) homogenous dehydrocoupling polymerization reaction (using a transition metal as a catalyst) of hydrosilane (i.e., Cp_2ZrCl_2/*n*-BuLi, Wilkinson's catalyst), (b) ring-opening polymerization (ROP), (c) anionic polymerization, and (d) electrochemical reduction (electro polymerization).[128,137,138]

Compared to polysilanes, polygermanes, with the heavier Ge atoms in the backbone, show a stronger σ-conjugation and a narrower band gap; they usually are synthesized by Wurtz-type polymerization.[139] However, the reaction conditions are very harsh, requiring alkali metals (i.e., Na, Li, K) as the reducing agent (alkali metals /toluene, reflux) (Figure 1-13). Although a variety of alkyl and aryl (R_1, R_2) derivatives can be used, the synthesis is still not friendly to many electronically active functional groups. Besides, Wurtz-type polymerization cannot prepare high molecular weight polygermanes efficiently; their yield is usually less than 25%.[140]

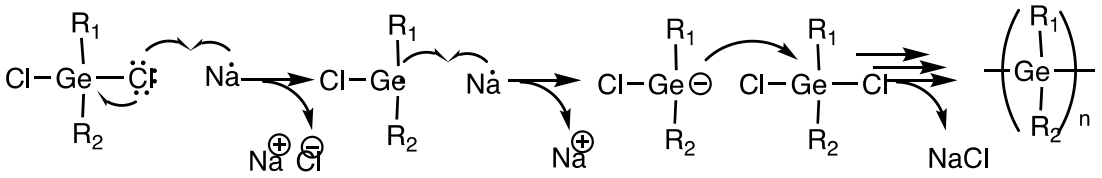

Figure 1-13. Proposed mechanism for polygermane synthesis by a Wurtz-type reduction from dichlorogermanes and sodium, where R_1, R_2 = alkyl or aryl.[139]

The electrochemical reduction or electro-reduction with an Mg electrode is another promising method (Figure 1-14), which forms repeated Ge–Ge bonds under electrochemical conditions. It usually can be divided into two reactions (cathodic and anodic). Figure 1-14 only shows the cathodic reactions, while the anodic reaction is $2/n\mathrm{M} \rightarrow 2/n\mathrm{M}^{n+} + 2\mathrm{e}^-$. The conditions are $LiClO_4$ in tetrahydrofuran (THF) as the solvent, Mg as the cathode and anode under sonication, in a cell with ~3 F/mol. The electrochemical reduction produces polygermane, with moderate molecular weight distribution but less efficiency.[136,141]

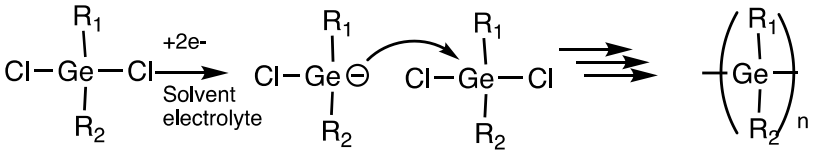

Figure 1-14. Proposed mechanism for polygermane synthesis by electrochemical reduction, where R_1, R_2 = alkyl or aryl.[141]

Homogenous dehydrocoupling polymerization is used widely to prepare polysilane, but it cannot be applied to the synthesis of polymgermanes, especially those with high molecular weight.[139,142] Harrod et al. published the dehydrocoupling of Ph_2GeH_2 using Cp_2TiCl_2 as a catalyst, which only formed the H–$[Ph_2Ge]_4$–H oligomer.[142] Choi et al. reported the dehydrocoupling of $PhGeH_3$ taking Cp_2ZrCl_2/*n*-BuLi as a catalyst. The resulting polymers only had a small molecular weight (<100 Da) with a partial network structure.[143]

Another approach of synthesis involves the ruthenium-catalyzed demethanative coupling of $HGeMe_3$. Reichl et al. demonstrated that high yield polygermanes could be synthesized by $Ru(PMe_3)_4(GeMe_3)_2$ at room temperature, which formed CH_4 as a by-product.[144–146] Later, Katz et al. from the same group proposed a mechanism for those

demethanative couplings (Figure 1-15).[145] Although these reactions offer polygermanes with a relatively high molecular weight, they are limited by the availability of dimethyl- or dihalide- germane precursors.

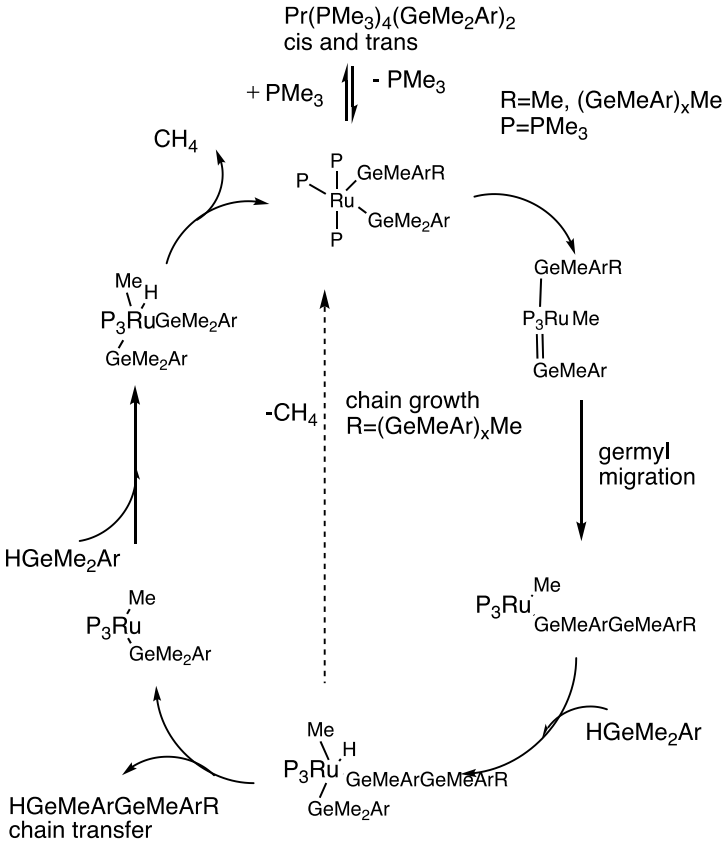

Figure 1-15. Proposed mechanism for linear polygermane formation by demethanative coupling.[145,146]

Nowadays, many researchers are working still on the synthesis of polygermanes because, not only do the previous synthesis routes have limitations (i.e., moderate molecular weight products and a limit of substituent functionalities), but also because the polygermanes have many promising properties, including semiconductivity, photoconductivity, and photoluminesce.[141] Thus, Royen et al. demonstrated a new approach: a solid-state synthesis of poly(dihydrogermane). Poly(dihydrogermane) is the simplest form of polygermane containing only Ge and H, which can be made from Zintl precursor CaGe. It can be synthesized by a deintercalation reaction of the Zintl phase CaGe in the acid environment, resulting in a yellow/orange solid with a high molecular weight.[147] Based on that, Yu et al. prepared a high-quality gram-scale

poly(dihydrogermane) from CaGe, taking a two-step deintercalation reaction instead of one-step (Figure 1-16). The resulting products have a more ordered linear fabric morphology, a stronger Ge–Ge bond strength, and are more stable than the traditional ones.[148]

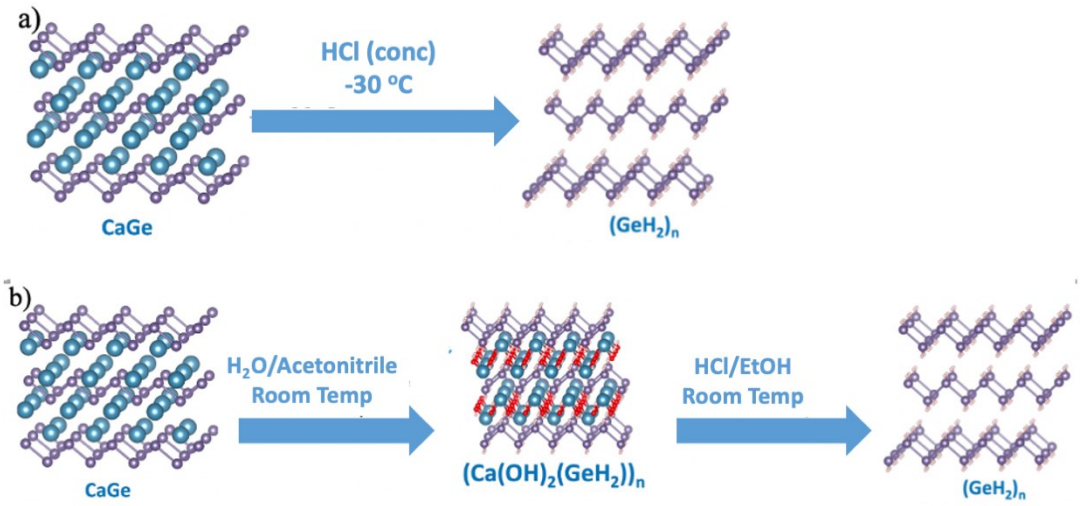

Figure 1-16. Synthesis of $[GeH_2]_n$ from CaGe by (a) Royen et al.[147] and (b) Yu et al.[148] where the blue spheres are Ca atoms, the purple spheres are Ge atoms, the pink spheres are H atoms, and the red spheres are O atoms.

1.6 Ca–Ge System

The Ca–Ge alloy system (phase diagram) can help us target and prepare various Ge nanosystems providing the fundamental information to prepare different Ca–Ge Zintl phases. The phase diagram (Figure 1-17) provides five intermetallic compounds: Ca_2Ge, Ca_5Ge_3, Ca_7Ge_6, CaGe, and $CaGe_2$, which are treated as stoichiometric phases. With the crystallographic data for the intermediate phases,[91,149–151] all the Ca–Ge intermetallic compounds can be determined and synthesized, while not all the compounds can be used as ideal precursors.

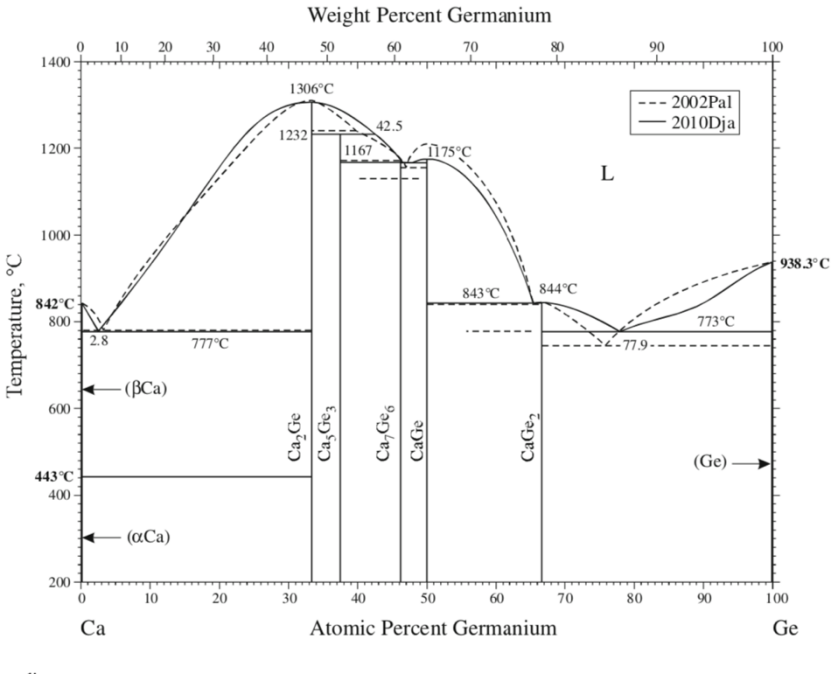

Figure 1-17. Ca–Ge phase diagram.[152,153] [Reprinted and adapted with permission from Copyright 2013 ASM International.]

$Ca_{33}Ge$ and Ca_7Ge combine a large percentage of electropositive atoms (i.e., Ca) with a small number of electronegative atoms (i.e., Ge) and do not obey the Zintl-Klemm concept.[154] Ca_2Ge also has limited potential as a precursor because of isolated anions (all the Ge atoms are four-coordinated with a Ca atom) and impossible deintercalation. Ca_5Ge_3 (Figure 1-18) only contains Ge_2 dumbbells and isolated Ge atoms, which could form GeH_4 and Ge_2H_6 gas easily after acid deintercalation.

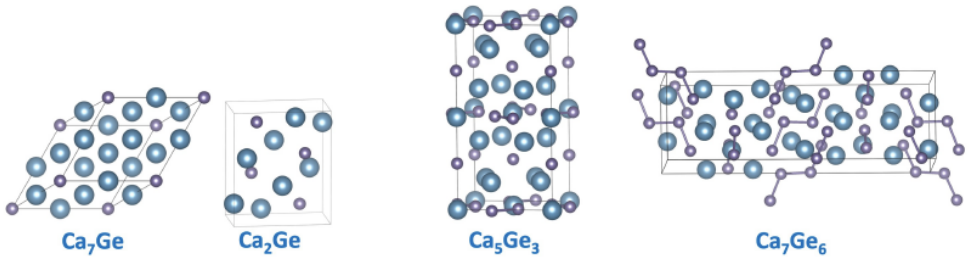

Figure 1-18. The structure of Ca_7Ge, Ca_2Ge, Ca_5Ge_3, and Ca_7Ge_6, where Ca and Ge atoms are represented by light blue and purple spheres, respectively.[91]

Ca_7Ge_6 is formed by a peritectic reaction in the Ge-containing range of 37.5–50% Ge, which indicates that at a mixed temperature and composition, mixing one

solid phase (Ca_7Ge_6) with liquid (L) can form another single solid phase (CaGe).[149] The liquid phase can change between CaGe and Ca_7Ge_6, but it is difficult to reach equilibrium. It is interesting to note that in the investigations outlined in Chapter 3, a small amount of Ca_7Ge_6 impurity is formed during the synthesis of CaGe and is removed easily during acid/water treatment and centrifugation.

CaGe is prepared by congruently melting the elements at 1175 °C.[151] The structure of this alloy is shown in Figure 1-19. Ge subunits are arranged in planar zigzag chains and aligned in a parallel fashion. These Ge chains are separated by two layers of Ca atoms.

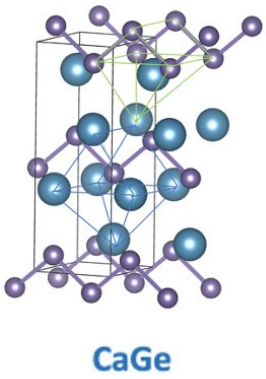

Figure 1-19. Scheme of the structure of CaGe, where Ca and Ge atoms are represented by light blue and purple spheres, respectively.[91]

$CaGe_2$ congruently melts at 844 °C and possesses a structure similar to that of $CaSi_2$ (Figure 1-9). Four polytypes (2H, 3R, 1T, and 6R) have been reported,[155,156] all containing anion (germanene) layers stabilized by cations (Ca).[157] The 2H and 1T polytypes have a hexagonal crystal system, with two and one layers of germanene stacked in the AB and A order, respectively. The 3R and 6R polytypes have a trigonal rhombohedral crystal system, with three and six layers of germanene stacked in the ABC and AA'BB'CC' order, respectively. However, not all structures can be used as precursors. A survey of the literature showed that only 6R-Ge (or β-$CaGe_2$) and 2H-Ge (or α-$CaGe_2$) were thermodynamically stable $CaGe_2$ compounds (Figure 1-20).[91,157]

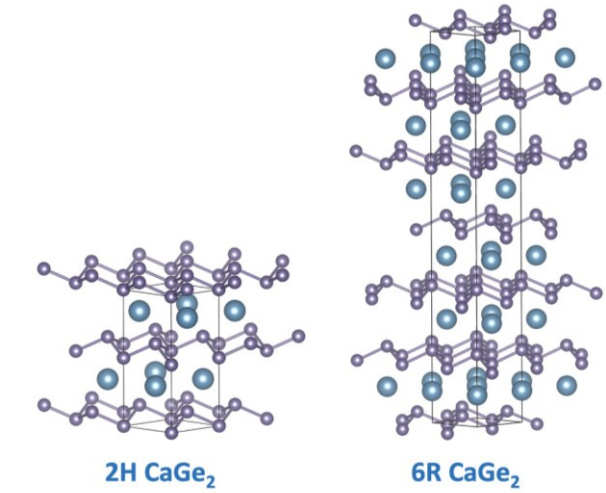

Figure 1-20. Scheme of the structures of α-$CaGe_2$ and β-$CaGe_2$. where Ca and Ge atoms are represented by light blue and purple spheres, respectively.[91]

1.7 Layered Materials Exfoliation

Zintl phases are the starting materials. However, after acid deintercalation, the resulting layered materials cannot be used directly for further application because the layered materials are packed in the bulk structures, which cannot fulfill optical, catalytic, or electronic properties (Figure 1-21).[158] Thus, it is necessary to produce large-scale mono- or few-layers from the bulk structures.[159]

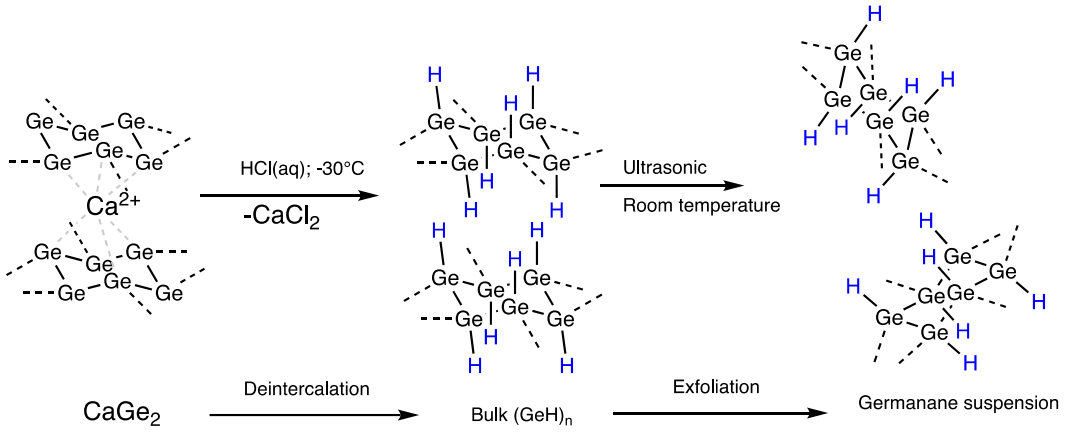

Figure 1-21. The structure of $CaGe_2$, bulk layered germanane (Ge_6H_6), and germanane dispersion.[115]

Currently, liquid-phase exfoliation is one of the most common and useful approaches to prepare suspended layered materials from their corresponding bulk materials.[115] After deintercalation, the Van der Waals (vdw) forces between the layers are weaker. The exfoliation step facilitates the separation and release of each layer in the solution. In other words, liquid-phase exfoliation must take place in a proper solvent.[160]

The type of solvent plays a critical role, not only in the efficiency of the exfoliation but also in the quality and properties of the exfoliated materials, which is determined by testing a large number of solvents through a trial-and-error process. In this study, after deintercalation of the Zintl phase precursor, the resulting germananes and polygermanes show the stacked structures of Ge_6H_6 and $–(GeH_2)_n–$, respectively, which can be described as bulk materials without Ca^{2+}. In 2018, Nakamura and Nakano studied the liquid-phase exfoliation of germananes with 35 different solvents (as shown in Table 1-1).[115] They found that the best solvent was the one with a low boiling point, good dispersibility, extraordinarily large δD value, and a moderately larger δH value. The best solvents selected for the exfoliation of Ge_6H_6 are also applicable to the exfoliation of polygermanes.[115]

Table 1-1. List of Probe Liquids for Hydrogen-terminated Germanane (Ge_6H_6) Dispersibility Tests.[115]

	Liquid name		Liquid name		Liquid name
1	Acetone	**13**	Acetonitrile	**25**	2-Butanol
2	Toluene	**14**	Tetrachloroethylene	**26**	n-Butyl Acetate
3	2-Propanol	**15**	Acetic Acid	**27**	Carbon Disulfide
4	Methyl Ethyl Ketone	**16**	Ethanol	**28**	Diether Ether
5	N-Methyl-2-pyrrolidone	**17**	Cyclopentanone	**29**	1,3-Butanediol
6	Dimethyl Formamide	**18**	Ethyl Acetate	**30**	Cyclohexylchloride
7	Hexane	**19**	Formic Acid	**31**	Dimethyl Sulfoxide
8	Formamide	**20**	Ethylene Glycol	**32**	1,3-Dioxolane
9	1,4-Dioxane	**21**	Tetrahydronaphthalene	**33**	Caprolactone
10	Propylene Carbonate	**22**	Chloroform	**34**	Methylene Dichloride
11	o-Dichlorobenzene	**23**	Methylal	**35**	1-Bromonaphthalene
12	Benzyl Alcohol	**24**	Cyclohexanol		

1.8 Surface Functionalization

Group 14 elemental nanomaterials have been used in many applications. However, they still have some disadvantageous properties, such as a small band gap and poor thermodynamic and chemical stability, which limit their applications. Hence, we must modulate their properties, improve their stability and widen their band gaps. Surface modification or functionalization is one of the most common ways for this purpose.

The physicist Wolfgang Pauli said that "God made the bulk, but the surface was invented by the devil."[161] Surface plays such an important role because, different from those of the inner atoms, the surface atoms share their borders with the outside world. Inside the bulk, each atom is surrounded by other similar atoms that have much the same environment, while the surface atoms can have interactions with other different atoms. Therefore, the surface properties of a material can be tunable, which is also applicable to all nanomaterials. In the following section, different functionalization approaches on various nanomaterials will be introduced.

1.8.1 Surface Functionalization on Wafer/Bulk Si/Ge (111)

Before functionalization, single-crystal Si and Ge wafers have a specific orientation because of the arrangement of the Si or Ge atoms in a unit cell. Their arrangements are in the same pattern as diamond, in a face-centered cubic (fcc) structured lattice. Therefore, as in diamond, both silicon and germanium crystals would have the octahedral structure in the plane of (111) because it has the highest network density (Figure 1-22). In the next paragraph, only the Si/Ge (111) surface is discussed.

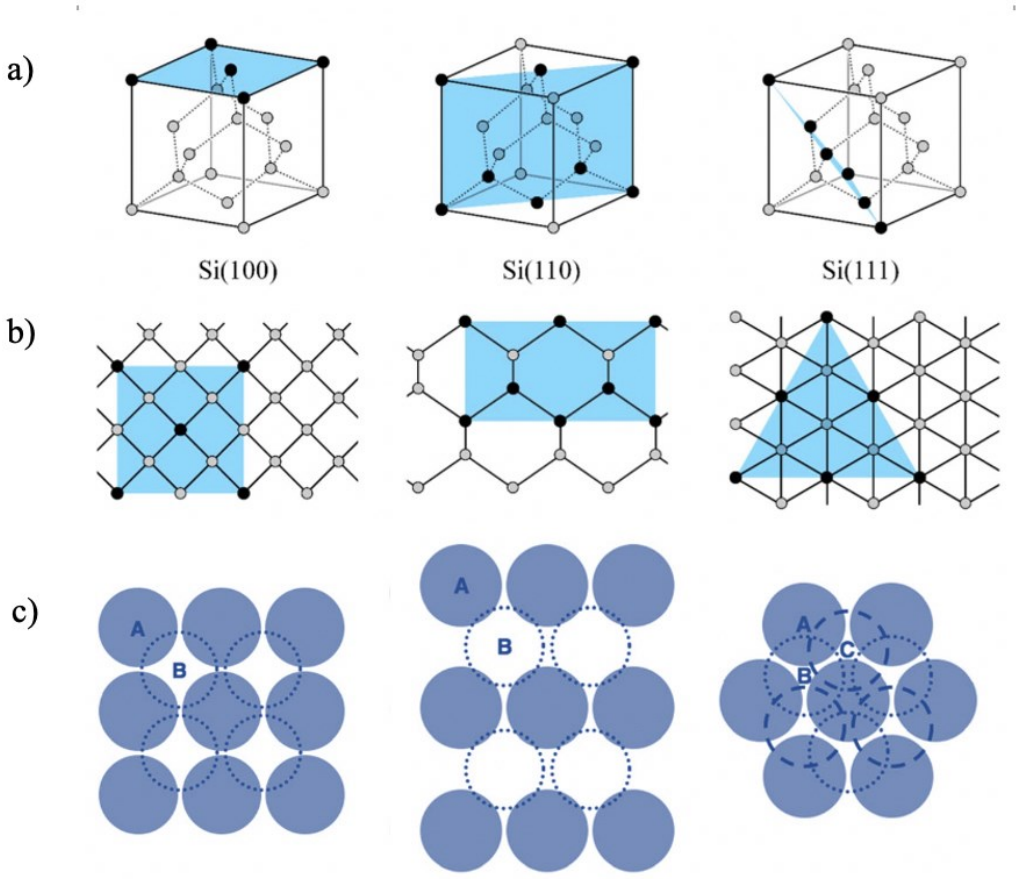

Figure 1-22. (a) Unit cell, (b) top view and (c) stacking sequences in (100), (110), and (111) orientation. Gray and black spheres represent silicon with different link-set types.[162,163] [(a, b) Reprinted and adapted with permission from Copyright 1998 IEEE and (c) from Copyright 2013 RSC.]

Nowadays, the surface functionalization of Si/Ge materials has been studied by wet chemistry (Figure 1-23).[164,165] An appropriate wet chemical treatment of the wafer surface is necessary for the further functionalization process to remove most of the oxidation but also some other organic and metallic contaminants.[166–168] The surfaces can be cleaned with fluoride-based etching (40% NH_4F or aqueous HF, must contain fluoride ion) to prepare a flat H-Si (111) surface[169] and a rough H-Ge (111) surface.[170] The halogenation on the surface can be achieved by introducing halogen sources (i.e., PCl_5, Cl_2, CCl_3Br, or N-bromosuccinimide) onto the H-Si/Ge (111) surface under high temperature using benzoyl peroxide or ultraviolet light as a radical initiator.[171–173] One-step halogenation can be achieved by treating the oxidized wafer surface with 10% HCl for 10 min; this can be functionalized further.[108,174]

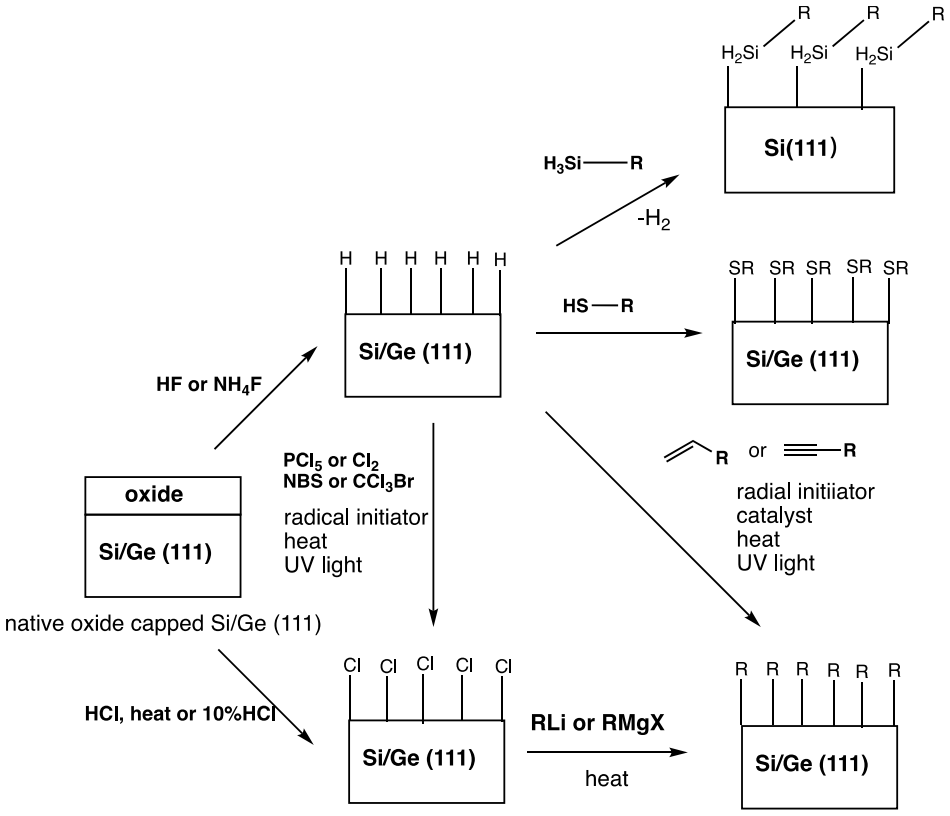

Figure 1-23. Functionalization on Si/Ge (111) surface via wet chemistry.

After chemical etching, the halide-terminated or hydride-terminated surface can be functionalized by attaching various organic ligands. Hydrosilylation/hydrogermylation can be explained as the addition of an unsaturated bond (i.e., alkynes, alkenes) into the Si–H/Ge–H group and formation of Si–C/Ge–C under high temperature (usually >150 °C),[175,176,177] with the addition of an initiator (i.e., diacyl peroxide, 4-nitro,[178] or bromobenzene diazonium salt[179]), or with a catalyst.[164,180] The first example of hydrosilylation on a Si(111) –H surface was demonstrated in 1993 by Linford et al.[181–184] With the diacyl peroxide as the radical initiator, alkenes passivated on the Si–H surface formed a stable monolayer in different environments, including boiled solvents, water, base, or acid (i.e., HF) solutions. A Grignard reagent also can be applied to a halogenated Si(111) surface from H-Si(111), while it does not work for H-Ge(111).[184–186] Halide-terminated Si/Ge(111) reacting with a strong organic base, such as a Grignard reagent and organolithium is another approach.[187,188] The resulting products functionalized via halogenation usually have a high surface

coverage of small ligands, while hydrosilylation/hydrogermylation is much faster (a couple of hours).[108,189] Furthermore, thiols can be grafted covalently to a Si/Ge (111) surface through the reaction between H-Si/Ge (111) and thiols.[190–192] The Si–Si bond also can be formed by dehydrogenative coupling using a transition metal catalyst (i.e., Cp_2TiCl_2 and Cp_2ZrCl_2/*n*-BuLi).[193]

Neither H-Si(111),[194] H-Ge (111), nor Br-Si(111)[171] can prevent from being oxidized in the presence of air, although they are good candidates for functionalization.[195] However, after functionalization, organic ligand functionalized Si/Ge (111) surface can be stable in the air for days or even weeks.[171,190] Furthermore, the functionalized surface also exhibits thermal stability. For example, alkyl-S-Ge (111) can be stable up to 177 °C (desorption at 277 °C).[190] Alkyl-Ge (111) can be stable up to even higher temperatures (i.e., 200–400 °C).[174,187] Similar situations can be found in Si (111); For example, alkyl-Si (111) can be stable up to 300–350 °C.[173,196]

1.8.2 Surface Functionalization on Si/Ge Quantum dots (QDs)

Most functionalization methods mentioned above have been applied also to the QD surfaces.[197–200] Actually, surface modification of Si QDs commonly is achieved via the reaction of surface hydrides or halides (i.e., Cl) with appropriate ligands. Although only hydride-terminated Si QDs are studied in this thesis, a brief scheme of the functionalization of halide-terminated silicon nanocrystals is illustrated here (Figure 1-24).

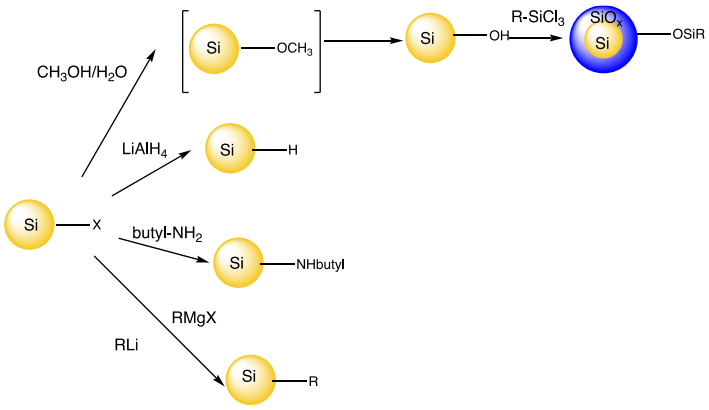

Figure 1-24. Scheme of X-SiQD (X = Cl, or Br) surface modification via reaction of surface halides with nucleophiles.[201]

Hydrosilylation is the most widely used surface modification method for the surfaces of H–Si QDs because it can be applied independently of the size or the shape of QDs.[175–177,180,202] It can be used to functionalize hydride-terminated Si QDs, where unsaturated ligands are inserted between Si–H bonds to form stable Si–C linkages with high surface coverage. It can be achieved by radical-initiated,[197] photochemical (AIBN 60 °C, BP 85 °C),[203] thermal,[204] platinum-catalyzed,[205] diazonium salt-initiated,[206] and boranes catalyzed[177] without heat, light, or catalyst (Figure 1-25).[207]

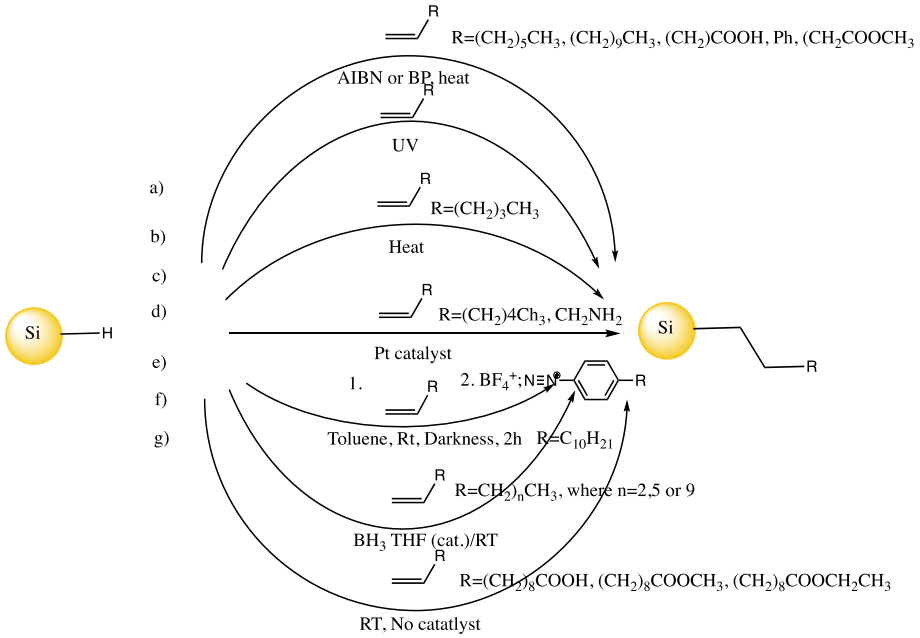

Figure 1-25. Scheme of common hydrosilylations on hydride-terminated Si QDs are (a) radical-initiated hydrosilylation,[197] (b) photochemical hydrosilylation,[203] (c) thermal hydrosilylation,[204] (d) platinum-catalyzed hydrosilylation,[205] (e) diazonium salt-initiated hydrosilylation,[206] (f) borane catalyzed hydrosilylation,[177] and (g) hydrosilylation without heat, light, or catalyst.[207]

Thermal hydrosilylation is the most common method, usually carried out in the temperature range between 100 and 190 °C with the assistance of alkene/alkyne as the reagent solvent. Unfortunately, this temperature is so high that it can boil some short-chain organic ligands. Tilley et al. prepared water-soluble amine-terminated Si QDs using chloroplatinic acid (H_2PtCl_6) as a catalyst to produce hydrosilylation at room temperature.[205] Yang et al. carried out a low-temperature radical-initiated (i.e., AIBN, 60 °C) hydrosilylation, which allows for a wide range of functional group tolerance with high surface coverage (64%).[204,208] Hohlein et al. developed a series of organic

soluble diazonium salts for hydrosilylation on H-Si QDs.[197,206] Purkait et al. reported the hydrosilylation using Lewis acid BH_3·THF to functionalize short-chain ligands (pentene and pentyne) on the surface of H-Si QDs.[177] Korgel et al. investigated a room-temperature hydrosilylation approach to functionalize with bifunctional ligands without any external triggers (i.e., heat, light, or catalyst).[207] However, this reaction is very time-consuming, requiring 12–120 h. Xenon difluoride (XeF_2)-mediated functionalization was reported by Mobarok et al. XeF_2 and PCl_5 are etchants[162] that can cleave Si–Si α bonds.[55] They can generate a large number of fluorine or chlorine radicals that rapidly strip off surface Si atoms and leave dangling bonds (≡Si•). The fluorine or chlorine radicals can remove a significant portion of surface Si–H_x species in the form of hydrofluorosilane or hydrochorosilane byproducts.

Although hydrosilylation has been well developed in the past, there are some alternative methods for the functionalization of Si QDs. Hohlein et al. functionalized Si QDs using alkyl aryl lithium reagents (organolithium reagent based).[197] The approach based on Grignard reagents is not as effective as hydrosilylation because the former requires the reactive Si–Li (after Si–Si cleavage) to get further functionalization with bromoalkene and epoxide. Dasog et al.[30,54,209] functionalized H-Si QDs with trialkylphosphine oxide (TOPO), carbon dioxide (CO_2), and amines (RNH_2) (Figure 1-26). The amine or carbon dioxide functionalized Si QDs are not stable under ambient conditions, but TOPO passivated Si QDs are colloidally stable.

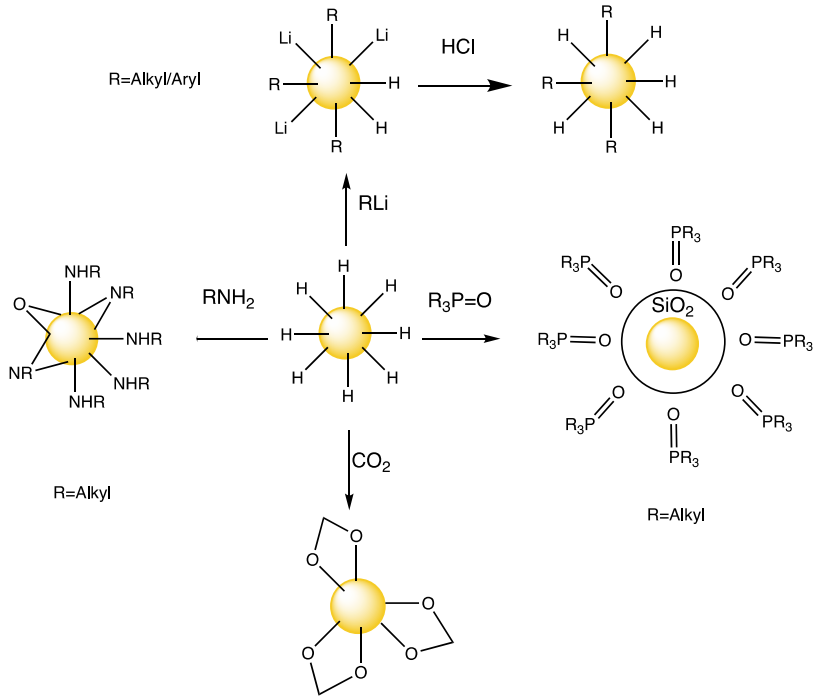

Figure 1-26. Surface functionalization of hydride-terminated silicon QDs with organolithium (LiR), trialkylphosphine oxide ($R_3P = O$), carbon dioxide (CO_2), and amines (RNH_2).[30]

Furthermore, hydride-terminated Si QDs can be transformed into halide-terminated Si QDs, which are good precursors for further functionalization with different organic ligands (i.e., alcohols, amines, Grignard, or organolithium reagents, silanols, or lithium aluminum hydride) (Figure 1-27). Recent research by Dasog et al. extended the two-step functionalization by using different halide sources (i.e., PCl_5, Br_2, and I_2).[30,54,216–218] Figure 1-27 shows that there is a significant etching of Si QDs using chloride or bromide Grignard reagents but an undetectable etching using iodide. As a result, only Cl-Si QDs and Br-Si QDs can be used to prepare alkyl-passivated SiQDs efficiently with Grignard reagents, while I-Si QDs would be oxidized easily.

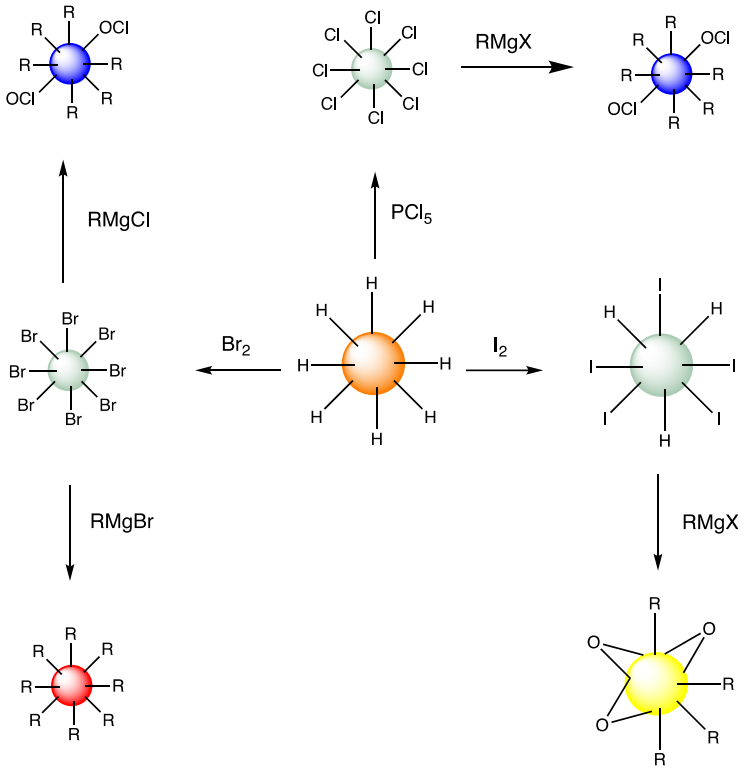

Figure 1-27. Halide-terminated surfaces derived from hydride-terminated SiQDs, followed by Grignard reactions. The color of the SiQDs corresponds to the resulting PL, reflecting the influence of the halide on SiQDs optical properties.[54]

Many different ligands have been used to functionalize Ge QDs as well. In the same way as Si QDs, hydride-terminated Ge QDs also can be functionalized with an alkyl group (i.e., alkane, alkene, or alkyne) by heat, UV, or a catalyst initiated hydrogermylation to form stable Ge–C bonds (Figure 1-28 g). For example, Wilcoxon et al. reduced GeX_4 (where X = Cl, Br, or I) at room temperature with hydride-containing reductants, such as $LiAlH_4$, before functionalization.[212]

There are some alternative surfaces capable of being functionalized. For example, chloride terminated 4 nm Ge QDs can be functionalized with acetal and alkyl via Grignard reagents (Figure 1-28 a).[213] Lambert et al. partially exchanged the ligands from hexadecylamine (HAD) to tri-octylphosphine (TOP) or oxtadecanthiol (ODT) on the 3–5 nm Ge QDs' surface (Figure 1-28 b).[214] Ruddy et al. prepared 4 nm $Ge_{1-x}E_x$ alloyed QDs functionalized with an octadecyl (OED) or OAM, which could then be exchanged to amine termination (i.e., hexylamine, polyamine) (Figure 1-28 c).[215,216] Purkait et al. prepared hydrophobic 5.25 nm Ge QDs functionalized with dodecyl

(stable in non-polar solvents) and with 3-dimethylamino-1-propene (stable in polar solvent) (Figure 1-28 d).[34,177,217] Holmes et al. found effects of OAM, dodecanethiol (DDT), and N4,N4,N4',N4'-tertraphenylbiphenyl-4,4'-diamine (TPD).[218] OAM can be replaced by either DDT or TPD with hydrazine or direct displacement (Figure 1-28 e). Ge QDs papered in RF plasma can be functionalized via ligand exchanging. Specifically, the OAM ligand can be replaced by many different compounds (i.e., hexadecylamine, CTA+, dodecylammonium, methylammonium, hydrazinium, and even sodium or potassium metals) (Figure 1-28 f).[219]

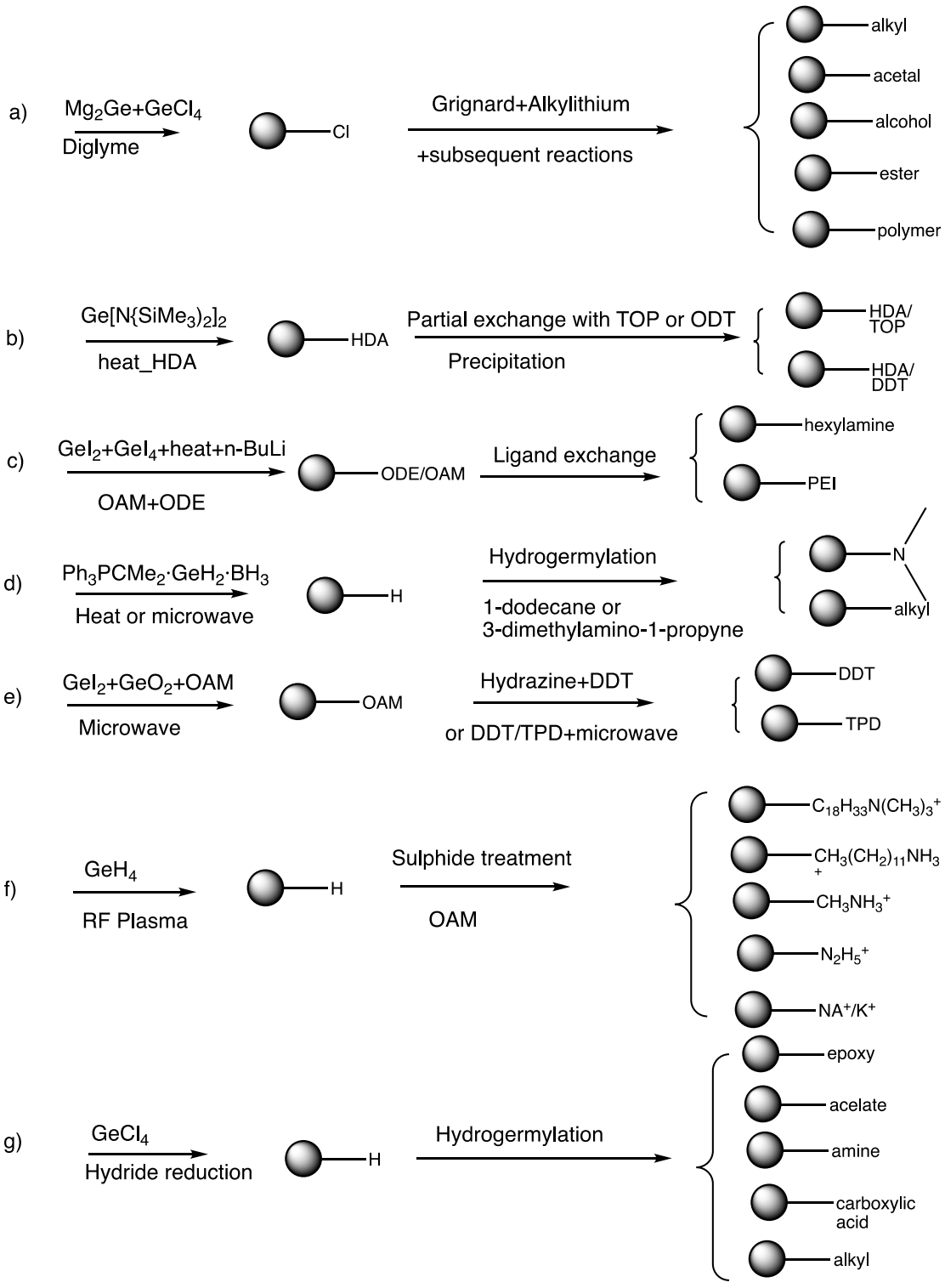

Figure 1-28. Scheme of functionalities to the Ge QDs.[220]

To address the issues of hydride-terminated reduction of germanium compounds (Figure 1-29) further, Fok et al. used solid GeI_4 instead of volatile $GeCl_4$ and reduced a toluene solution of GeI_4 in cetyltrimethylammonium bromide (CTAB) with $LiAlH_4$.[198] Refluxing of the produced hydro-terminated Ge QDs with *n*-undecene led to *n*-undecyl terminated Ge QDs, which showed PL around 390 nm.

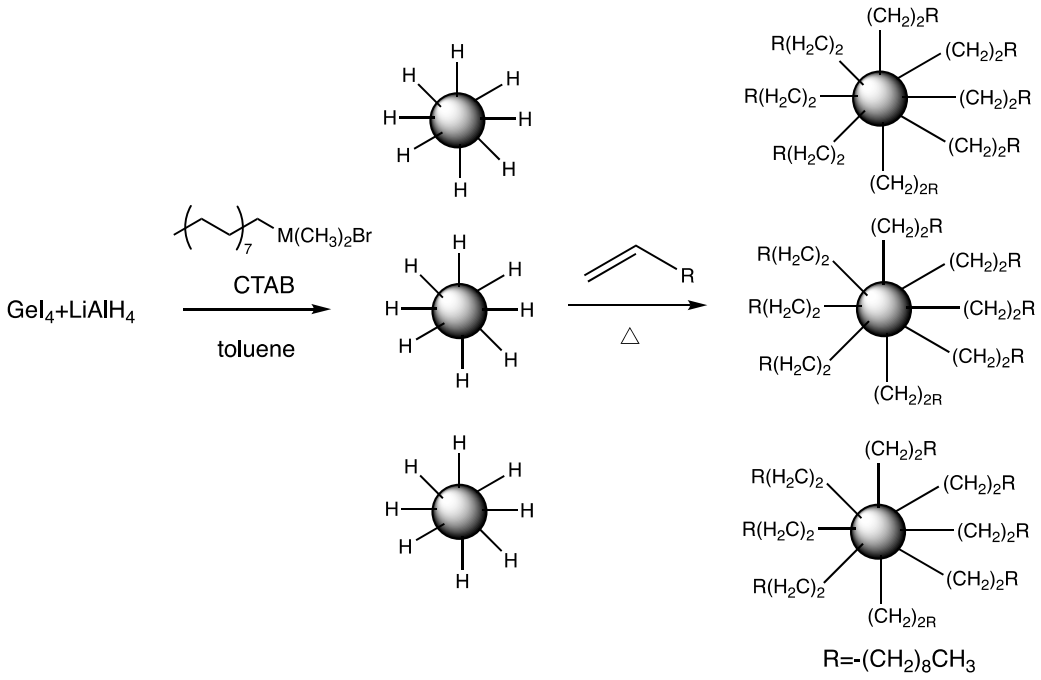

Figure 1-29. Scheme of the synthesis and surface derivatization of Ge QDs.[198]

1.8.3 Surface Functionalization on 2D Si/Ge

There are many similarities among surface functionalization of 2D Si/Ge materials, QDs, and bulk materials. As mentioned in Section 1.4, transition metal-catalyzed ($H_2PtCl_6 \cdot 6H_2O$),[105] radical-based (diazonium and iodonium salts, AIBN and thermal)[221–224] Lewis acid 3-coordinate B/Al catalyzed (i.e., $BH_3 \cdot S(CH_3)_2$, BF_3, BCF/$B(C_6F_5)_3$, and ACF/$Al(C_6F_5)_3$) hydrosilylation[225] have been reported for hydride-terminated silicane (Figure 1-30). In addition, hydride-terminated silicane can be functionalized using organoamines to yield Si–NHR and Si–(NR) –Si at 60 °C for 12 to 24 h (Figure 1-9).[226,227] Besides hydrosilylation, Grignard reagents also are applied widely. Sugiyama et al. showed that hydride-terminated silicane can be functionalized by Grignard reagent (PhMgBr) at 70 °C for 2 days to prepare phenyl-terminated Si NSs

(band gap = 2.7 to 2.9 eV).[226] The starting materials also can be the Zintl precursor, like $CaSi_2$ or $CaGe_2$. For example, Ohashi et al. in 2019 reacted $CaSi_2$ with neat benzyl bromide at 150 °C to yield a yellow benzyl-modified silicane.[228]

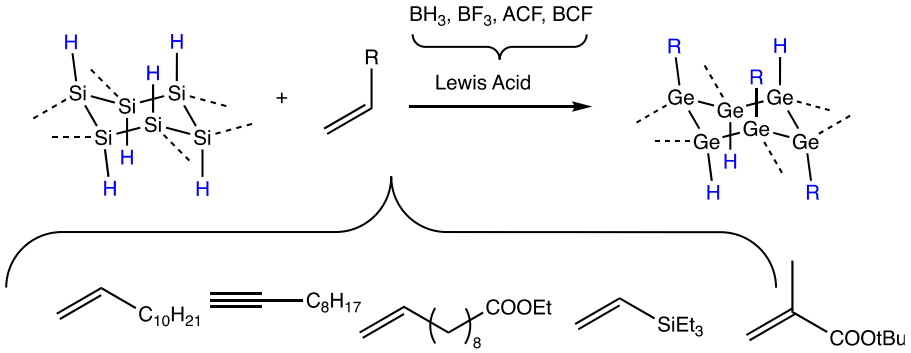

Figure 1-30. Scheme of Lewis acid catalyzed hydrosilylation, where $BH_3{\cdot}SMe_2$ = borane dimethylsulfide, BF_3 = Trifluoroborane, ACF = tris(pentafluorophenyl)alane, and BCF = tris(pentafluorophenyl)borane.[225]

Radical-based (AIBN and thermal), Lewis acid ($BH_3{\cdot}THF$), and etchant (XeF_2) hydrogermylation have been reported for germanane.[106,122] Specifically, Yu et al. functionalized the hydride-terminated germanane by radically-induced and thermally-induced hydrogermylation using dodecane.[122] The suspension of germanane must be ultrasonicated before adding a radical initiator (azobis(isobutyronitrile)) or heating (190 °C) because a bilayer or multilayer always is formed. The radical-induced hydrogermylation prepared germanane covered 55% of the surface, while the thermal-induced germanane covered 103% because of its partial oligomerization of the ligands. Furthermore, there was a redshift in Ge_6H_6 (radically-induced functionalized germanane) from 1.7 eV to 1.5 eV and 1.1 eV (thermally-induced functionalized germanane). They also found that functionalization would affect the chemical and thermal stability of germanane. After it was functionalized, dodecyl-GeNSs did not lose a lot of mass at temperatures lower than 365 °C. Radical and thermal-induced functionalized GeNSs would not lose the surface group until the temperature was raised to 470 °C and 475 °C. Yu et al. also functionalized the hydride-terminated germanane with both primary hydridosilanes ($H_3SiC_{18}H_{37}$, $H_3Si(CH_2)_2(CH_2)_6CF_3$) and tertiary hydridosilanes ($HSi(Me)(C_{18}H_{37})$, $HSi(CH_{17})_3$) simply by thermal heating.[123] Also, the

same method worked well with hydride-terminated Si QDs (3–64 nm). Once Si–Ge was formed, the bright red PL was quenched.

On the other hand, Jiang et al. established the synthesis, properties, and surface functionalization of germananes (see Section 1.4). Since 2014, their alkylation method was successful, with over 95% surface coverage, and produced a library of germananes terminated with different organic ligands (Figure 1-31). They established the effect of ligand size (greater size) and electronegativity (more electronegative) on the electron structures (lower band gap). Simply by changing the identity of the organic ligand, the band gap of germanane can be tuned by about 15%.[83,116]

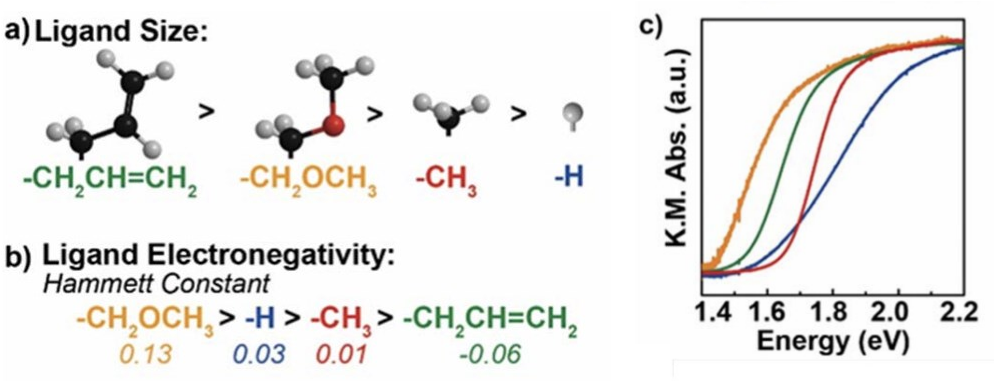

Figure 1-31. Ligand effect on the band gap. (a) The relative size of the four ligands decreases from left to right. (b) Relative electronegativity of the four ligands decreases from left to right. (c) DRA of the GeR terminated with these four ligands increasing from $GeCH_2OCH_3$ (orange) to $GeCH_2CH = CH_2$ (olive) to GeH (blue) to $GeCH_3$ (red).[116] [Reprinted and adapted with permission from Copyright 2016 American Chemical Society, further permissions related to the material excerpted should be directed to the American Chemical Society, https://pubs.acs.org/doi/full/10.1021/acs.chemmater.6b04309.]

1.9 Scope of this Thesis

In Chapter 1, we give a brief introduction on the definition, classification, synthesis, precursor, and surface functionalization of the Group 14 nanomaterials, especially on silicon and germanium. We first introduce different methods for the preparation of Si/Ge nanomaterials by various morphologies, including 1D polymers and 2D nanosheets. We also mention the history of the development of these nanomaterials. The synthesis strategies of 1D polygermanes include Wurtz-type coupling, electrochemical reduction, and dehydrocoupling. The synthesis strategies of 2D nanosheets can be categorized into deposition on metallic

substrates and deintercalation of Zintl phases. The surface functionalization on Ge wafer surfaces, porous surfaces, quantum dots, polygermanes, and Ge nanosheets are summarized, including hydrogermylation, Grignard, organolithium reagents, dehydrocoupling reaction, amination, and thiolation. Figure 1-32 summarizes the methods that have been used to functionalize hydride-terminated Si and Ge QDs, as discussed earlier in this chapter. The study is relevant to the development of nanomaterials since the previous synthesis routes have limitations (i.e., moderate molecular weight products and limit of substituent functionalities). Besides, the prepared nanomaterials have many promising properties including semiconductivity, photoconductivity, and photoluminescence.

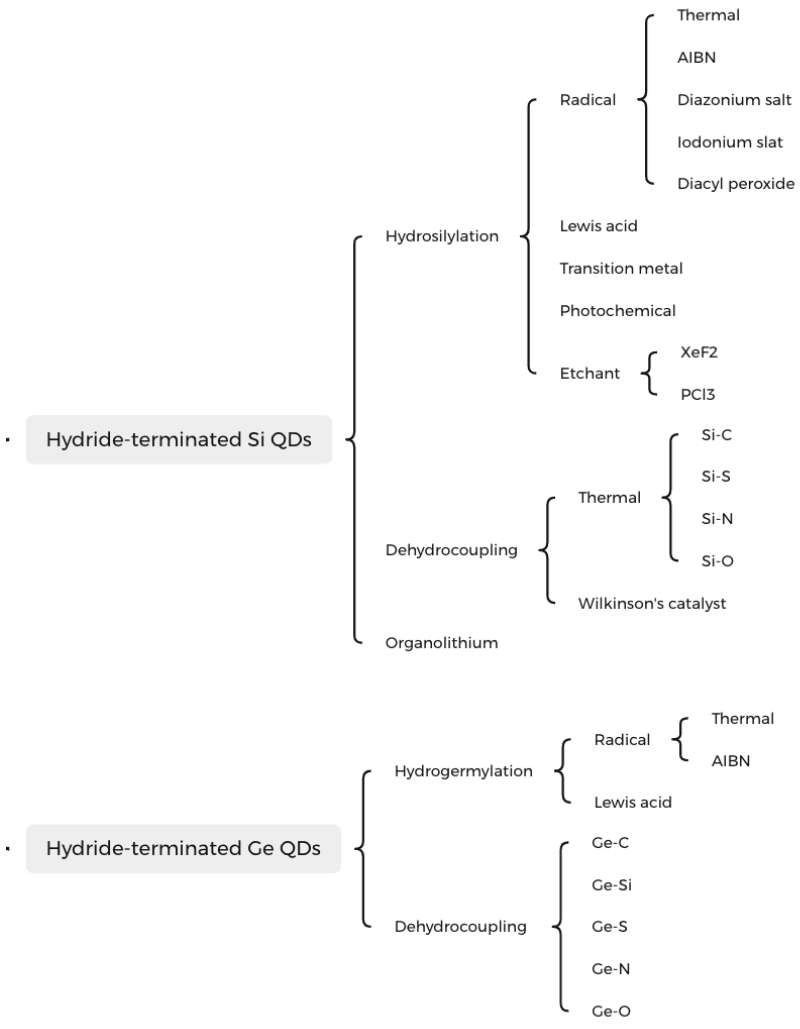

Figure 1-32. Summary of the synthetic pathway of hydride-terminated Si and Ge QDs.

Chapter 2 concentrated on the functionalization on Si QD surface with different self-synthesized dicarboxylic acid ligands, as the precursors for the dissipative reaction chemical cycle. A series of experiments conducted in this study discovered the combined effects of the two acids and SiNCs. Through analyzing the combined effects, dicarboxylic acids such as aspartic and succinic acid showcase assembly properties while SiNCs demonstrate the property of luminescence. On the condition of adding EDC to functionalized SiNCs, the type of SiNCs that aspartic acid terminated fails to show dissipative self-assembly, whereas the type of SiNCs that were terminated by succinic acid reacted partially as expected.

In Chapter 3, we present the thiolation on the hydride-terminated polygermane and Ge nanosheets to produce Ge–S bonding by simple heating of the reaction with thiols and disulfide. After the completion of the chemical reaction, the Ge–H bonds were consumed, and C–H and C–S vibration modes were observed in FTIR spectra. In the end, a series of characterizations were carried out to confirm the thiol-termination.

Finally, Chapter 4 shows a summary from Chapters 1 to 3 and describes the outlook to prepare other functionalization.

References

(1) Eberhard, W. G.; Wcislo, W. T. Plenty of Room at the Bottom? *Am. Sci.* **2012**, *100* (3), 226–233.

(2) Bayda, S.; Adeel, M.; Tuccinardi, T.; Cordani, M.; Rizzolio, F. The History of Nanoscience and Nanotechnology: From Chemical-Physical Applications to Nanomedicine. *Molecules* **2020**, *25* (1), 1–15.

(3) Wang, G. Nanotechnology: The new features. https://arxiv.org/abs/1812.04939 (accessed Aug 30, 2021).

(4) Ramsden, J. J. What Is Nanotechnology? *Nanotechnol. Perceptions* **2005**, *1* (1), 3–17.

(5) Toné, S.; Kubo, T.; Ohyama, T.; Kusakabe, T.; Minatogawa, Y. Quantitation of MRNA Using in Vitro RNA Amplification and Northern Hybridization. *Anal. Biochem.* **2000**, *284* (2), 420–422.

(6) Radical Nanotechnology. *Introduction to Nanoscience and Nanotechnology* **2010**, 263–280.

(7) Dolez, P. I. *Nanomaterials Definitions, Classifications, and Applications*; **2015**.

(8) Asha, A. B.; Narain, R. *Nanomaterials Properties*; Elsevier Inc., **2020**.

(9) Suresh, S. Semiconductor Nanomaterials, Methods and Applications: A Review. *Nanosci. Nanotechnol.* **2013**, *3* (3), 62–74.

(10) de Mello Donegá, C. Synthesis and Properties of Colloidal Heteronanocrystals. *Chem. Soc. Rev.* **2011**, *40* (3), 1512–1546.

(11) Rossetti, R.; Nakahara, S.; Brus, L. E. Quantum Size Effects in the Redox Potentials, Resonance Raman Spectra, and Electronic Spectra of CdS Crystallites in Aqueous Solution. *J. Chem. Phys.* **1983**, *79* (2), 1086–1088.

(12) Ekimov, A. I.; Efros, A. L.; Onushchenko, A. A. Quantum Size Effect in Semiconductor Microcrystals. *Solid State Commun.* **1985**, *56* (11), 921–924.

(13) Weller, H.; Koch, U.; Gutierrez, M.; Henglein, A. Photochemistry of Colloidal Metal Sulfides. Absorption and Fluorescence of Extremely Small ZnS Particles (The World of the Neglected Dimensions) H.. *Berichte der Bunsengesellschaft/Physical Chem. Chem. Phys.* **1984**, *88* (7), 649–656.

(14) Weller, H. Colloidal Semiconductor Q-Particles: Chemistry in the Transition Region Between Solid State and Molecules. *Angew. Chemie Int. Ed. English* **1993**, *32* (1), 41–53.

(15) Murray, C. B.; Norris, D. J.; Bawendi, M. G. Synthesis and Characterization of Nearly Monodisperse CdE (E = S, Se, Te) Semiconductor Nanocrystallites. *J. Am. Chem. Soc.* **1993**, *115* (19), 8706–8715.

(16) Katari, J. E. B.; Colvin, V. L.; Alivisatos, A. P. X-Ray Photoelectron Spectroscopy of CdSe Nanocrystals with Applications to Studies of the Nanocrystal Surface. *J. Phys. Chem.* **1994**, *98* (15), 4109–4117.

(17) Hines, M. A.; Guyot-Sionnest, P. Synthesis and Characterization of Strongly Luminescing ZnS-Capped CdSe Nanocrystals. *J. Phys. Chem.* **1996**, *100* (2), 468–471.

(18) Smith, A. M.; Nie, S. Semiconductor Nanocrystals: Structure, Properties, and Band Gap Engineering. *Acc. Chem. Res.* **2010**, *43* (2), 190–200.

(19) Hartman, T.; Sofer, Z. Beyond Graphene: Chemistry of Group 14 Graphene Analogues: Silicene, Germanene, and Stanene. *ACS Nano* **2019**, *13* (8), 8566–8576.

(20) Takagahara, T.; Takeda, K. Theory of the Quantum Confinement Effect on Excitons in Quantum Dots of Indirect-Gap Materials. *Phys. Rev. B* **1992**, *46* (23), 15578–15581.

(21) Mansur, H. S. Quantum Dots and Nanocomposites. *Wiley Interdiscip. Rev. Nanomedicine Nanobiotechnology* **2010**, *2* (2), 113–129.

(22) Algar, W. R.; Susumu, K.; Delehanty, J. B.; Medintz, I. L. Semiconductor Quantum Dots in Bioanalysis: Crossing the Valley of Death. *Anal. Chem.* **2011**, *83* (23), 8826–8837.

(23) Zhou, H. S.; Sasahara, H.; Honma, I.; Komiyama, H.; Haus, J. W. Coated Semiconductor Nanoparticles: The CdS/PbS System's Photoluminescence Properties. *Chem. Mater.* **1994**, *6* (9), 1534–1541.

(24) Honma, I.; Sano, T.; Komiyama, H. Surface-Enhanced Raman Scattering (SERS) for

Semiconductor Microcrystallites Observed in Ag-CdS Hybrid Particles. *J. Phys. Chem.* **1993**, *97* (25), 6692–6695.

(25) Kortan, A. R.; Hull, R.; Opila, R. L.; Bawendi, M. G.; Steigerwald, M. L.; Carroll, P. J.; Brus, L. E. Nucleation and Growth of CdSe on ZnS Quantum Crystallite Seeds, and Vice Versa, in Inverse Micelle Media. *J. Am. Chem. Soc.* **1990**, *112* (4), 1327–1332.

(26) Hanifi, D. A.; Bronstein, N. D.; Koscher, B. A.; Nett, Z.; Swabeck, J. K.; Takano, K.; Schwartzberg, A. M.; Maserati, L. Threshold Quantum Yield. *Science (80-.).* **2019**, *1202* (March), 1199–1202.

(27) Pan, Z.; Zhang, H.; Cheng, K.; Hou, Y.; Hua, J.; Zhong, X. Highly E Ffi Cient Inverted Type-I CdS / CdSe Core / Shell Structure. **2012**, No. 5, 3982–3991.

(28) Kim, S.; Fisher, B.; Bawendi, M. Type-II Quantum Dots : CdTe / CdSe (Core / Shell) and CdSe / ZnTe (Core / Shell) Heterostructures. **2003**, 11466–11467.

(29) Thuy, U. T. D.; Tu, L. A.; Loan, N. T.; Chi, T. T. K.; Liem, N. Q. Comparative Photoluminescence Properties of Type-I and Type-II CdTe/CdS Core/Shell Quantum Dots. *Opt. Mater. (Amst).* **2016**, *53*, 34–38.

(30) Dasog, M.; Kehrle, J.; Rieger, B.; Veinot, J. G. C. Silicon Nanocrystals and Silicon-Polymer Hybrids: Synthesis, Surface Engineering, and Applications. *Angew. Chemie - Int. Ed.* **2016**, *55* (7), 2322–2339.

(31) Zhong, Y.; Song, B.; Peng, F.; Wu, Y.; Wu, S.; Su, Y.; He, Y. In Situ Rapid Growth of Fluorescent Silicon Nanoparticles at Room Temperature and under Atmospheric Pressure. *Chem. Commun.* **2016**, *52* (92), 13444–13447.

(32) Park, J. H.; Gu, L.; Von Maltzahn, G.; Ruoslahti, E.; Bhatia, S. N.; Sailor, M. J. Biodegradable Luminescent Porous Silicon Nanoparticles for in Vivo Applications. *Nat. Mater.* **2009**, *8* (4), 331–336.

(33) Erogbogbo, F.; Yong, K.; Roy, I.; Xu, G.; Prasad, P. N.; Swihart, M. T. Biocompatible Luminescent Silicon. *ACS Nano* **2008**, *2* (5), 873–878.

(34) Bhattacharjee, S.; Rietjens, I. M. C. M.; Singh, M. P.; Atkins, T. M.; Purkait, T. K.; Xu, Z.; Regli, S.; Shukaliak, A.; Clark, R. J.; Mitchell, B. S.; Alink, G. M.; Marcelis, A. T. M.; Fink, M. J.; Veinot, J. G. C.; Kauzlarich, S. M.; Zuilhof, H. Cytotoxicity of Surface-Functionalized Silicon and Germanium Nanoparticles: The Dominant Role of Surface Charges. *Nanoscale* **2013**, *5* (11), 4870–4883.

(35) Exley, C. Silicon in Life:A Bioinorganic Solution to Bioorganic Essentiality1JD Birchall Memorial Lecture.1. *J. Inorg. Biochem.* **1998**, *69* (3), 139–144.

(36) Canham, L. T. Silicon Quantum Wire Array Fabrication by Electrochemical and Chemical Dissolution of Wafers. *Appl. Phys. Lett.* **1990**, *57* (10), 1046–1048.

(37) Behray, M.; Webster, C. A.; Pereira, S.; Ghosh, P.; Krishnamurthy, S.; Al-Jamal, W. T.; Chao, Y. Synthesis of Diagnostic Silicon Nanoparticles for Targeted Delivery of Thiourea to

Epidermal Growth Factor Receptor-Expressing Cancer Cells. *ACS Appl. Mater. Interfaces* **2016**, *8* (14), 8908–8917.

(38) Kang, Z.; Tsang, C. H. A.; Zhang, Z.; Zhang, M.; Wong, N. B.; Zapien, J. A.; Shan, Y.; Lee, S. T. A Polyoxometalate-Assisted Electrochemical Method for Silicon Nanostructures Preparation: From Quantum Dots to Nanowires. *J. Am. Chem. Soc.* **2007**, *129* (17), 5326–5327.

(39) Bley, R. A.; Kauzlarich, S. M. A Low-Temperature Solution Phase Route for the Synthesis of Silicon Nanoclusters. *J. Am. Chem. Soc.* **1996**, *118* (49), 12461–12462.

(40) Heinrich, J. L.; Curtis, C. L.; Credo, G. M.; Kavanagh, K. L.; Sailor, M. J. Luminescent Colloidal Silicon Suspensions from Porous Silicon. *Science (80-.).* **1992**, *255* (5040), 66–68.

(41) Anglin, E. J.; Cheng, L.; Freeman, W. R.; Sailor, M. J. Porous Silicon in Drug Delivery Devices and Materials. *Adv. Drug Deliv. Rev.* **2008**, *60* (11), 1266–1277.

(42) Heath, J. R. A Liquid-Solution-Phase Synthesis of Crystalline Silicon. *Science (80-.).* **1992**, *258* (5085), 1131–1133.

(43) Zou, J.; Baldwin, R. K.; Pettigrew, K. A.; Kauzlarich, S. M. Solution Synthesis of Ultrastable Luminescent Siloxane-Coated Silicon Nanoparticles. *Nano Lett.* **2004**, *4* (7), 1181–1186.

(44) Rosso-Vasic, M.; Spruijt, E.; Van Lagen, B.; De Cola, L.; Zuilhof, H. Alkyl-Functionalized Oxide-Free Silicon Nanoparticles: Synthesis and Optical Properties. *Small* **2008**, *4* (10), 1835–1841.

(45) Li, Q.; He, Y.; Chang, J.; Wang, L.; Chen, H.; Tan, Y. W.; Wang, H.; Shao, Z. Surface-Modified Silicon Nanoparticles with Ultrabright Photoluminescence and Single-Exponential Decay for Nanoscale Fluorescence Lifetime Imaging of Temperature. *J. Am. Chem. Soc.* **2013**, *135* (40), 14924–14927.

(46) Kanemitsu, Y.; Okamoto, S.; Otobe, M.; Oda, S. Photoluminescence Mechanism in Surface-Oxidized Silicon Nanocrystals. *Phys. Rev. B - Condens. Matter Mater. Phys.* **1997**, *55* (12), R7375–R7378.

(47) Mangolini, L.; Thimsen, E.; Kortshagen, U. HIGH-Yield Plasma Synthesis of Luminescent Silicon Quantum Dots. *2005 Proc. 4th ASME Conf. Integr. Nanosyst. Des. Synth. Appl.* **2005**, 73–74.

(48) Jurbergs, D.; Rogojina, E.; Mangolini, L.; Kortshagen, U. Silicon Nanocrystals with Ensemble Quantum Yields Exceeding 60%. *Appl. Phys. Lett.* **2006**, *88* (23), 1–3.

(49) Saitow, K. I. Silicon Nanoclusters Selectively Generated by Laser Ablation in Supercritical Fluid. *J. Phys. Chem. B* **2005**, *109* (9), 3731–3733.

(50) Hessel, C. M.; Henderson, E. J.; Veinot, J. G. C. Hydrogen Silsesquioxane: A Molecular Precursor for Nanocrystalline Si-SiO2 Composites and Freestanding Hydride-Surface-Terminated Silicon Nanoparticles. *Chem. Mater.* **2006**, *18* (26), 6139–6146.

(51) Holmberg, V. C.; Bogart, T. D.; Chockla, A. M.; Hessel, C. M.; Korgel, B. A. Optical Properties of Silicon and Germanium Nanowire Fabric. *J. Phys. Chem. C* **2012**, *116* (42), 22486–22491.

(52) Roberto, J.; Núñez, R. Photoluminescence and Patterning of Silicon Nanocrystals. **2012**, 236.

(53) Rodríguez Núñez, J. R.; Kelly, J. A.; Henderson, E. J.; Veinot, J. G. C. Wavelength-Controlled Etching of Silicon Nanocrystals. *Chem. Mater.* **2012**, *24* (2), 346–352.

(54) Dasog, M.; Bader, K.; Veinot, J. G. C. Influence of Halides on the Optical Properties of Silicon Quantum Dots. *Chem. Mater.* **2015**, *27* (4), 1153–1156.

(55) Mobarok, M. H.; Purkait, T. K.; Islam, M. A.; Miskolzie, M.; Veinot, J. G. C. Instantaneous Functionalization of Chemically Etched Silicon Nanocrystal Surfaces. *Angew. Chemie - Int. Ed.* **2017**, *56* (22), 6073–6077.

(56) Islam, M. A.; Mobarok, M. H.; Sinelnikov, R.; Purkait, T. K.; Veinot, J. G. C. Phosphorus Pentachloride Initiated Functionalization of Silicon Nanocrystals. *Langmuir* **2017**, *33* (35), 8766–8773.

(57) Yu, Y.; Fan, G.; Fermi, A.; Mazzaro, R.; Morandi, V.; Ceroni, P.; Smilgies, D. M.; Korgel, B. A. Size-Dependent Photoluminescence Efficiency of Silicon Nanocrystal Quantum Dots. *J. Phys. Chem. C* **2017**, *121* (41), 23240–23248.

(58) Clark, R. J.; Aghajamali, M.; Gonzalez, C. M.; Hadidi, L.; Islam, M. A.; Javadi, M.; Mobarok, M. H.; Purkait, T. K.; Robidillo, C. J. T.; Sinelnikov, R.; Thiessen, A. N.; Washington, J.; Yu, H.; Veinot, J. G. C. From Hydrogen Silsesquioxane to Functionalized Silicon Nanocrystals. *Chem. Mater.* **2017**, *29* (1), 80–89.

(59) Sugimoto, H.; Fujii, M.; Imakita, K. Synthesis of Boron and Phosphorus Codoped All-Inorganic Colloidal Silicon Nanocrystals from Hydrogen Silsesquioxane. *Nanoscale* **2014**, *6* (21), 12354–12359.

(60) Geim, A. K.; Novoselov, K. S. The Rise of Graphene PROGRESS. *Nat. Mater.* **2007**, *6* (3), 183–191.

(61) Geim, A. K. Graphene Prehistory. *Physica Scripta* **2012**, *T146*, 014003.

(62) Novoselov, K. S.; Geim, A. K.; Morozov, S. V.; Jiang, D.; Katsnelson, M. I.; Grigorieva, I. V.; Dubonos, S. V.; Firsov, A. A. Two-Dimensional Gas of Massless Dirac Fermions in Graphene. *Nature* **2005**, *438* (7065), 197–200.

(63) Liu, N.; Bo, G.; Liu, Y.; Xu, X.; Du, Y.; Dou, S. X. Recent Progress on Germanene and Functionalized Germanene: Preparation, Characterizations, Applications, and Challenges. *Small* **2019**, *15* (32), 1–11.

(64) Baringhaus, J.; Ruan, M.; Edler, F.; Tejeda, A.; Sicot, M.; Taleb-Ibrahimi, A.; Li, A. P.; Jiang, Z.; Conrad, E. H.; Berger, C.; Tegenkamp, C.; De Heer, W. A. Exceptional Ballistic Transport in Epitaxial Graphene Nanoribbons. *Nature* **2014**, *506* (7488), 349–354.

(65) Fowler, J. D.; Allen, M. J.; Tung, V. C.; Yang, Y.; Kaner, R. B.; Weiller, B. H. Practical Chemical Sensors from Chemically Derived Graphene. *ACS Nano* **2009**, *3* (2), 301–306.

(66) Eda, G.; Chhowalla, M. Chemically Derived Graphene Oxide: Towards Large-Area Thin-Film Electronics and Optoelectronics. *Adv. Mater.* **2010**, *22* (22), 2392–2415.

(67) Miao, X.; Tongay, S.; Petterson, M. K.; Berke, K.; Rinzler, A. G.; Appleton, B. R.; Hebard, A. F. High Efficiency Graphene Solar Cells by Chemical Doping. *Nano Lett.* **2012**, *12* (6), 2745–2750.

(68) Qu, L.; Liu, Y.; Baek, J. B.; Dai, L. Nitrogen-Doped Graphene as Efficient Metal-Free Electrocatalyst for Oxygen Reduction in Fuel Cells. *ACS Nano* **2010**, *4* (3), 1321–1326.

(69) Ohsuna, T.; Yaokawa, R.; Nakano, H. 2D Crystal Structure Determination of Bilayer Silicene and Germanene Using Transmission Electron Microscopy. *R&D Rev. Toyota CRDL* **2019**, *50* (1), 27–37.

(70) Vogt, P.; De Padova, P.; Quaresima, C.; Avila, J.; Frantzeskakis, E.; Asensio, M. C.; Resta, A.; Ealet, B.; Le Lay, G. Silicene: Compelling Experimental Evidence for Graphenelike Two-Dimensional Silicon. *Phys. Rev. Lett.* **2012**, *108* (15), 1–5.

(71) Fleurence, A.; Friedlein, R.; Ozaki, T.; Kawai, H.; Wang, Y.; Yamada-Takamura, Y. Experimental Evidence for Epitaxial Silicene on Diboride Thin Films. *Phys. Rev. Lett.* **2012**, *108* (24), 1–5.

(72) Meng, L.; Wang, Y.; Zhang, L.; Du, S.; Wu, R.; Li, L.; Zhang, Y.; Li, G.; Zhou, H.; Hofer, W. A.; Gao, H. J. Buckled Silicene Formation on Ir(111). *Nano Lett.* **2013**, *13* (2), 685–690.

(73) Enriquez, H.; Vizzini, S.; Kara, A.; Lalmi, B.; Oughaddou, H. Silicene Structures on Silver Surfaces. *Journal of Physics: Condensed Matter* **2012**, *24* (31), 314211.

(74) Dávila, M. E.; Xian, L.; Cahangirov, S.; Rubio, A.; Le Lay, G. Germanene: A Novel Two-Dimensional Germanium Allotrope Akin to Graphene And Silicene. *New Journal of Physics* **2014**, *16* (9), 095002.

(75) Kharadi, M. A.; Malik, G. F. A.; Khanday, F. A.; Shah, K. A.; Mittal, S.; Kaushik, B. K. Review—Silicene: From Material to Device Applications. *ECS J. Solid State Sci. Technol.* **2020**, *9* (11), 115031.

(76) Bianco, E.; Butler, S.; Jiang, S.; Restrepo, O. D.; Windl, W.; Goldberger, J. E. Stability and Exfoliation of Germanane: A Germanium Graphane Analogue. *ACS Nano* **2013**, *7* (5), 4414–4421.

(77) Butler, S. Z.; Hollen, S. M.; Cao, L.; Cui, Y.; Gupta, J. A.; Gutiérrez, H. R.; Heinz, T. F.; Hong, S. S.; Huang, J.; Ismach, A. F.; Johnston-Halperin, E.; Kuno, M.; Plashnitsa, V. V.; Robinson, R. D.; Ruoff, R. S.; Salahuddin, S.; Shan, J.; Shi, L.; Spencer, M. G.; Terrones, M.; Windl, W.; Goldberger, J. E. Progress, Challenges, and Opportunities in Two-Dimensional Materials beyond Graphene. *ACS Nano* **2013**, *7* (4), 2898–2926.

(78) Lew Yan Voon, L. C.; Sandberg, E.; Aga, R. S.; Farajian, A. A. Hydrogen Compounds of Group-IV Nanosheets. *Appl. Phys. Lett.* **2010**, *97* (16), 3–5.

(79) Houssa, M.; Dimoulas, A.; Molle, A. Silicene: A Review of Recent Experimental and Theoretical Investigations. *J. Phys. Condens. Matter* **2015**, *27* (25).

(80) Quhe, R.; Fei, R.; Liu, Q.; Zheng, J.; Li, H.; Xu, C.; Ni, Z.; Wang, Y.; Yu, D.; Gao, Z.; Lu, J.

Tunable and Sizable Band Gap in Silicene by Surface Adsorption. *Scientific Reports* **2012**, *2* (1).

(81) Ding, Y.; Wang, Y. Electronic Structures of Silicene Fluoride and Hydride. *Applied Physics Letters* **2012**, *100* (8), 083102.

(82) Kaloni, T. P.; Singh, N.; Schwingenschlögl, U. Prediction of a Quantum Anomalous Hall State in Co-Decorated Silicene. *Phys. Rev. B - Condens. Matter Mater. Phys.* **2014**, *89* (3), 1–5.

(83) Jiang, S.; Butler, S.; Bianco, E.; Restrepo, O. D.; Windl, W.; Goldberger, J. E. Improving the Stability and Optical Properties of Germanane via One-Step Covalent Methyl-Termination. *Nat. Commun.* **2014**, *5*, 1–6.

(84) Li, L.; Lu, S. Z.; Pan, J.; Qin, Z.; Wang, Y. Q.; Wang, Y.; Cao, G. Y.; Du, S.; Gao, H. J. Buckled Germanene Formation on Pt(111). *Adv. Mater.* **2014**, *26* (28), 4820–4824.

(85) Xu, Y.; Tang, P.; Zhang, S. C. Large-Gap Quantum Spin Hall States in Decorated Stanene Grown on a Substrate. *Phys. Rev. B - Condens. Matter Mater. Phys.* **2015**, *92* (8), 1–5.

(86) Liu, C. C.; Feng, W.; Yao, Y. Quantum Spin Hall Effect in Silicene and Two-Dimensional Germanium. *Phys. Rev. Lett.* **2011**, *107* (7), 1–4.

(87) Georgakilas, V.; Otyepka, M.; Bourlinos, A. B.; Chandra, V.; Kim, N.; Kemp, K. C.; Hobza, P.; Zboril, R.; Kim, K. S. Functionalization of Graphene: Covalent and Non-Covalent Approaches, Derivatives and Applications. *Chem. Rev.* **2012**, *112* (11), 6156–6214.

(88) Mortazavi, B.; Dianat, A.; Cuniberti, G.; Rabczuk, T. Application of Silicene, Germanene and Stanene for Na or Li Ion Storage: A Theoretical Investigation. *Electrochim. Acta* **2016**, *213*, 865–870.

(89) Zhu, F. F.; Chen, W. J.; Xu, Y.; Gao, C. L.; Guan, D. D.; Liu, C. H.; Qian, D.; Zhang, S. C.; Jia, J. F. Epitaxial Growth of Two-Dimensional Stanene. *Nat. Mater.* **2015**, *14* (10), 1020–1025.

(90) Fang, Y.; Huang, Z. Q.; Hsu, C. H.; Li, X.; Xu, Y.; Zhou, Y.; Wu, S.; Chuang, F. C.; Zhu, Z. Z. Quantum Spin Hall States in Stanene/Ge(111). *Sci. Rep.* **2015**, *5* (111), 1–8.

(91) Schäfer, H.; Eisenmann, B.; Müller, W. Zintl Phases: Transitions between Metallic and Ionic Bonding. *Angew. Chemie Int. Ed. English* **1973**, *12* (9), 694–712.

(92) Beekman, M.; Kauzlarich, S. M.; Doherty, L.; Nolas, G. S. Zintl Phases as Reactive Precursors for Synthesis of Novel Silicon and Germanium-Based Materials. *Materials (Basel).* **2019**, *12* (7).

(93) Kauzlarich, S. M. Zintl Compounds. *Encycl. Inorg. Bioinorg. Chem.* **2011**.

(94) Nesper, R. The Zintl-Klemm Concept - A Historical Survey. *Zeitschrift fur Anorg. und Allg. Chemie* **2014**, *640* (14), 2639–2648.

(95) Nesper, R. Structure and Chemical Bonding in Zintl-Phases Containing Lithium. *Prog. Solid State Chem.* **1990**, *20* (1), 1–45.

(96) Kurylyshyn, I. M.; Fässler, T. F.; Fischer, A.; Hauf, C.; Eickerling, G.; Presnitz, M.; Scherer, W. Probing the Zintl-Klemm Concept: A Combined Experimental and Theoretical Charge Density Study of the Zintl Phase CaSi. *Angew. Chemie - Int. Ed.* **2014**, *53* (11), 3029–3032.

(97) Qiu, J.; Fu, H.; Xu, Y.; Zhou, Q.; Meng, S.; Li, H.; Chen, L.; Wu, K. From Silicene to Half-Silicane by Hydrogenation. *ACS Nano* **2015**, *9* (11), 11192–11199.

(98) Wöhler, F. Ueber Verbindungen Des Siliciums Mit Sauerstoff Und Wasserstoff. J*ustus Liebigs Ann. Chem*. **1863**, *127* (3), 257–274.

(99) Kautsky, H. Über einige ungesättigte Siliciumverbindungen. *Z. Anorg. Allg. Chem.* **1921,** 117, 209-242.

(100) Weiss, A.; Beil, G.; Meyer, H. The Topochemical Reaction of CaSi2 to a Two-Dimensional Subsiliceous Acid Si6H3(OH)3 (= Kautskys' Siloxene). *Zeitschrift fur Naturforsch. - Sect. B J. Chem. Sci.* **1980**, *35* (1), 25–30.

(101) Fraser, S. Structure R. B. *Phys. Rev. B* **1993**, *48* (24), 872–877.

(102) Yamanaka, S.; Matsu-ura, H.; Ishikawa, M. New Deintercalation Reaction of Calcium from Calcium Disilicide. *Mater. Res. Bull.* **1996**, *31* (3), 307–316.

(103) Ali, M. A.; Tchalala, M. R. Chemical Synthesis of Silicon Nanosheets from Layered Calcium Disilicide. *J. Phys. Conf. Ser.* **2014**, *491* (1).

(104) Dean, J. A. *Lange's Hendbook of CHEMISTRY*; 1999.

(105) Nakano, H.; Nakano, M.; Nakanishi, K.; Tanaka, D.; Sugiyama, Y.; Ikuno, T.; Okamoto, H.; Ohta, T. Preparation of Alkyl-Modified Silicon Nanosheets by Hydrosilylation of Layered Polysilane (Si 6H 6). *J. Am. Chem. Soc.* **2012**, *134* (12), 5452–5455.

(106) Sugiyama, Y.; Okamoto, H.; Mitsuoka, T.; Morikawa, T.; Nakanishi, K.; Ohta, T.; Nakano, H. Synthesis and Optical Properties of Monolayer Organosilicon Nanosheets. *J. Am. Chem. Soc.* **2010**, *132* (17), 5946–5947.

(107) Okamoto, H.; Kumai, Y.; Sugiyama, Y.; Mitsuoka, T.; Nakanishi, K.; Ohta, T.; Nozaki, H.; Yamaguchi, S.; Shirai, S.; Nakano, H. Silicon Nanosheets and Their Self-Assembled Regular Stacking Structure. *J. Am. Chem. Soc.* **2010**, *132* (8), 2710–2718.

(108) Knapp, D.; Brunschwig, B. S.; Lewis, N. S. Chemical, Electronic, and Electrical Properties of Alkylated Ge(111) Surfaces. *J. Phys. Chem. C* **2010**, *114* (28), 12300–12307.

(109) Vogg, G. U.; Brandt, M. S.; Stutzmann, M.; Albrecht, M. From CaSi2 to Siloxene: Epitaxial Silicide and Sheet Polymer Films on Silicon. *J. Cryst. Growth* **1999**, *203* (4), 570–581.

(110) Vogg, G.; Brandt, M. S.; Stutzmann, M.; Genchev, I.; Bergmaier, A.; Go, L.; Dollinger, G. Epitaxial CaGe " Lms on Germanium. **2000**, *212*, 148–154.

(111) Vogg, G.; Miesner, C.; Brandt, M. S.; Stutzmann, M.; Abstreiter, G. Epitaxial Alloy Films of Zintl-Phase Ca(Si1-XGex)2. *J. Cryst. Growth* **2001**, *223* (4), 573–576.

(112) Vogg, G.; Meyer, L. J. P.; Miesner, C.; Brandt, M. S.; Stutzmann, M. Polygermanosilyne Calcium Hydroxide Intercalation Compounds Formed by Topotactic Transformation of Ca(Si1-XGex)2 Alloy Zintl Phases in Ambient Atmosphere. *Monatshefte fur Chemie* **2001**, *132* (10), 1125–1135.

(113) Vogg, G.; Meyer, A. J. P.; Miesner, C.; Brandt, M. S.; Stutzmann, M. Efficient Tunable

Luminescence of SiGe Alloy Sheet Polymers. *Appl. Phys. Lett.* **2001**, *78* (25), 3956–3958.

(114) Jiang, S.; Arguilla, M. Q.; Cultrara, N. D.; Goldberger, J. E. Improved Topotactic Reactions for Maximizing Organic Coverage of Methyl Germanane. *Chem. Mater.* **2016**, *28* (13), 4735–4740.

(115) Nakamura, D.; Nakano, H. Liquid-Phase Exfoliation of Germanane Based on Hansen Solubility Parameters. *Chem. Mater.* **2018**, *30* (15), 5333–5338.

(116) Jiang, S.; Krymowski, K.; Asel, T.; Arguilla, M. Q.; Cultrara, N. D.; Yanchenko, E.; Yang, X.; Brillson, L. J.; Windl, W.; Goldberger, J. E. Tailoring the Electronic Structure of Covalently Functionalized Germanane via the Interplay of Ligand Strain and Electronegativity. *Chem. Mater.* **2016**, *28* (21), 8071–8077.

(117) Hartman, T.; Šturala, J.; Luxa, J.; Sofer, Z. Chemistry of Germanene: Surface Modification of Germanane Using Alkyl Halides. *ACS Nano* **2020**, *14* (6), 7319–7327.

(118) Restrepo, O. D.; Krymowski, K. E.; Goldberger, J.; Windl, W. A First Principles Method to Simulate Electron Mobilities in 2D Materials. *New Journal of Physics* **2014**, *16* (10), 105009.

(119) Rosli, N. F.; Rohaizad, N.; Sturala, J.; Fisher, A. C.; Webster, R. D.; Pumera, M. Siloxene, Germanane, and Methylgermanane: Functionalized 2D Materials of Group 14 for Electrochemical Applications. *Adv. Funct. Mater.* **2020**, *30* (21), 1–11.

(120) Amamou, W.; Odenthal, P. M.; Bushong, E. J.; O'Hara, D. J.; Luo, Y. K.; Van Baren, J.; Pinchuk, I.; Wu, Y.; Ahmed, A. S.; Katoch, J.; Bockrath, M. W.; Tom, H. W. K.; Goldberger, J. E.; Kawakami, R. K. Large Area Epitaxial Germanane for Electronic Devices. *2D Mater.* **2015**, *2* (3).

(121) Liu, Z.; Wang, Z.; Sun, Q.; Dai, Y.; Huang, B. Methyl-Terminated Germanane GeCH 3 Synthesized by Solvothermal Method with Improved Photocatalytic Properties. *Appl. Surf. Sci.* **2019**, *467–468* (June 2018), 881–888.

(122) Yu, H.; Helbich, T.; Scherf, L. M.; Chen, J.; Cui, K.; Fässler, T. F.; Rieger, B.; Veinot, J. G. C. Radical-Initiated and Thermally Induced Hydrogermylation of Alkenes on the Surfaces of Germanium Nanosheets. *Chem. Mater.* **2018**, *30* (7), 2274–2280.

(123) Yu, H.; Thiessen, A. N.; Hossain, M. A.; Kloberg, M. J.; Rieger, B.; Veinot, J. G. C. Thermally-Induced Dehydrogenative Coupling of Organosilanes and H-Terminated Silicon Quantum Dots onto Germanane Surfaces. *Chem. Mater.* **2020**. *32* (11), 4536–4543

(124) Clark, T. J.; Lee, K.; Manners, I. Transition-Metal-Catalyzed Dehydrocoupling: A Convenient Route to Bonds between Main-Group Elements. *Chem. - A Eur. J.* **2006**, *12* (34), 8634–8648.

(125) Su, B.; Wu, Y.; Jiang, L. The Art of Aligning One-Dimensional (1D) Nanostructures. *Chem. Soc. Rev.* **2012**, *41* (23), 7832–7856.

(126) Tsuji, H.; Michl, J.; Tamao, K. Recent Experimental and Theoretical Aspects of the Conformational Dependence of UV Absorption of Short Chain Peralkylated Oligosilanes. *J. Organomet. Chem.* **2003**, *685* (1–2), 9–14.

(127) Schepers, T.; Michl, J. Optimized Ladder C and Ladder H Models for Sigma Conjugation: Chain

Segmentation in Polysilanes. *J. Phys. Org. Chem.* **2002**, *15* (8), 490–498.

(128) Miller, R. D.; Michl, J. Polysilane High Polymers. *Chem. Rev.* **1989**, *89* (6), 1359–1410.

(129) Fukazawa, A.; Tsuji, H.; Tamao, K. All-Anti-Octasilane: Conformation Control of Silicon Chains Using the Bicyclic Trisilane as a Building Block. *J. Am. Chem. Soc.* **2006**, *128* (21), 6800–6801.

(130) Tsuji, H.; Toshimitsu, A.; Tamao, K. Unique Reactivity of a Diphenyldisilane Unit Incorporated in a Bicyclic Ring System: Generation of a Disilanyllithium via the Silicon-Phenyl Bond Cleavage with Lithium. *Khimiya Geterotsiklicheskikh Soedin.* **2001**, *37* (11), 1500–1505.

(131) Tamao, K.; Tsuji, H.; Terada, M.; Asahara, M.; Yamaguchi, S.; Toshimitsu, A. Conformation Control of Oligosilanes Based on Configurationally Constrained Bicyclic Disilane Units. *Angew. Chemie - Int. Ed.* **2000**, *39* (18), 3287–3290.

(132) Tsuji, H.; Fukazawa, A.; Yamaguchi, S.; Toshimitsu, A.; Tamao, K. All-Anti-Pentasilane: Conformation Control of Oligosilanes Based on the Bis(Tetramethylene)-Tethered Trisilane Unit. *Organometallics* **2004**, *23* (14), 3375–3377.

(133) Sato, K.; Tsuji, H.; Hirakuri, K.; Fukata, N.; Yamauchi, Y. Controlled Chemical Etching for Silicon Nanocrystals with Wavelength-Tunable Photoluminescence. *Chem. Commun.* **2009**, No. 25, 3759–3761.

(134) West, R.; Miller, R. D. Organometallics 1985, 4, 1318-1319 Registry. **1985**, No. 266, 1318–1319.

(135) Kipping, F. S.; Sands, J. E. XCIV.—Organic derivatives of silicon. Part XXVI. Piperidine as an analytical reagent. **1921**, No. 848, 848–850.

(136) Kashimura, S.; Ishifune, M.; Yamashita, N.; Bu, H. B.; Takebayashi, M.; Kitajima, S.; Yoshiwara, D.; Kataoka, Y.; Nishida, R.; Kawasaki, S. I.; Murase, H.; Shono, T. Electroreductive Synthesis of Polysilanes, Polygermanes, and Related Polymers with Magnesium Electrodes. *J. Org. Chem.* **1999**, *64* (18), 6615–6621.

(137) Koe, J. Contemporary Polysilane Synthesis and Functionalisation. *Polym. Int.* **2009**, *58* (3), 255–260.

(138) Marro, E. A.; Klausen, R. S. Conjugated Polymers Inspired by Crystalline Silicon †. *Chem. Mater.* **2019**, *31* (7), 2202–2211.

(139) Amadoruge, M. L.; Weinert, C. S. Singly Bonded Catenated Germanes: Eighty Years of Progress. *Chem. Rev.* **2008**, *108* (10), 4253–4294.

(140) Mochida, K.; Chiba, H. Synthesis, Absorption Characteristics and Some Reactions of Polygermanes. *J. Organomet. Chem.* **1994**, *473* (1–2), 45–54.

(141) Shono, T.; Kashimura, S.; Murase, H. Electroreductive Synthesis of Polygermane and Germane-Silane Copolymer. *J. Chem. Soc. Chem. Commun.* **1992**, *19900* (12), 896–897.

(142) Aitken, C.; Harrod, J. F.; Malek, A.; Samuel, E. Oligomerization of Phenylgermanes by Catalytic Dehydrocoupling. *J. Organomet. Chem.* **1988**, *349* (3), 285–291.

(143) Choi, N.; Tanaka, M. Zirconocene-Catalyzed Dehydrogenative Coupling of Phenylgermane and Properties of the Resulting Partially Network Polyphenylgermanes. *J. Organomet. Chem.* **1998**, *564* (1–2), 81–84.

(144) Baumgartner, T.; Jäkle, F. *Main Group Strategies towards Functional Hybrid Materials*; 2017.

(145) Katz, S. M.; Reichl, J. A.; Berry, D. H. Catalytic Synthesis of Poly(Arylmethylgermanes) by Demethanative Coupling: A Mild Route to σ-Conjugated Polymers. *J. Am. Chem. Soc.* **1998**, *120* (38), 9844–9849.

(146) Reichl, J. A.; Popoff, C. M.; Gallagher, L. A.; Remsen, E. E.; Berry, D. H. Ruthenium-Catalyzed Demethanative Coupling of HGeMe3: A High Yield Route to Polygermanes. *J. Am. Chem. Soc.* **1996**, *118* (39), 9430–9431.

(147) Royen, P.; Rocktäschel, C. Zur Kenntnis Niedere Hydride Des Siliciums Und Germaniums. *ZAAC - J. Inorg. Gen. Chem.* **1966**, *346* (5–6), 279–289.

(148) Yu, H.; Ni, C.; Thiessen, A. N.; Li, Z.; Veinot, J. G. C. Synthesis, Properties, and Derivatization of Poly(Dihydrogermane): A Germanium-Based Polyethylene Analogue. *ACS Nano* **2021**. *15* (6), 9368–9378

(149) Palenzona, A.; Manfrinetti, P.; Fornasini, M. L. The Phase Diagram of the Ca-Ge System. *J. Alloys Compd.* **2002**, *345* (1–2), 144–147.

(150) Leon-Escamilla, E. A.; Corbett, J. D. Hydrogen Impurity Effects. A5Tt3 Intermetallic Compounds between A = Ca, Sr, Ba, Eu and Tt = Si, Ge, Sn with Cr5B3-like Structures That Are Stable Both as Binary and as Ternary Hydride and Fluoride Phases. *J. Solid State Chem.* **2001**, *159* (1), 149–162.

(151) Borchardt-Ott, W. Die Kristallstruktur. **1990**, *319* (1926), 21–26.

(152) Alloy, B.; Diagrams, P.; Okamoto, H.; Subramanian, P. R.; Kacprzak, L. Ca (Calcium) Binary Alloy Phase Diagrams. *Alloy Phase Diagrams* **2018**, *3*, 228–238.

(153) Djaballah, Y.; Pasturel, A.; Belgacem-Bouzida, A. Thermodynamic Assessment of the Calcium-Germanium System. *J. Alloys Compd.* **2010**, *497* (1–2), 74–79.

(154) Schafer, H. Work for the Modern Chemistry of Intermetallics. *Annu. Rev. Mater. Sci.* **1985**, *15*, 1–41.

(155) Arguilla, M. Q.; Cultrara, N. D.; Scudder, M. R.; Jiang, S.; Ross, R. D.; Goldberger, J. E. Optical Properties and Raman-Active Phonon Modes of Two-Dimensional Honeycomb Zintl Phases. *J. Mater. Chem. C* **2017**, *5* (43),

(156) Cultrara, N. D.; Wang, Y.; Arguilla, M. Q.; Scudder, M. R.; Jiang, S.; Windl, W.; Bobev, S.; Goldberger, J. E. Synthesis of 1T, 2H, and 6R Germanane Polytypes. *Chem. Mater.* **2018**, *30* (4), 1335–1343.

(157) Tobash, P. H.; Bobev, S. Synthesis, Structure and Electronic Structure of a New Polymorph of CaGe2. *J. Solid State Chem.* **2007**, *180* (5), 1575–1581.

(158) Ambrosi, A.; Pumera, M. Exfoliation of Layered Materials Using Electrochemistry. *Chem. Soc.*

Rev. **2018**, *47* (19), 7213–7224.

(159) Halim, U.; Zheng, C. R.; Chen, Y.; Lin, Z.; Jiang, S.; Cheng, R.; Huang, Y.; Duan, X. A Rational Design of Cosolvent Exfoliation of Layered Materials by Directly Probing Liquid-Solid Interaction. *Nat. Commun.* **2013**, *4*, 1–7.

(160) Wu, W.; Xu, J.; Tang, X.; Xie, P.; Liu, X.; Xu, J.; Zhou, H.; Zhang, D.; Fan, T. Two-Dimensional Nanosheets by Rapid and Efficient Microwave Exfoliation of Layered Materials. *Chem. Mater.* **2018**, *30* (17), 5932–5940.

(161) Cardon, M. The Devil and the Surfaces. *Physics (College. Park. Md).* **1945**, 1945–1945.

(162) Kovacs, G. T. A.; Maluf, N. I.; Petersen, K. E. Bulk Micromachining of Silicon. *Proc. IEEE* **1998**, *86* (8), 1536–1551.

(163) K.E. Jensen.; D. Pennachio.; D. Recht.; D.A. Weitz.; F. Spaepen, "Rapid growth of large, defect-free colloidal crystals", **2013**, Soft Matter 9: 320-328.

(164) Buriak, J. M. Organometallic Chemistry on Silicon and Germanium Surfaces. *Chem. Rev.* **2002**, *102* (5), 1271–1308.

(165) Loscutoff, P. W.; Bent, S. F. Reactivity of the Germanium Surface: Chemical Passivation and Functionalization. *Annu. Rev. Phys. Chem.* **2006**, *57*, 467–495.

(166) Maeda, Y. Visible Photoluminescence from Nanocrystallite Ge Embedded in a Glassy SiO2 Matrix: Evidence in Support of the Quantum-Confinement Mechanism. *Phys. Rev. B* **1995**, *51* (3), 1658–1670.

(167) Maeda, Y.; Tsukamoto, N.; Yazawa, Y.; Kanemitsu, Y.; Masumoto, Y. Visible Photoluminescence of Ge Microcrystals Embedded in SiO2 Glassy Matrices. *Appl. Phys. Lett.* **1991**, *59* (24), 3168–3170.

(168) Cho, S.; Man Kang, I.; Rok Kim, K.; Park, B.-G.; Harris, J. S. Silicon-Compatible High-Hole-Mobility Transistor with an Undoped Germanium Channel for Low-Power Application. *Applied Physics Letters* **2013**, *103* (22), 222102.

(169) Higashi, G. S.; Chabal, Y. J.; Trucks, G. W.; Raghavachari, K. Ideal Hydrogen Termination of the Si (111) Surface. *Appl. Phys. Lett.* **1990**, *56* (7), 656–658.

(170) Deegan, T.; Hughes, G. An X-Ray Photoelectron Spectroscopy Study of the HF Etching of Native Oxides on Ge(111) and Ge(100) Surfaces. *Appl. Surf. Sci.* **1998**, *123–124*, 66–70.

(171) He, J.; Patitsas, S. N.; Preston, K. F.; Wolkow, R. A.; Wayner, D. D. M. Covalent Bonding of Thiophenes to Si(111) by a Halogenation/Thienylation Route. *Chemical Physics Letters*. **1998**, pp 508–514.

(172) Okubo, T.; Tsuchiya, H.; Sadakata, M.; Yasuda, T.; Tanaka, K. Organic Functional Group Introduced to Si(1 1 1) via Silicon-Carbon Bond: A Liquid-Phase Approach. *Appl. Surf. Sci.* **2001**, *171* (3–4), 252–256.

(173) Bansal, A.; Li, X.; Lauermann, I.; Lewis, N. S.; Yi, S. I.; Weinberg, W. H. Alkylation of Si Surfaces Using a Two-Step Halogenation/Grignard Route. *J. Am. Chem. Soc.* **1996**, *118* (30),

7225–7226.

(174) Wong, K. T.; Kim, Y. G.; Soriaga, M. P.; Brunschwig, B. S.; Lewis, N. S. Synthesis and Characterization of Atomically Flat Methyl-Terminated Ge(111) Surfaces. *J. Am. Chem. Soc.* **2015**, *137* (28), 9006–9014.

(175) Warner, J. H.; Hoshino, A.; Yamamoto, K.; Tilley, R. D. Water-Soluble Photoluminescent Silicon Quantum Dots. *Angew. Chemie - Int. Ed.* **2005**, *44* (29), 4550–4554.

(176) Sieval, A. B.; Linke, R.; Zuilhof, H.; Sudhölter, E. J. R. High-Quality Alkyl Monolayers on Silicon Surfaces. *Adv. Mater.* **2000**, *12* (19), 1457–1460.

(177) Purkait, T. K.; Iqbal, M.; Wahl, M. H.; Gottschling, K.; Gonzalez, C. M.; Islam, M. A.; Veinot, J. G. C. Borane-Catalyzed Room-Temperature Hydrosilylation of Alkenes/Alkynes on Silicon Nanocrystal Surfaces. *J. Am. Chem. Soc.* **2014**, *136* (52), 17914–17917.

(178) Ciampi, S.; Harper, J. B.; Gooding, J. J. Wet Chemical Routes to the Assembly of Organic Monolayers on Silicon Surfaces via the Formation of Si-C Bonds: Surface Preparation, Passivation and Functionalization. *Chem. Soc. Rev.* **2010**, *39* (6), 2158–2183.

(179) Wang, D.; Buriak, J. M. Trapping Silicon Surface-Based Radicals. *Langmuir* **2006**, *22* (14), 6214–6221.

(180) Liu, F.; Luber, E. J.; Huck, L. A.; Olsen, B. C.; Buriak, J. M. Nanoscale Plasmonic Stamp Lithography on Silicon. *ACS Nano* **2015**, *9* (2), 2184–2193.

(181) Yang, L.; Lua, Y. Y.; Lee, M. V.; Linford, M. R. Chemomechanical Functionalization and Patterning of Silicon. *Acc. Chem. Res.* **2005**, *38* (12), 933–942.

(182) Shirahata, N.; Linford, M. R.; Furumi, S.; Pei, L.; Sakka, Y.; Gates, R. J.; Asplund, M. C. Laser-Derived One-Pot Synthesis of Silicon Nanocrystals Terminated with Organic Monolayers. *Chem. Commun.* **2009**, No. 31, 4684–4686.

(183) Linford, M. R.; Chidsey, C. E. D.; Fenter, P.; Eisenberger, P. M. Alkyl Monolayers on Silicon Prepared from 1-Alkenes and Hydrogen-Terminated Silicon. *J. Am. Chem. Soc.* **1995**, *117* (11), 3145–3155.

(184) Wagner, P.; Nock, S.; Spudich, J. A.; Volkmuth, W. D.; Chu, S.; Cicero, R. L.; Wade, C. P.; Linford, M. R.; Chidsey, C. E. D. Bioreactive Self-Assembled Monolayers on Hydrogen-Passivated Si(111) as a New Class of Atomically Flat Substrates for Biological Scanning Probe Microscopy. *J. Struct. Biol.* **1997**, *119* (2), 189–201.

(185) Boukherroub, R.; Petit, A.; Loupy, A.; Chazalviel, J. N.; Ozanam, F. Microwave-Assisted Chemical Functionalization of Hydrogen-Terminated Porous Silicon Surfaces. *J. Phys. Chem. B* **2003**, *107* (48), 13459–13462.

(186) Boukherroub, R.; Morin, S.; Bensebaa, F.; Wayner, D. D. M. New Synthetic Routes to Alkyl Monolayers on the Si(111) Surface. *Langmuir* **1999**, *15* (11), 3831–3835.

(187) Gerlich, D.; Cullen, G. W.; Amick, J. A. The Stabilization of Germanium Surfaces by Ethylation. *J. Electrochem. Soc.* **1962**, *109* (2), 133.

(188) Truong, K. D.; Rowntree, P. A. Formation of Self-Assembled Butanethiol Monolayers on Au Substrates: Spectroscopic Evidence for Highly Ordered Island Formation in Sub-Monolayer Films. *J. Phys. Chem.* **1996**, *100* (51), 19917–19926.

(189) Yu, H.; Webb, L. J.; Heath, J. R.; Lewis, N. S. Scanning Tunneling Spectroscopy of Methyl- and Ethyl-Terminated Si(111) Surfaces. *Appl. Phys. Lett.* **2006**, *88* (25), 2–4.

(190) Han, S. M.; Ashurst, W. R.; Carraro, C.; Maboudian, R. Formation of Alkanethiol Monolayer on Ge(111). *J. Am. Chem. Soc.* **2001**, *123* (10), 2422–2425.

(191) Choi, K.; Buriak, J. M. Hydrogermylation of Alkenes and Alkynes on Hydride-Terminated Ge(100) Surfaces. *Langmuir* **2000**, *16* (20), 7737–7741.

(192) Li, Y. H.; Wang, D.; Buriak, J. M. Molecular Layer Deposition of Thiol - Ene Multilayers on Semiconductor Surfaces. *Langmuir* **2010**, *26* (2), 1232–1238.

(193) Li, Y. H.; Buriak, J. M. Dehydrogenative Silane Coupling on Silicon Surfaces via Early Transition Metal Catalysis. *Inorg. Chem.* **2006**, *45* (3), 1096–1102.

(194) Chuah, L. S.; Hassan, Z.; Hassan, H. A. Visible-Light Emission Due to Quantum Size Effects in Porous Crystalline Silicon. *AIP Conf. Proc.* **2010**, *1250* (September), 385–388.

(195) Bodlaki, D.; Yamamoto, H.; Waldeck, D. H.; Borguet, E. Ambient Stability of Chemically Passivated Germanium Interfaces. *Surf. Sci.* **2003**, *543* (1–3), 63–74.

(196) Kluth, G. J.; Sung, M. M.; Maboudian, R. Thermal Behavior of Alkylsiloxane Self-Assembled Monolayers on the Oxidized Si(100) Surface. *Langmuir* **1997**, *13* (14), 3775–3780.

(197) Höhlein, I. M. D.; Angi, A.; Sinelnikov, R.; Veinot, J. G. C.; Rieger, B. Functionalization of Hydride-Terminated Photoluminescent Silicon Nanocrystals with Organolithium Reagents. *Chem. - A Eur. J.* **2015**, *21* (7), 2755–2758.

(198) Fok, E.; Shih, M.; Meldrum, A.; Veinot, J. G. C. Preparation of Alkyl-Surface Functionalized Germanium Quantum Dots via Thermally Initiated Hydrogermylation. *Chem. Commun.* **2004**, *4* (4), 386–387.

(199) Yu, Y.; Rowland, C. E.; Schaller, R. D.; Korgel, B. A. Synthesis and Ligand Exchange of Thiol-Capped Silicon Nanocrystals. *Langmuir* **2015**, *31* (24), 6886–6893.

(200) Holmberg, V. C.; Korgel, B. A. Corrosion Resistance of Thiol- and Alkene-Passivated Germanium Nanowires. *Chem. Mater.* **2010**, *22* (12), 3698–3703.

(201) Cheng, X.; Lowe, S. B.; Ciampi, S.; Magenau, A.; Gaus, K.; Reece, P. J.; Gooding, J. J. Versatile "Click Chemistry" Approach to Functionalizing Silicon Quantum Dots: Applications toward Fluorescent Cellular Imaging. *Langmuir* **2014**, *30* (18), 5209–5216.

(202) Veinot, J. G. C. Synthesis, Surface Functionalization, and Properties of Freestanding Silicon Nanocrystals. *Chem. Commun.* **2006**, No. 40, 4160–4168.

(203) Thiessen, A. N.; Zhang, L.; Oliynyk, A. O.; Yu, H.; O'Connor, K. M.; Meldrum, A.; Veinot, J. G. C. A Tale of Seemingly "Identical" Silicon Quantum Dot Families: Structural Insight into Silicon Quantum Dot Photoluminescence. *Chem. Mater.***2020**, *32* (16), 6838–6846

(204) Yang, Z.; Iqbal, M.; Dobbie, A. R.; Veinot, J. G. C. Surface-Induced Alkene Oligomerization: Does Thermal Hydrosilylation Really Lead to Monolayer Protected Silicon Nanocrystals? *J. Am. Chem. Soc.* **2013**, *135* (46), 17595–17601.

(205) Tilley, R. D.; Warner, J. H.; Yamamoto, K.; Matsui, I.; Fujimori, H. Micro-Emulsion Synthesis of Monodisperse Surface Stabilized Silicon Nanocrystals. *Chem. Commun.* **2005**, No. 14, 1833–1835.

(206) Höhlein, I. M. D.; Kehrle, J.; Helbich, T.; Yang, Z.; Veinot, J. G. C.; Rieger, B. Diazonium Salts as Grafting Agents and Efficient Radical-Hydrosilylation Initiators for Freestanding Photoluminescent Silicon Nanocrystals. *Chem. - A Eur. J.* **2014**, *20* (15), 4212–4216.

(207) Yu, Y.; Hessel, C. M.; Bogart, T. D.; Panthani, M. G.; Rasch, M. R.; Korgel, B. A. Room Temperature Hydrosilylation of Silicon Nanocrystals with Bifunctional Terminal Alkenes. *Langmuir* **2013**, *29* (5), 1533–1540.

(208) Yang, Z.; Gonzalez, C. M.; Purkait, T. K.; Iqbal, M.; Meldrum, A.; Veinot, J. G. C. Radical Initiated Hydrosilylation on Silicon Nanocrystal Surfaces: An Evaluation of Functional Group Tolerance and Mechanistic Study. *Langmuir* **2015**, *31* (38), 10540–10548.

(209) Dasog, M.; De Los Reyes, G. B.; Titova, L. V.; Hegmann, F. A.; Veinot, J. G. C. Size vs Surface: Tuning the Photoluminescence of Freestanding Silicon Nanocrystals Across the Visible Spectrum via Surface Groups. *ACS Nano* **2014**, *8* (9), 9636–9648.

(210) Dasog, M.; Yang, Z.; Regli, S.; Atkins, T. M.; Faramus, A.; Singh, M. P.; Muthuswamy, E.; Kauzlarich, S. M.; Tilley, R. D.; Veinot, J. G. C. Chemical Insight into the Origin of Red and Blue Photoluminescence Arising from Freestanding Silicon Nanocrystals. *ACS Nano* **2013**, *7* (3), 2676–2685.

(211) Dasog, M.; Veinot, J. G. C. Size Independent Blue Luminescence in Nitrogen Passivated Silicon Nanocrystals. *Phys. Status Solidi Appl. Mater. Sci.* **2012**, *209* (10), 1844–1846.

(212) Wilcoxon, J. P.; Provencio, P. P.; Samara, G. A. Synthesis and Optical Properties of Colloidal Germanium Nanocrystals. *Phys. Rev. B - Condens. Matter Mater. Phys.* **2001**, *64* (3), 1–9.

(213) Tanke, R. S.; Kauzlarich, S. M.; Patten, T. E.; Pettigrew, K. A.; Murphy, D. L.; Thompson, M. E.; Lee, H. W. H. Synthesis of Germanium Nanoclusters with Irreversibly Attached Functional Groups : Acetals , Alcohols , Esters , and Polymers. **2003**, No. 15, 1682–1689.

(214) Lambert, T. N.; Andrews, N. L.; Gerung, H.; Boyle, T. J.; Oliver, J. M.; Wilson, B. S.; Han, S. M. Water-Soluble Germanium (0) Nanocrystals : Cell Recognition and Near-Infrared Photothermal Conversion Properties. **2007**, *87131*, 691–699.

(215) Ruddy, D. A.; Erslev, P. T.; Habas, S. E.; Seabold, J. A.; Neale, N. R. Surface Chemistry Exchange of Alloyed Germanium Nanocrystals: A Pathway Toward Conductive Group IV Nanocrystal Films. **2013**. *4* (3), 416–421

(216) Near-, S. S.; Ruddy, D. A.; Johnson, J. C.; Smith, E. R.; Neale, N. R. Size and Bandgap Control in The. **2010**, *4* (12), 7459–7466.

(217) Iqbal, M.; Purkait, T. K.; Goss, G. G.; Bolton, J. R.; Gamal El-Din, M.; Veinot, J. G. C. Application of Engineered Si Nanoparticles in Light-Induced Advanced Oxidation Remediation of a Water-Borne Model Contaminant. *ACS Nano* **2016**, *10* (5), 5405–5412.

(218) Holmes, A. L.; Hütges, J.; Reckmann, A.; Muthuswamy, E.; Meerholz, K.; Kauzlarich, S. M. Probing Electronics as a Function of Size and Surface of Colloidal GERMANIUM NANOCRYSTALS. *The Journal of Physical Chemistry C* **2015**, *119* (10), 5671–5678.

(219) Wheeler, L. M.; Nichols, A. W.; Chernomordik, B. D.; Anderson, N. C.; Beard, M. C.; Neale, N. R. All-Inorganic Germanium Nanocrystal Films By Cationic LIGAND EXCHANGE. *Nano Letters* **2016**, *16* (3), 1949–1954.

(220) Carolan, D. Recent Advances in Germanium Nanocrystals: Synthesis, Optical Properties and Applications. *Prog. Mater. Sci.* **2017**, *90*, 128–158.

(221) Helbich, T.; Lyuleeva, A.; Ludwig, T.; Scherf, L. M.; Fässler, T. F.; Lugli, P.; Rieger, B. One-Step Synthesis of Photoluminescent Covalent Polymeric Nanocomposites from 2D Silicon Nanosheets. *Adv. Funct. Mater.* **2016**, *26* (37), 6711–6718.

(222) Helbich, T.; Lyuleeva, A.; Höhlein, I. M. D.; Marx, P.; Scherf, L. M.; Kehrle, J.; Fässler, T. F.; Lugli, P.; Rieger, B. Radical-Induced Hydrosilylation Reactions for the Functionalization of Two-Dimensional Hydride Terminated Silicon Nanosheets. *Chem. - A Eur. J.* **2016**, *22* (18), 6194–6198.

(223) Lyuleeva, A.; Holzmüller, P.; Helbich, T.; Stutzmann, M.; Brandt, M. S.; Becherer, M.; Lugli, P.; Rieger, B. Charge Transfer Doping in Functionalized Silicon Nanosheets/P3HT Hybrid Material for Applications in Electrolyte-Gated Field-Effect Transistors. *J. Mater. Chem. C* **2018**, *6* (27), 7343–7352.

(224) Lyuleeva, A.; Helbich, T.; Rieger, B.; Lugli, P. Polymer-Silicon Nanosheet Composites: Bridging the Way to Optoelectronic Applications. *J. Phys. D. Appl. Phys.* **2017**, *50* (13).

(225) Helbich, T.; Lyuleeva, A.; Marx, P.; Scherf, L. M.; Purkait, T. K.; Fässler, T. F.; Lugli, P.; Veinot, J. G. C.; Rieger, B. Lewis Acid Induced Functionalization of Photoluminescent 2D Silicon Nanosheets for the Fabrication of Functional Hybrid Films. *Adv. Funct. Mater.* **2017**, *27* (21).

(226) Okamoto, H.; Sugiyama, Y.; Nakanishi, K.; Ohta, T.; Mitsuoka, T.; Nakano, H. Surface Modification of Layered Polysilane with n -Alkylamines, α,ω-Diaminoalkanes, and ω-Aminocarboxylic Acids. *Chem. Mater.* **2015**, *27* (4), 1292–1298.

(227) Ohshita, J.; Yamamoto, K.; Tanaka, D.; Nakashima, M.; Kunugi, Y.; Ohashi, M.; Nakano, H. Preparation and Photocurrent Generation of Silicon Nanosheets with Aromatic Substituents on the Surface. *J. Phys. Chem. C* **2016**, *120* (20), 10991–10996.

(228) Ohashi, M.; Shirai, S.; Nakano, H. Direct Chemical Synthesis of Benzyl-Modified Silicane from Calcium Disilicide. *Chem. Mater.* **2019**, *31* (13), 4720–4725.

Chapter 2

Dissipative Self-assembly of Dicarboxylic Acid Functionalized SiNCs

2.1 Introduction

Self-assembly is a process in which building blocks in a disordered system spontaneously and autonomously form a stable and organized supermolecule, structure, or pattern.[1] These building blocks (i.e., amphiphiles, gelators, peptides, etc.)[2–4] can be held together by noncovalent interactions that lead to different properties or functions as assemblies. The design of the building blocks can determine the type of assembly and its properties.[5,6] Silicon nanocrystals (SiNCs) can have great potential for many applications due to their tunable photoluminescence, biocompatibility, and low toxicity.[7–10] These properties can be tuned through surface functionalization, which relies on the formation of covalent bonds. Unfortunately, there are some limitations for the properties of dynamic materials to adapt to environmental changes due to the static nature of the bonds. Thus, one can envision how their utility could be expanded greatly if they could be used as a building block in dissipative self-assembly.

In dissipative self-assembly, the assembly process is driven by a chemical reaction cycle, which can be sub-divided into two reactions, activation and deactivation.[4,11–14] For the activation reaction, precursors are converted into active products, with irreversible consumption of a high energy molecule (i.e., chemical fuel) or photon (i.e., light). The metastable products, in the limited lifetime, can self-assemble because it is more energy favorable. The second reaction, the deactivation is a spontaneous process, which converts the products back to the original precursors. This conversion back to the precursor leads to disassembly and the dissipative nature of the process (Figure 2-1).[15,16]

Dissipative self-assembly was reported first in 2015 and has grown into an intriguing field of research.[4,13,17] Maiti et al. reported the ATP-fueled dissipative self-assembly of amphiphiles into vesicular nanoreactors,[13] and Tena-Solsona et al.

described the carbodiimide-fueled dissipative self-assembly of dicarboxylate forming the colloid, which can deliver hydrophobic agents.[18] There are also examples of the dissipative assembly of nanocrystals. Klajn et al. functionalized the surface of Au/Ag NCs to self-assemble into a self-erasing ink in light-driven dissipative self-assembly.[19,20] Grötsch et al. activated carboxylate surface groups terminated 3 nm SiNCs with a transient N-hydroxysuccinimide (NHS) ester through the consumption of EDC.[21]

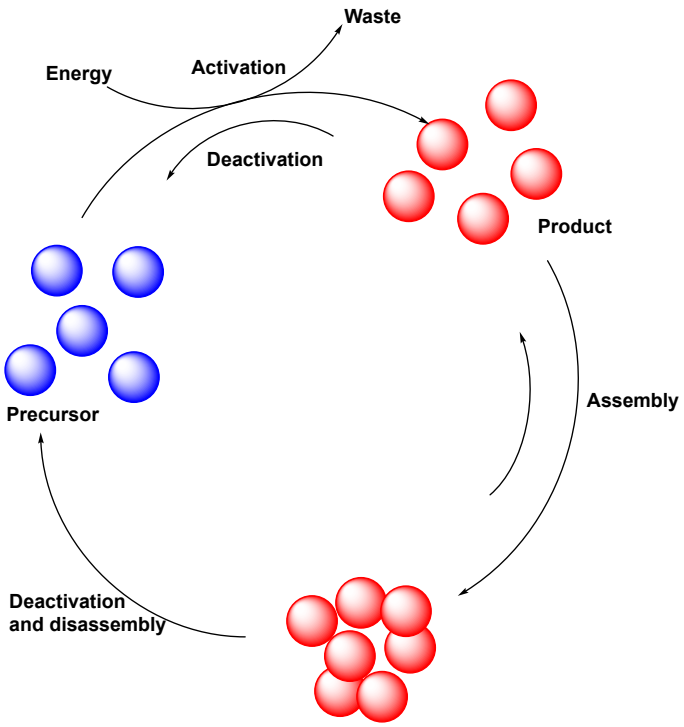

Figure 2-1. Dissipative self-assembly chemical reaction cycle: For the activation reaction, the precursors are inactive. With the addition of energy, the precursors convert into active products irreversibly. The deactivation is a spontaneous process, which converts the products back to precursors. The active products can self-assemble.[22]

While promising, the EDC fueled self-assembly of hexenoic acid functionalized SiNCs required the addition of excess NHS. The lifetime of NHS ester is extremely long, leading to a half-life of 3.88 h; this leads to long-lived assemblies that are present for up to 12 h. The study outlined in this chapter aims to develop a shorter lifetime chemical reaction cycle and converts a dicarboxylate SiNCs precursor into a transient anhydride without extra addition of NHS (Figure 2-2 a).

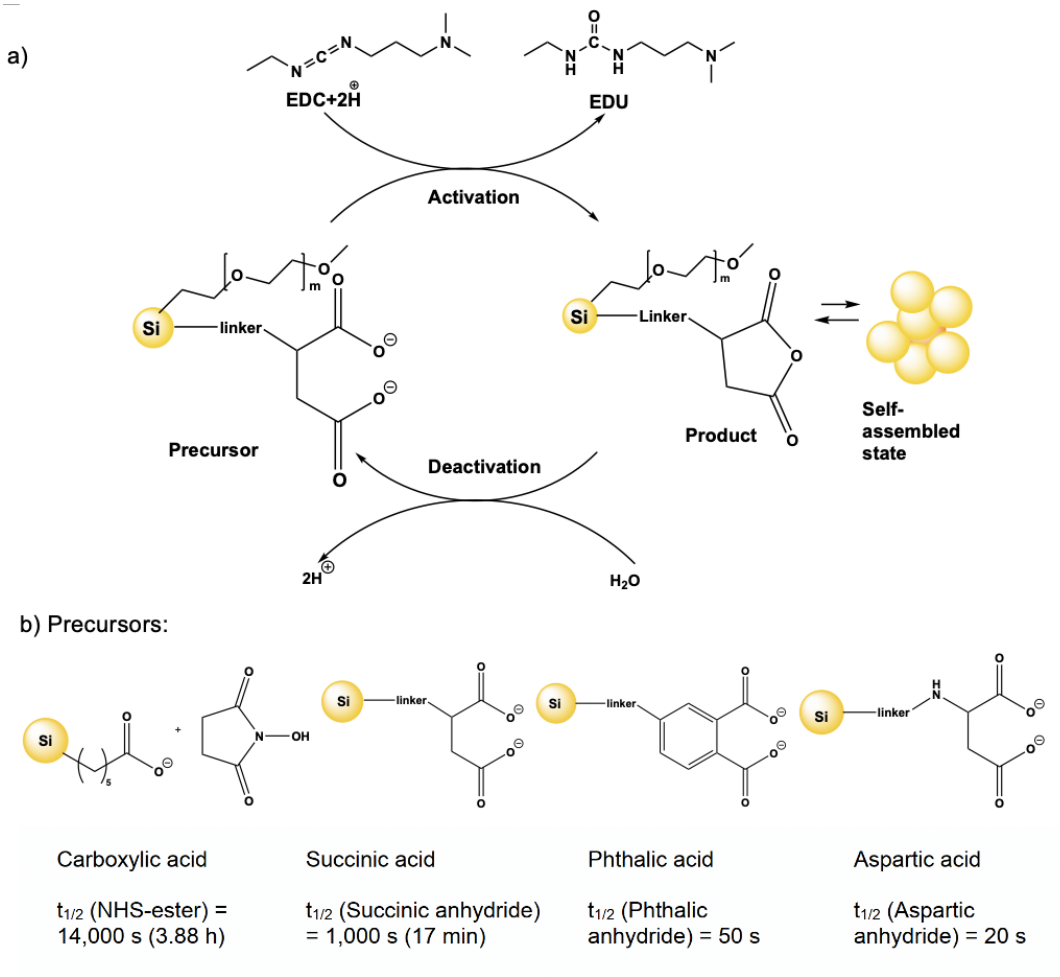

Figure 2-2. (a) Scheme of the chemical reaction cycle developed in this study. The dicarboxylate functionalized SiNCs are converted into the metastable (anhydride) product by consumption of the EDC. The detailed mechanism can be found in Figure 2-S2. (b) The molecular of dicarboxylate functionalized SiNCs precursors and their anhydride lifetimes, allyloxy poly(ethylene oxide)methyl ether was omitted for clarity.

2.2 Chemicals and Synthesis

2.2.1 Chemicals

Electronic-grade hydrofluoric acid ($HF_{(aq)}$, 48%) was purchased from Fisher Scientific and used directly. Reagent grade sulfuric acid (H_2SO_4, 95–98%) was purchased from Caledon Laboratory Chemicals. Allyloxy poly(ethylene oxide)methyl ether [PEG, 9–12 ethylene oxide units, molecular weight ≈ 450 g/mol, density = 1.076 g/mL] was purchased from Gelest Inc. Undecanoic acid [molecular weight = 184.28 g/mol, density = 0.912 g/mL, 98.0%], N-(3-dimethylaminopropyl)-N′-ethylcarbodiimide

hydrochloride [EDC, ≥98.0%], N-hydroxysulfosuccinimide [Sulfo-NHS, ≥98.0%], D-aspartic acid [99.0%], 2-oxopiperidine-4-carboxylic acid [molecular weight = 143.14 g/mol, density = 1.24 g/mL, 95.0%], fuming sulfuric acid (reagent grade, 20% free SO_3 bases) and trichlorosilane [molecular weight = 135.45 g/mol, density = 1.342 g/mL, 99%] were purchased from Sigma-Aldrich and used directly. Deionized (DI) water was obtained from a Milli-Q® Reference water purification system. Toluene was purified by a Pure-Solv purification system (Innovative Technologies, Inc.). Hexane and ethanol were purchased from EMD Millipore. All chemicals were used without further purification unless otherwise indicated. ^{1}H NMR was measured on a 400 MHz spectrometer at 25 °C in $CDCl_3$ or CD_3OD, as appropriate.

2.2.2 Synthesis of Hydrogen Silsesquioxane (HSQ)

HSQ, short for hydrogen silsesquioxane was synthesized, based on a well-established literature procedure,[23] by selective oxidization of trichlorosilane with sulfuric acid. Dry toluene (210.0 mL) in the top addition funnel was added to a mixture of concentrated (70.0 mL) and fuming (32.5 mL) sulfuric acid in an Ar-filled round bottom flask (Figure 2-S1). Subsequently, trichlorosilane (75 mL) in dry toluene (510 mL) was introduced to the addition funnel and was added dropwise (1 gtt/sec) to the solution in the round flask over a few hours. The final mixture was stirred for an extra 30 min, isolated, and washed with a 33% aqueous sulfuric acid solution (600 mL). The product in the organic solvent was dried over a mixture of magnesium sulfate (~5 g) neutralized with calcium carbonate (~5 g) for 12–16 h. After that, the toluene was removed by rotary evaporation, followed by in vacuo. The white solid product (yield: 28 g, 98%) was stored under vacuum until further use.

2.2.3 Synthesis of H-SiNCs

H-SiNCs were synthesized based on a well-established literature procedure published by the Veinot group.[24] Thermal processing of HSQ (5 g) was performed in a standard Lindberg blue tube furnace at 1100 °C under a flowing H_2 5%; Ar 95% atmosphere for 1 h. (Heating profile: the temperature was set from 25 to 1100 °C with a ramp rate of 18 °C/min; then the temperature was fixed at 1100 °C for 1 h and was decreased to 25 °C over a time frame of 12 h.)

The resulting dark amber SiNC/SiO_2 composite was transferred to an agate mortar with the addition of 100% ethanol to mechanically grind it, yielding a fine dark brown slurry. The slurry (d = 3 mm) was placed into a thick-walled flask with borosilicate glass beads and shaken for 8 h. The powder was suspended in 100% ethanol and collected via Millipore 0.54 μm PVDF hydrophilic membrane filter (vacuum filtration). H-SiNCs were prepared by chemical etching using a 1:1:1 solution of 100% ethanol: DI water: 49% HF.[24] A 1 g of composite requires 30 mL of etching solution in a typical procedure. The composite was immersed into the etching solution in a Teflon beaker, under stirring with a PTFE-coated stirring bar, for 50 min. The resulting cloudy, yellow mixture separated into two layers after extra toluene was added. The top layer was transferred into a test tube, which was centrifuged at 3000 rpm for 5–10 min to separate out the H-SiNCs. The clear, colorless supernatant was discarded, and the step was repeated two more times. The H-SiNCs used for the following reaction were redispersed into toluene, with the addition of active molecular sieves (4 Å beads, 4–8 mesh). The molecular sieves can remove residual moisture from H-SiNCs.

2.2.4 Synthesis of Water-soluble SiNCs

Water-soluble SiNCs were prepared following a literature procedure.[24] H-SiNCs prepared from etched SiNC/SiO_2 (600 mg) were dispersed with excess undecanoic acid (7.14 mmol, 1.5 mL) and allyloxy poly(ethylene oxide)methyl (10.76 mmol, 4.5 mL), and the suspension was transferred into an Ar charged Schlenk flask equipped with a magnetic stir bar. The mixture was exposed to three freeze-pump-thaw degassing cycles with an Ar charged Schlenk line. After the last thaw, the Schlenk flask was refilled with Ar and heated to 170 ℃ with stirring. The yellow, cloudy suspension became an orange, transparent solution in 1 h, and the reaction was kept heating for 3 h in total. Then, these SiNCs would be extracted by liquid-liquid extraction with hexanes/DI water two times, filtered through a hydrophilic dialysis membrane filter (12,000–14,000 Dalton), and isolated using (30,000 Dalton) centrifugal filter units (Millipore) by multiple centrifugations (5 × 3000 rpm, 15 min).[25] The final product was characterized by FTIR, TGA, and TEM.

2.2.5 Functionalized Water-soluble SiNCs with Aspartic Acid

EDC (10 mg, 0.064 mmol) and sulfo-NHS (10mg, 0.046 mmol) were dissolved in 20 mM HEPES buffer (895 μL, pH 7) to create a clear solution. Water dispersion of water-soluble SiNCs (100 μL) was added, rendering the solution orange to yellowish orange luminescent. The solution was stirred for 30 min at 25 °C, and then D-aspartic acid (0.075 mmol, 10 mg) was added, which weakened the luminescence slightly. Finally, the solution was stirred overnight at 25 °C, and the resulting yellow luminescent mixture was purified using (30,000 Dalton) centrifugal filter units (Millipore) by multiple centrifugations (5 × 3000 rpm, 15 min rounds). The resulting SiNCs were freeze-dried and stored in a freezer (–30 °C). The final product was characterized by FTIR, UV, TGA, and XPS.

2.2.6 Typical Procedure for Ring-opening in Acidic Condition of (RS)-2-oxopiperodome-4-carboxylic Acid

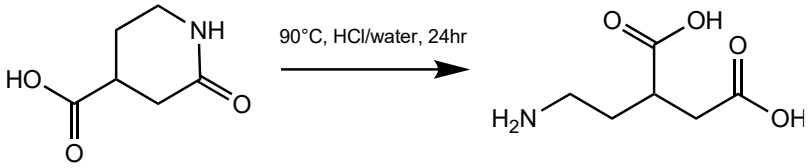

(RS)-2-[2-aminoethyl] butandioic acids were prepared following a literature procedure.[26] A 6 M aqueous hydrochloric acid (60 mmol, 10 mL) solution was added with (RS)-2-oxopiperodome-4-carboxylic acid (1 mmol, 0.14 g) into a small glass vial, and the mixture was stirred at 90 °C for 24 h. The compounds were completely dried under a high vacuum for 24 h.

(RS)-2-[2-Aminoethyl] butandioic acid, hydrochloride is a viscous, colorless oil. ^{1}H NMR (400 MHz, CD_3OD, T = 25 °C**)**: The peak at 2.71 ppm, 2.56 ppm, 1.99–2.08 ppm, 1.84–1.93 ppm, 2.97–3.09 ppm, and 2.83–2.91 ppm were attributed to -COOH- and -CH-, -CH_2-COO- and other -CH_2- on the chain, respectively.

2.2.7 Functionalized Water-soluble SiNCs with Derivatives of Succinic Acid

EDC (10 mg, 0.064 mmol) and sulfo-NHS (10 mg, 0.046 mmol) were dissolved in 20 mM HEPES buffer (895 µL, pH 7) to create a clear solution. Water dispersion of water-soluble SiNCs (100 µL) was added, rendering the solution orange to red luminescent. The solution was stirred for 30 min at 25 °C, and then synthesized (RS)-2-[2-aminoethyl] butandioic acid (10 mg, 0.069 mmol) was added. The aqueous workup procedure is the same as that in Section 2.2.4. The final product was characterized by FTIR, UV, TGA, and XPS.

2.2.8 Characterization and Analytical Methods

Titration of Dicarboxylic Acid Functionalized SiNCs

A small portion (10%) of the freeze-dried functionalized SiNCs (100 µL) were dispersed in DI water and sonicated for at least 3 h until the sample completely dissolved. The SiNCs (in DI water) were set pH at 10.5 by adding concentrated NaOH (1 M). The sample was titrated against HCl (0.1 M) to calculate the pK_a of the sample (Figure 2-S3).

Addition of EDC to Precursor Solution for the Self-assembly

The remaining SiNCs were dispersed in degassed MES Buffer (0.2 M, pH = 5–7.4) to prepare a 5 mM solution. To activate the cycle, EDC was added from a high-concentration stock solution, i.e., a 25–100 µM EDC fuel was added to a precursor solution according to the target concentrations of each sample.

Fourier-Transform Infrared Spectroscopy (FT-IR)

FTIR spectra were collected using a Thermo Nicolet Magna 750 IR Spectrometer (32 scans). FTIR samples were prepared by drop coating a DI water dispersion of the sample in question onto an electronic-grade Si-wafer and dried under air or nitrogen atmosphere.

Transmission Electron Microscopy (TEM)

Bright-field transmission electron microscopy (TEM) images were obtained using a JEOL JEM-ARM200CF S/TEM electron microscope operated at 200 keV. TEM samples were prepared by depositing a small droplet (~0.01 mL) of DI water suspension of the functionalized SiNCs onto a 200-mesh carbon-coated copper grid, which was purchased from Electron Microscopy Inc. Excess solvent was drawn off using standard filter paper. The grid on which the sample was mounted was maintained in a vacuum chamber for at least 24 h prior to image acquisition. The SiNC size was averaged for more than 100 particles using software ImageJ.

X-ray Photoelectron Spectroscopy (XPS)

XP spectra were obtained using a Kratos Axis Ultra instrument operating in energy spectrum mode. Samples were prepared by depositing a solution of functionalized SiNCs in DI water onto a copper foil substrate (thickness = 0.25 mm) and allowing it to dry. The operating chamber pressure was maintained at 10–7 Pa. A monochromatic Al Kα source (λ = 8.34 Å) at 210W irradiated the samples, and the spectra were collected with a bandpass energy of 20 eV, 0.1 eV step size, electron take-off angle of 90°. CasaXPS software (VAMAS) was used to interpret high-resolution spectra. All high-resolution spectra were calibrated to the C 1s emission (284.8 eV), and a Shirley-type background was applied to remove most of the extrinsic loss structure. The Si 2p emission (Si $2p_{1/2}$ to Si $2p_{3/2}$ peak area ratio) were fitted to a doublet at 0.5 with the same full-width-at-half-maximum for both components and 0.6 eV energy separation.

UV-visible Absorbance and Photoluminescence (PL)

UV/VIS-absorbance measurements were performed using a SpectraMax i3x multimode microplate reader. The DI water suspension of functionalized SiNCs was dropped in small droplets (~0.01 mL) onto a 96 well plate with a wavelength range of 200 nm to 800 nm. After the assay started, the samples in the plate were shaken before the measurement and between each measurement by the instrument. The absorbance was recorded every 2 min. Photoluminescence (PL) spectra also were recorded using a SpectraMax i3x multimode microplate reader. The PL samples were prepared in the

same way as in the UV measurements and were measured with an excitation wavelength of 365 nm with excitation and emission slits widths of 5.

Thermogravimetric Analysis (TGA)

Thermogravimetric analysis (TGA) data were obtained using a Mettler Toledo TGA/DSC 1 Star System under an Ar atmosphere (25–800 °C, 10 °C/min). Functionalized SiNC samples were freeze-dried into a solid residue and placed on a platinum pan. The surface coverage can be calculated based on TGA weight loss (Equation 2-S1).

Dynamic Light Scattering (DLS)

DLS was measured by a Malvern Zetasizer Nano ZS from Malvern with a laser wavelength of 633 nm. The functionalized SiNCs in DI water were measured using a disposable polystyrene cuvette. Each measurement consisted of six acquisitions (1 acquisition time = 20 s).

Confocal Fluorescence Microscopy

The confocal fluorescence microscopy image was collected on a Leica TCS SP8 confocal microscope using a 63x water immersion objective. Samples were placed on a microscope slide, covered with a coverslip (d = 12 mm), and 20 µL of the sample were taken before EDC, and after 5 min, 20 min, and 2 h. Samples were excited with laser (543 nm) and imaged (580–700 nm).

2.3 Results and Discussion

A wide variety of chemically fuel-driven, self-assembly reaction cycles have been reported (e.g., EDC-fueled NHS-ester formation).[18,21,27,28] Most of those cycles require very long periods (i.e., several hours or even days) to complete. In contrast, the EDC-fueled anhydride formation cycle using dicarboxylic acids as precursor proceeds comparatively quickly (i.e., several minutes or a few hours).[18,29]

In this work, we use water-soluble dicarboxylic acid-terminated SiNCs with a diameter of 3 nm as precursors in the chemical reaction cycle (Figure 2-2 b). The synthesis strategy used to achieve water solubility is shown in Figure 2-3. PEG and undecanoic acid-terminated SiNCs were synthesized first as the core. Subsequently,

the surface was modified with different acid groups (i.e., aspartic acid and succinic acid derivatives) via EDC coupling.

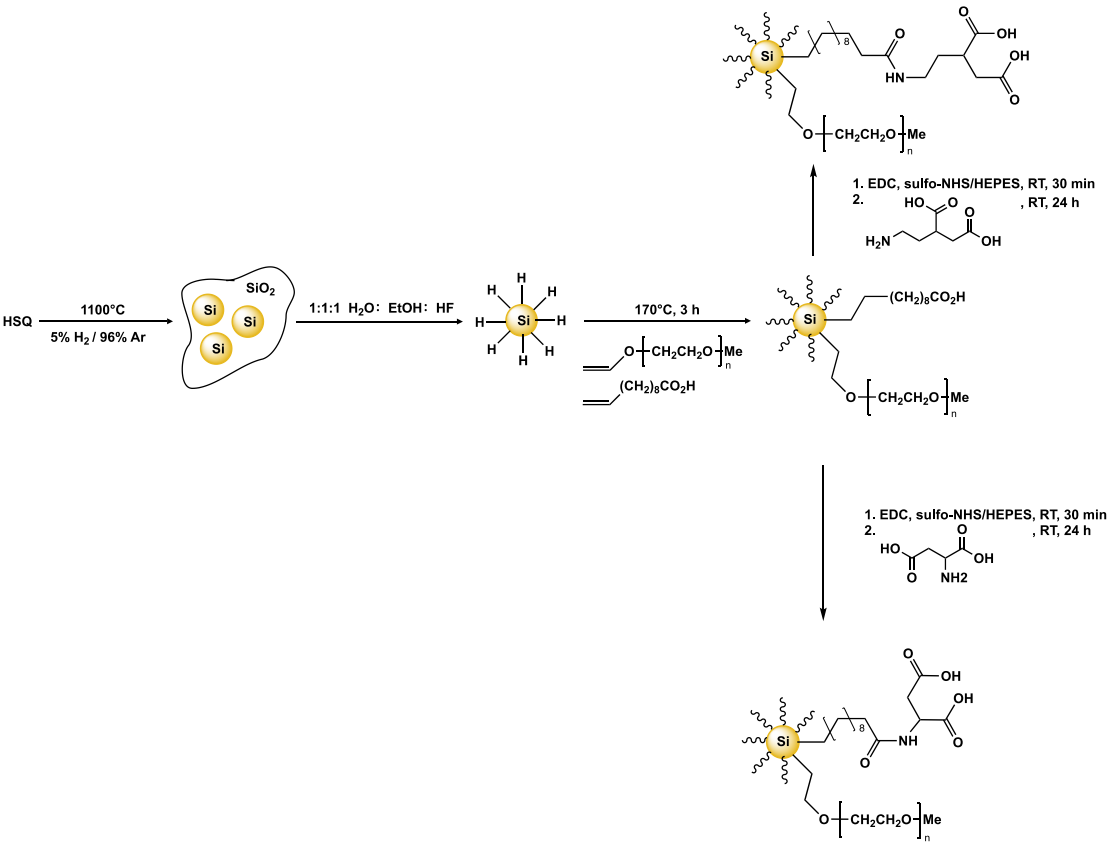

Figure 2-3. A schematic representation of the synthesis of aspartic acid-terminated SiNCs and derivatives of succinic acid-terminated SiNCs. More details can be found in Figures 2-S12, 2-S13, and 2-S14.

2.3.1 Characterizations of the Precursors—Dicarboxylic Acid-Terminated SiNCs

FTIR spectroscopy allows identification of the chemical functional groups present in a given material, while simultaneously offering a convenient approach to evaluating NCs surface modification. The successful surface functionalization of SiNCs with dicarboxylic acid was confirmed. Figure 2-4 shows the aliphatic sp^3 C–H stretching presence (~3000–2800 cm^{-1}), C–O/C–C stretches (~1100 cm^{-1}), and carboxylic acid hydroxyl feature (~3000 cm^{-1}).[25,30] We also note that Si-H_x features at approximately 2100 cm^{-1}, evident in the spectra of hydride-terminated SiNCs (Figure 2-S4), are not detected in the spectra of the functionalized systems. The additional features at ~1670 cm^{-1} and 1690 cm^{-1} (C=O stretching) and ca. 1540 cm^{-1} (amide N–H bending) are the presence of characteristic amide feature resulting from EDC coupling.[31,32]

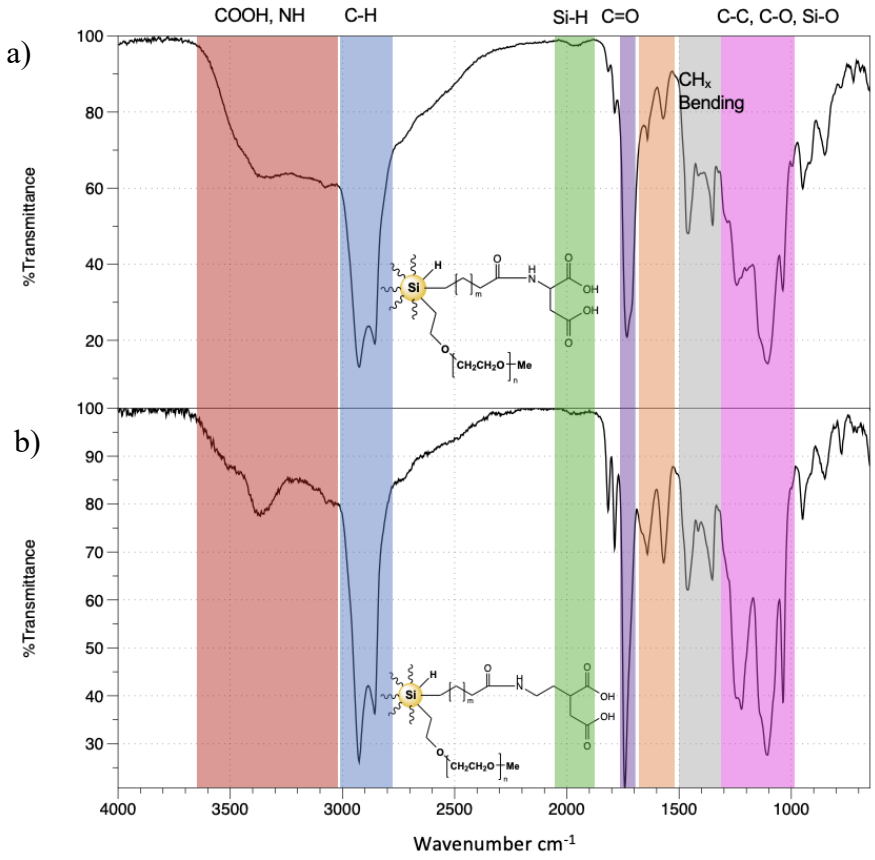

Figure 2-4. FTIR spectra of (a) aspartic acid-terminated SiNCs and (b) succinic acid-terminated SiNCs. Insets show corresponding illustrations of respective structures.

Figure 2-S6 displays the UV-visible absorption and PL measurement of aspartic acid functionalized SiNCs (asp-SiNCs, blue line) and derivatives of succinic acid functionalized SiNCs (suc-SiNCs, red line). Both asp-SiNCs and asp-SiNCs (Figure 2-S6 a) show strong absorptions at wavelengths from 270 nm to 400 nm, with a tail from 400 nm across the visible (creating the orange-yellow color, as shown in Figure 2-S6). They have PL maximum at ~656 nm (Figure 2-S6 b). This is consistent with other functionalized 3 nm SiNCs.[24]

Further exploration of the functionalized SiNCs was performed using XPS. The C 1s region of the XPS of asp-SiNCs and suc-SiNCs (Figure 2-5 a,b, respectively) show a strong peak at ~286.5 eV, which corresponds to C–N/C–O; a strong peak at ~284.9 eV, which attributed to C–C/C–H (aliphatic carbon); as well as a weak peak at ~288.3 eV, which corresponds to HCOOR/–CONH– (amide group).[33,34] What is more, expected emissions associated with conjugated amino acid can be detected at ~400.0 eV in the N 1s region (Figure 2-5 b,c).[35] Last but not least, the Si 2p XPS of asp-SiNCs and suc-SiNCs are shown in Figure 1-5 e,f, which were fitted to the Si $2p_{3/2}$ (higher BE) and $2p_{1/2}$ (lower BE) spin-orbit couple. The pink peaks attributed to silicon of oxidation state of 3 and the green peaks attributed to silicon dioxide with silicon of oxidation state of 4, which are the results of surface ligands and suboxides.[24]

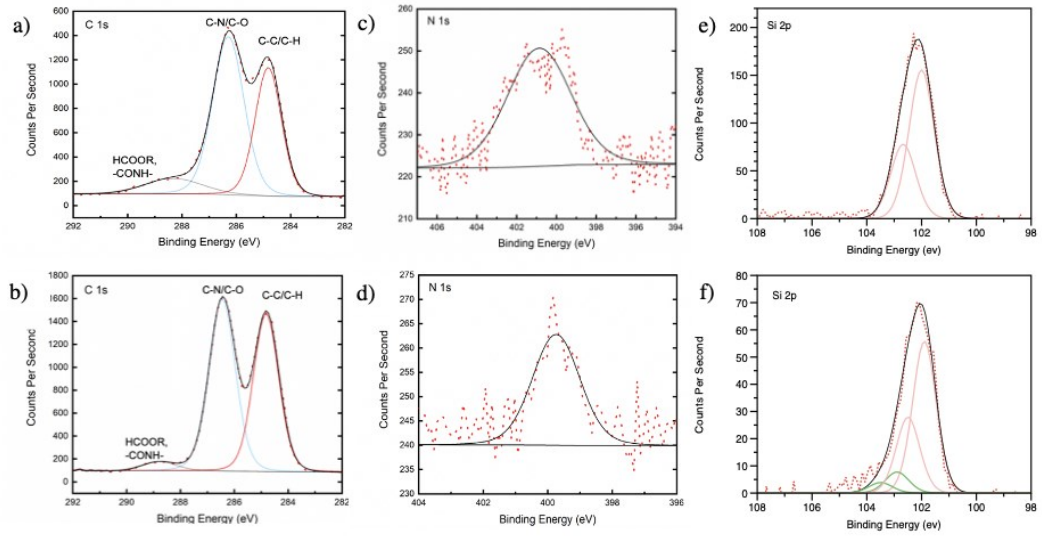

Figure 2-5. C 1s for a) asp-SiNCs, b) suc-SiNCs; N 1s for c) asp-SiNCs, d) suc-SiNCs; Si 2p for e) asp-SiNCs, f) suc-SiNCs.

Thermogravimetric analysis (TGA) of water-soluble SiNCs, asp-SiNCs, and suc-SiNCs were performed (Figure 2-6), showing a substantial weight loss consistent with loss of surface groups with heating.

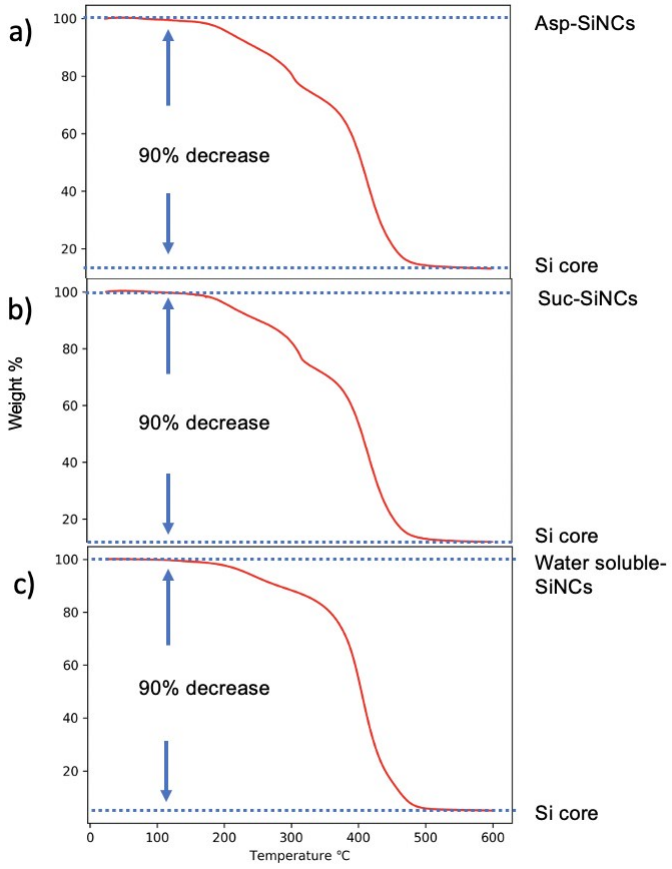

Figure 2-6. TGA data of (a) asp-SiNCs, (b) suc-SiNCs, and (c) water-soluble SiNCs.

2.3.2 Test on Fueled Transient Anhydride Formation

At this point, we can conclude that precursors, asp-SiNCs and suc-SiNCs, were synthesized successfully. In order to investigate their activation, asp-SiNCs were fueled with EDC; no apparent visibly obvious changes were noted after up to 24 h, and fluorescence microscopy showed a homogeneous fluorescent solution.

Since the asp-SiNCs cannot assemble, the suc-SiNCs were fueled with EDC. First and foremost, without any stirring, clusters were observed 10 min after 25 mM EDC addition, but there was no visible turbidity in the solution, and the clusters did not disassemble after 24 h. This can be explained by the physical crosslinking between the

surface ligands. Thus, in the following experiment, the same reaction condition was maintained but with stirring.

Without EDC addition, the fluorescence microscopy showed no assemblies (Figure 2-7 a). By contrast, 20 min after the addition of EDC, small fluorescent (green) clusters were observed, there is no fluorescent emission in the surrounding solution (Figure 2-7 c), and still, no turbidity can be observed. After 2 h, a homogeneous photoluminescent solution was observed.

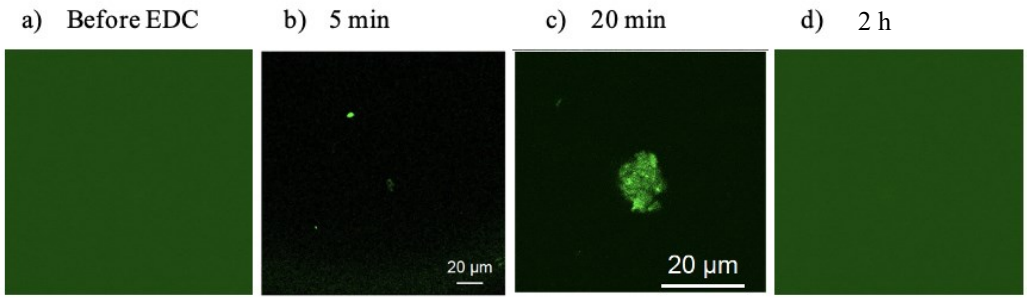

Figure 2-7. Confocal fluorescence microscopy images were collected before (a) and 5 min (b), 20 min (c) and 2 h (d) after adding EDC.

In order to determine the lifetime, a dynamic light scattering (DLS) measurement was required. From the DLS (Figure 2-S9), we note that the diameter decreased in the first 10 min (~90 nm to 10 nm) after EDC addition, then increased and stayed constant. Also, the count rate decreased minimally after EDC was added. Based on that, we cannot conclude that assembly did happen because the size should become bigger and the count rate should become very small if most of the clusters form. This might have happened because of the unfavorable buffer conditions, such as pH and concentration.

Thus, in the following experiment, both the pH and the concentration of MES buffer were changed. In a neutral solution (i.e., pH = 7.4, d = 4 nm), there were no assemblies and no turbidity. If we lowered the pH to 6–6.5, the diameter increased to 80–140 nm, and if we kept lowering the pH to 5.3, the average diameter increased to 400 nm (the real pH with the SiNCs should be 5.5); this might be aggregation due to the low pH value.

At a lower buffer concentration (25 mM and 50 mM), there was only a tiny number of assemblies, but if we used the buffer with a higher concentration (100 mM and 200 mM), more aggregation occurred; this happened probably because the ions in the buffer can interact with SiNCs. The higher buffer concentration also means a higher ion concentration, which can interact more with SiNCs. Thus, in order to test the newly found condition again, we tried different concentrations of SiNCs, shown in Figure 2-S10 and Figure 2-S11. With a higher concentration of SiNCs (10 mM), there was no change in diameter, no turbidity, and no NC formed clusters (Figure 2-S11). The situation of the lower concentration samples is very similar (Figure 2-S12).

Conclusion

In conclusion, we describe the new development of a fast dissipative reaction based on Grotsch's work. Asp-SiNCs and suc-SiNCs were synthesized successfully as precursors in a dissipative self-assembly chemical cycle, and a series of characterizations were carried out. Unfortunately, asp-SiNCs were not able to dissipative self-assemble upon the addition of EDC, and we still need to find a proper condition for suc-SiNCs.

References

(1) Grötsch, R. K.; Boekhoven, J. *Unique Properties of Supramolecular Biomaterials through Nonequilibrium Self-Assembly*; Elsevier Ltd., 2018.

(2) Mitchison, T. J.; Biol, J. C.; Kelleher, J. F.; Atkinson, S. J.; Pollard, T. D.; Biol, J. C.; Hartgerink, J. D.; Beniash, E.; Stupp, S. I. Self-Assembly and Mineralization of Peptide-Amphiphile Nanofibers. **2001**, *294* (November), 1684–1689.

(3) Israelachvili, J. N.; Mitchell, D. J.; Ninham, B. W. Theory of Self-Assembly of Hydrocarbon Amphiphiles into Micelles and Bilayers. *J. Chem. Soc. Faraday Trans. 2 Mol. Chem. Phys.* **1976**, *72*, 1525–1568.

(4) Van Rossum, S. A. P.; Tena-Solsona, M.; Van Esch, J. H.; Eelkema, R.; Boekhoven, J. Dissipative Out-of-Equilibrium Assembly of Man-Made Supramolecular Materials. *Chem. Soc. Rev.* **2017**, *46* (18), 5519–5535.

(5) Silva, G. A.; Czeisler, C.; Niece, K. L.; Beniash, E.; Harrington, D. A.; Kessler, J. A.; Stupp, S. I. Selective Differentiation of Neural Progenitor Cells by High-Epitope Density Nanofibers.

Science (80-.). **2004**, *303* (5662), 1352–1355.

(6) Zhang, S. Fabrication of Novel Biomaterials through Molecular Self-Assembly. *Nat. Biotechnol.* **2003**, *21* (10), 1171–1178.

(7) Erogbogbo, F.; Yong, K.; Roy, I.; Xu, G.; Prasad, P. N.; Swihart, M. T. Biocompatible Luminescent Silicon. *ACS Nano* **2008**, *2* (5), 873–878.

(8) Hessel, C. M.; Rasch, M. R.; Hueso, J. L.; Goodfellow, B. W.; Akhavan, V. A.; Puvanakrishnan, P.; Tunnel, J. W.; Korgel, B. A. Alkyl Passivation and Amphiphilic Polymer Coating of Silicon Nanocrystals for Diagnostic Imaging. *Small* **2010**, *6* (18), 2026–2034.

(9) Dasog, M.; Veinot, J. G. C. Size Independent Blue Luminescence in Nitrogen Passivated Silicon Nanocrystals. *Phys. Status Solidi Appl. Mater. Sci.* **2012**, *209* (10), 1844–1846.

(10) Cheng, X.; Lowe, S. B.; Ciampi, S.; Magenau, A.; Gaus, K.; Reece, P. J.; Gooding, J. J. Versatile "Click Chemistry" Approach to Functionalizing Silicon Quantum Dots: Applications toward Fluorescent Cellular Imaging. *Langmuir* **2014**, *30* (18), 5209–5216.

(11) Sorrenti, A.; Leira-Iglesias, J.; Markvoort, A. J.; De Greef, T. F. A.; Hermans, T. M. Non-Equilibrium Supramolecular Polymerization. *Chem. Soc. Rev.* **2017**, *46* (18), 5476–5490.

(12) Heinen, L.; Heuser, T.; Steinschulte, A.; Walther, A. Antagonistic Enzymes in a Biocatalytic Ph Feedback System Program Autonomous DNA Hydrogel Life Cycles. *Nano Lett.* **2017**, *17* (8), 4989–4995.

(13) della Sala, F.; Neri, S.; Maiti, S.; Chen, J. L. Y.; Prins, L. J. Transient Self-Assembly of Molecular Nanostructures Driven by Chemical Fuels. *Curr. Opin. Biotechnol.* **2017**, *46*, 27–33.

(14) Merindol, R.; Walther, A. Materials Learning from Life: Concepts for Active, Adaptive and Autonomous Molecular Systems. *Chem. Soc. Rev.* **2017**, *46* (18), 5588–5619.

(15) Whitesides, G. M.; Boncheva, M. Beyond Molecules: Self-Assembly of Mesoscopic and Macroscopic Components. *Proc. Natl. Acad. Sci. U. S. A.* **2002**, *99* (8), 4769–4774.

(16) Patist, A.; Oh, S. G.; Leung, R.; Shah, D. O. Kinetics of Micellization: Its Significance to Technological Processes. *Colloids Surfaces A Physicochem. Eng. Asp.* **2001**, *176* (1), 3–16.

(17) Van Ravensteijn, B. G. P.; Hendriksen, W. E.; Eelkema, R.; Van Esch, J. H.; Kegel, W. K. Fuel-Mediated Transient Clustering of Colloidal Building Blocks. *J. Am. Chem. Soc.* **2017**, *139* (29), 9763–9766.

(18) Tena-Solsona, M.; Rieß, B.; Grötsch, R. K.; Löhrer, F. C.; Wanzke, C.; Käsdorf, B.; Bausch, A. R.; Müller-Buschbaum, P.; Lieleg, O.; Boekhoven, J. Non-Equilibrium Dissipative Supramolecular Materials with a Tunable Lifetime. *Nat. Commun.* **2017**, *8* (May), 1–8.

(19) Kundu, P. K.; Das, S.; Ahrens, J.; Klajn, R. Controlling the Lifetimes of Dynamic Nanoparticle Aggregates by Spiropyran Functionalization. *Nanoscale* **2016**, *8* (46), 19280–19286.

(20) Klajn, R.; Wesson, P. J.; Bishop, K. J. M.; Grzybowski, B. A. Writing Self-Erasing Images Using Metastable Nanoparticle "Inks." *Angew. Chemie - Int. Ed.* **2009**, *48* (38), 7035–7039.

(21) Grötsch, R. K.; Angı, A.; Mideksa, Y. G.; Wanzke, C.; Tena-Solsona, M.; Feige, M. J.; Rieger, B.; Boekhoven, J. Dissipative Self-Assembly of Photoluminescent Silicon Nanocrystals. *Angew. Chemie - Int. Ed.* **2018**, *57* (44), 14608–14612.

(22) Rieß, B.; Grötsch, R. K.; Boekhoven, J. The Design of Dissipative Molecular Assemblies Driven by Chemical Reaction Cycles. *Chem* **2020**, *6* (3), 552–578.

(23) Thiessen, A. N.; Zhang, L.; Oliynyk, A. O.; Yu, H.; O'Connor, K. M.; Meldrum, A.; Veinot, J. G. C. A Tale of Seemingly "Identical" Silicon Quantum Dot Families: Structural Insight into Silicon Quantum Dot Photoluminescence. *ChemRxiv* **2020**, No. 2.

(24) Robidillo, C. J. T.; Islam, M. A.; Aghajamali, M.; Faramus, A.; Sinelnikov, R.; Zhang, X.; Boekhoven, J.; Veinot, J. G. C. Functional Bioinorganic Hybrids from Enzymes and Luminescent Silicon-Based Nanoparticles. *Langmuir* **2018**, *34* (22), 6556–6569.

(25) Clark, R. J.; Dang, M. K. M.; Veinot, J. G. C. Exploration of Organic Acid Chain Length on Water-Soluble Silicon Quantum Dot Surfaces. *Langmuir* **2010**, *26* (19), 15657–15664.

(26) Zacharie, B.; Abbott, S. D.; Baigent, C. B.; Doyle, C.; Yalagala, R. S. An Efficient Two-Step Preparation of α-, β-, γ- or δ-Amino Acids from 2-Pyrazinones, 2-Hydroxypyrimidines or 2-Pyridones Respectively. *European J. Org. Chem.* **2018**, *2018* (46), 6486–6493.

(27) Kariyawasam, L. S.; Hartley, C. S. Dissipative Assembly of Aqueous Carboxylic Acid Anhydrides Fueled by Carbodiimides. *J. Am. Chem. Soc.* **2017**, *139* (34), 11949–11955.

(28) Boekhoven, J.; Brizard, A. M.; Kowlgi, K. N. K.; Koper, G. J. M.; Eelkema, R.; Van Esch, J. H. Dissipative Self-Assembly of a Molecular Gelator by Using a Chemical Fuel. *Angew. Chemie - Int. Ed.* **2010**, *49* (28), 4825–4828.

(29) Grötsch, R. K.; Wanzke, C.; Speckbacher, M.; Angl, A.; Rieger, B.; Boekhoven, J. Pathway Dependence in the Fuel-Driven Dissipative Self-Assembly of Nanoparticles. *J. Am. Chem. Soc.* **2019**. *141* (25), 9872–9878

(30) Hessel, C. M.; Henderson, E. J.; Veinot, J. G. C. Hydrogen Silsesquioxane: A Molecular Precursor for Nanocrystalline Si-SiO2 Composites and Freestanding Hydride-Surface-Terminated Silicon Nanoparticles. *Chem. Mater.* **2006**, *18* (26), 6139–6146.

(31) Tamm, L. K.; Tatulian, S. A. Infrared Spectroscopy of Proteins and Peptides in Lipid Bilayers. *Q. Rev. Biophys.* **1997**, *30* (4), 365–429.

(32) Jedlovszky-Hajdú, A.; Bombelli, F. B.; Monopoli, M. P.; Tombácz, E.; Dawson, K. A. Surface Coatings Shape the Protein Corona of SPIONs with Relevance to Their Application in Vivo. *Langmuir* **2012**, *28* (42), 14983–14991.

(33) Damodaran, V. B.; Fee, C. J.; Ruckh, T.; Popat, K. C. Conformational Studies of Covalently Grafted Poly(Ethylene Glycol) on Modified Solid Matrices Using X-Ray Photoelectron Spectroscopy. *Langmuir* **2010**, *26* (10), 7299–7306.

(34) Briggs, D.; Beamson, G. Primary and Secondary Oxygen-Induced C1s Binding Energy Shifts in X-Ray Photoelectron Spectroscopy of Polymers. *Anal. Chem.* **1992**, *64* (15), 1729–1736.

(35) Buhl, M.; Vonhören, B.; Ravoo, B. J. Immobilization of Enzymes via Microcontact Printing and Thiol-Ene Click Chemistry. *Bioconjug. Chem.* **2015**, *26* (6), 1017–1020.

Chapter 3

Thermally-Induced Dehydrocoupling of Thiol and Disulfide on the Surfaces of Polygermanes and Germanium Nanosheets

3.1 Introduction

Germanium nanomaterials, including quantum dots,[1–3] nanowires,[4] germanene,[5,6] and germanane (GeNSs)[7,8] are attractive platforms for a variety of far-reaching potential applications. Like other nanomaterials, many of their attractive properties (e.g., stability, reactivity, and processability) depend strongly on surface chemistry. Therefore, a variety of modification strategies, such as hydrogermylation[9–11]and dehydrocoupling,[12–14] have been explored. Of late, liberating structural motifs from solid-state compounds (e.g., Zintl phases) has emerged as an attractive approach to preparing various nanosystems;[15–17] this general methodology has provided access to two-dimensional germanium nanosheets (i.e., GeNSs)[18,19] and oligo/polygermanes (PGs).[13,20]

While GeNSs and PGs resemble other Ge nanosystems, their dimensions approach the atomic scale. $CaGe_2$-derived germanane is one atom thick and routinely denoted as '$(Ge_6H_6)_n$', where "*n*" is very large. Often, its structure is viewed as interconnected Ge_6 rings in 'chair' conformations, and its atomic arrangement is the same as that of the top surface of H-terminated Ge (111). CaGe-derived PG consists of fully hydrogenated, catenated Ge atoms, represented by an empirical formula $(GeH_2)_n$, where '*n*' is very large. In both cases, the established reactivity of the Ge–H functional groups makes derivatization/functionalization crucial to protecting the underlying Ge nanoarchitecture from deleterious effects of oxidation, imparting solution processability as well as tailoring chemical, optical, and electronic responses.

To date, approaches toward modifying GeNSs have included hydrogermylation,[12,13,21] heteronuclear dehydrocoupling,[22] and reactions with haloalkanes.[23] Reactions of PGs are studied far less and are limited to

hydrogermylation.[13] With some limited exceptions, most of these involve tethering functionalities via covalent Ge–C bonds. Exploring linkages involving other heteroatoms (e.g., sulfur) is expected to broaden the scope of reactivity of these intriguing systems and offer the possibility of tuning material electronic structure. Reactions with sulfur-containing species (e.g., thiols, disulfides) have provided protection of bulk Ge surfaces from oxidation,[24,25] rendered Ge nanoparticles solution compatible, and offer ligand exchange reactions,[26] as well as imparting corrosion resistance to Ge nanowires.[27,28] This demonstrated the versatility of the thiolation reaction drew our attention and motivated us to investigate thiol modification of GeNSs and PGs, as described herein (Scheme 3-1).

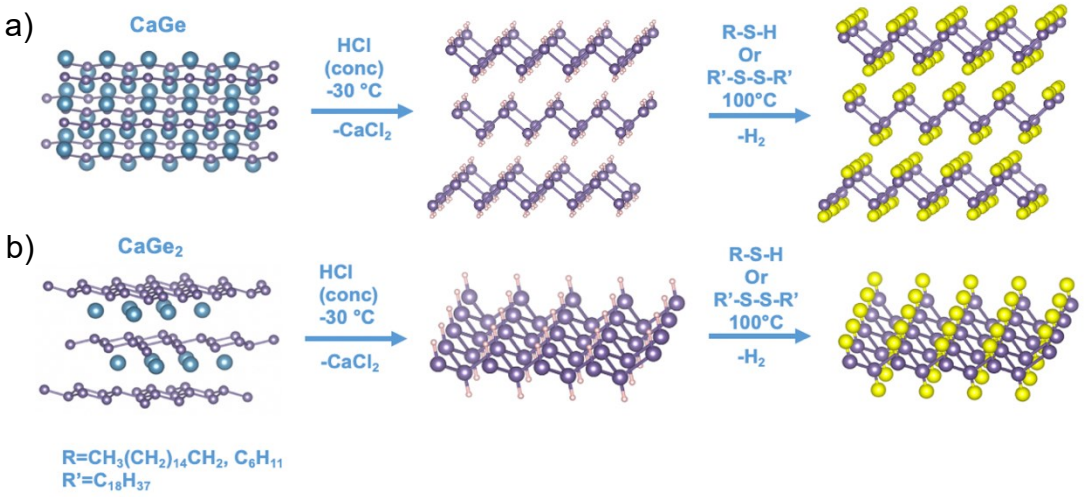

Scheme 3-1. A pictorial representation of the Zintl phase deintercalation-based preparation and post-synthesis thiolation of (a) polygermanes and (b) germanane. Purple spheres: Ge, blue: Ca, pink: yellow spheres H: sulfur atoms of ligands of choice.

3.2 Materials and Methods

3.2.1 Materials

Germanium metal [Ge; ≥ 99.99%], calcium metal [Ca; 99%], 1-hexanethiol [HT; $CH_3(CH_2)_4CH_2SH$; 95%], 1-octanethiol [OT; $CH_3(CH_2)_6CH_2SH$; ≥ 98.5%], 1-dodecanethiol [DDT; $CH_3(CH_2)_{10}CH_2SH$; ≥ 98%], and 1-cyclohexanethiol [CHT; $C_6H_{11}SH$; 97%], were purchased from Sigma-Aldrich. 1-Hexadecanethiol [HDT; $CH_3(CH_2)_{14}CH_2SH$; 97.0%] was obtained from Fisher Scientific. Di-*n*-octadecyl

disulfide [ODS; $C_{36}H_{74}S_2$, 98%] was obtained from Alfa Aesar. All reagents were used as received unless specified otherwise. All organic solvents were dried using an Innovative Technology, Inc., Grubbs-type solvent purification system.

3.2.2 Synthesis of CaGe and $CaGe_2$

CaGe and $CaGe_2$ were prepared using literature procedures.[8,20,29] Briefly, stoichiometric mixtures of Ca and Ge were pressed into a pellet, and the pellet was placed in an arc furnace. For both materials, the pellet was heated to 950–1050 °C, followed by cooling to room temperature, after which it was placed in hexane until further use. The resulting CaGe and $CaGe_2$ were ground to a fine powder (i.e., granular) using a mortar and pestle at ambient temperature and then used in the deintercalation procedures outlined below.

3.2.3 Synthesis of $(GeH_2)_n$

Polygermanes were prepared from CaGe using a procedure reported previously by our Group.[8,30] Briefly, uniformly ground CaGe powder (2.00 g; 17.8 mmol) was immersed fully in a mixture of acetonitrile (30 mL) and deionized water (0.960 mL; 53.4 mmol), cooled to -30 ^{o}C in a freezer. After 30 min, the original black solid becomes orange-red. This orange-red solid is stable in the solvent mixture at -30 ^{o}C for up to 2 d. To obtain the final GeH_2, the majority of the solvent mixture was decanted, and a mixture of concentrated hydrochloric acid and anhydrous ethanol (1:5; v:v) that had been previously cooled to -30 ^{o}C was added to the wet orange-red solid, mixed, and finally centrifuged (3000 rpm) for 5 min. The supernatant was discarded. This acid treatment/centrifugation was repeated once. The product of the final acid treatment was washed (i.e., suspended/centrifuged/isolated) with one aliquot of anhydrous ethanol (20 mL), followed by one aliquot of dry toluene (20 mL). The resulting $(GeH_2)_n$ (0.15 g, 2.0 mmol) was suspended in dry toluene (5 mL) with a standard freeze-pump-thaw procedure and covered with aluminum foil until further use and characterization using FTIR, X-ray photoelectron (XP), and Raman spectroscopies, transmission electron microscopy, and diffuse reflective analysis.

3.2.4 Synthesis of $(Ge_6H_6)_n$

To prepare germanane, freshly prepared $CaGe_2$ (1.00 g; 5.39 mmol) was added to a standard argon-filled Schlenk flask charged with -30 ºC concentrated hydrochloric acid (100 mL). The reaction mixture was maintained at -30 °C in a freezer in subdued light for at least 7 d and was shaken once daily at regular intervals. Subsequently, the reaction mixture was filtered using a glass frit under nitrogen to obtain a solid product consisting of gray flakes that exhibited a metallic sheen. The flakes were washed three times with degassed, anhydrous acetone, followed by drying under vacuum on the Schlenk line. The vial containing the final product was wrapped in aluminum foil and stored in a nitrogen-filled glovebox until further use. The product was characterized using FTIR, XP, and Raman spectroscopies, transmission electron microscopy, and diffuse reflective analysis.

3.2.5 Functionalization of $(GeH_2)_n$ and $(Ge_6H_6)_n$

In a nitrogen-filled glovebox, $(Ge_6H_6)_n$ (10 mg; equivalent to 0.14 mmol of Ge–H) or $(GeH_2)_n$ (10 mg; equivalent to 0.28 mmol of Ge–H), degassed dry toluene (1 mL), and an excess of the thiol reagent of choice (i.e., hexadecanethiol, 8 mL; 25 mmol: cyclohexanethiol, 8 mL; 65 mmol: octadecyl disulfide, 8 mL; 13 mmol) were loaded into a 20 mL Biotage® microwave tube containing a magnetic stir bar that had been pre-dried in a standard glassware oven at 140 °C. The reaction vessel was sealed and placed in a bath sonicator (Fisher Scientific FS30) for 3 h. The $(Ge_6H_6)_n$ and $(GeH_2)_n$ reaction mixtures appeared dark red and pale yellow, respectively (Figure 3-S4). Next, this mixture was heated to 100 °C in an oil bath with stirring and was maintained at that temperature for 15 h. After cooling, anhydrous ethanol (10 mL) was added, resulting in the formation of gas bubbles. The mixture was centrifuged at 3000 rpm (5 min) to separate unreacted $(Ge_6H_6)_n$ or $(GeH_2)_n$. At this point, the supernatant contained functionalized $(Ge_6H_6)_n$ or $(GeH_2)_n$. To isolate the functionalized systems, the supernatant was decanted to new centrifuge tubes, and toluene (10 mL) was added, followed by centrifugation at 3000 rpm for 30 min to provide black and orange-red solids. The clear, colourless supernatant was decanted and discarded, dry toluene (5 mL) and anhydrous ethanol (20 mL) were added, and the mixture was shaken to resuspend the solid. Then, the solid was isolated by centrifugation (3000 rpm) for 30

min. This suspension/centrifugation procedure was repeated three times with toluene/ethanol, followed by three additional times using only dry toluene (20 mL). Finally, the functionalized GeNSs or PGs were dispersed in 2–3 mL of toluene and stored in a glovebox in subdued light. The products were characterized using FTIR, XP, and Raman spectroscopies, transmission electron microscopy, and diffuse reflective analysis.

3.2.6 Material Characterization

Fourier-Transform Infrared (FTIR) Spectroscopy. FTIR spectra were collected using a Thermo Nicolet Magna 750 IR Spectrometer (32 scans). FTIR samples were prepared by drop coating a toluene dispersion of the sample in question onto an electronic-grade Si-wafer and dried under air or nitrogen atmosphere.

Transmission Electron Microscopy (TEM). Bright-field transmission electron microscopy (TEM) images were obtained using a JEOL JEM-ARM200CF S/TEM electron microscope operated at 200 keV. Samples were prepared by depositing a small drop (~0.01 mL) of a toluene suspension of the functionalized GeNSs or PGs onto a 200-mesh carbon-coated copper grid purchased from Electron Microscopy Inc. Excess solvent was drawn off using standard filter paper. The grid on which the sample was mounted was maintained in a vacuum chamber for at least 24 h prior to image acquisition. High-resolution (HR) TEM images were obtained using JEOL-2200FS TEM-STEM operated at 200 keV. HRTEM images were processed using Gatan Digital Micrograph software (calibration image size) and ImageJ (measuring).

X-ray Photoelectron Spectroscopy (XPS). XP spectra were acquired using a Kratos Axis Ultra instrument operating in energy spectrum mode. Samples were prepared by depositing functionalized GeNSs or PGs suspensions in toluene onto a copper foil substrate (thickness = 0.25 mm) and allowing it to dry. The operating chamber pressure was maintained at 10^{-7} Pa. Monochromatic Al Kα X-rays (λ = 8.34 Å) at 210 W was used to irradiate the sample, and the spectrum was collected with bandpass energy of 20 eV, 0.1 eV step size, and an electron take-off angle of 90°. All high-resolution spectra were calibrated to the C 1s emission (C–H and C–C) of adventitious carbon

(284.8 eV), and a Shirley-type background was applied using CasaXPS software (VAMAS) to account for intrinsic loss background. Spectra were fitted using Gaussian-Lorentzian curves considering the element-specific oxidation states and spin-orbit splitting parameters. The S 2p emissions were fitted to a doublet using a 1:2 peak area ratio with the same full-width-at-half-maximum for both components and 1.2 eV spin-orbit splitting.[31,32] The Ge 3d emission was fitted to Ge $3d_{3/2}$/Ge $3d_{5/2}$ partner lines using an intensity ratio of 0.68 as Ge $3d_{3/2}$/Ge $3d_{5/2}$. The spin orbit splitting was fixed at 0.6 eV with the same full-width-at-half-maximum of all peaks.

Raman Spectroscopy was performed using a Renishaw in*Via* Raman microscope with a 633 nm diode laser operating at a power of 3.98 mW. Samples were prepared by mounting the powders in question on a gold-coated glass slide. At least three spots were measured for each sample, with an integration of 5 scans on each spot and a laser power of 1–5%.

Diffuse Reflective Analysis (DRA) Diffuse reflective analysis was measured in a Cary 5000 UV-Vis-NIR spectrophotometer with a diffuse reflectance integrating sphere attachment. The grading filter and detector were changed at 900 nm. Samples were dried completely in a vacuum chamber for at least 24 h to get ideal powdered solid materials.

3.3 Results and Discussion

For the present study, functionalized polygermanes (PGs) and germanium nanosheets (GeNSs) were prepared from CaGe and $CaGe_2$ precursors, respectively (Scheme 3-1). These Zintl phase precursors were prepared by heating stoichiometric mixtures of the constituent metals, and their identities were confirmed using X-ray powder diffraction (Figure 3-1 a,c).[13,20] The established crystal structure of the CaGe Zintl phase shows chains of catenated Ge atoms in layers that are separated and charge balanced by Ca ions (Figure 3-1 c).[29] In contrast, the structure of $CaGe_2$ is made up of polyanionic Ge layers separated by interstitial Ca^{2+} ions (Figure 3-1 a).[18] To liberate the respective Ge structures, it is necessary to remove the Ca ions. This is achieved via controlled, low

temperature exposure to hydrochloric acid solutions; the procedures differ for each Zintl precursor, as described by the following equations:

$$3n\ CaGe_2 + 6n\ HCl \rightarrow (Ge_6H_6)_n + 3n\ CaCl_2 \quad (1\text{-}1)$$

$$n\ CaGe + 2n\ HCl \rightarrow (GeH_2)_n + n\ CaCl_2 \quad (1\text{-}2)$$

and the reader is directed to the experimental section for detailed descriptions. In both cases, HCl-based deintercalation removes the Ca ions and protons from the acid, providing charge balance. Figures 3-1b and d show the X-ray powder diffraction (XRD) patterns of the resulting materials, which are consistent with literature reports.[29,13] FTIR spectra (Figure 3-2) of the resulting materials show clear signatures of Ge–H bonds at 2010 cm^{-1} that provide a point of attachment for further functionalization via reaction with sulfur-based reagents, such as thiols (i.e., R–SH; R = $CH_3(CH_2)_{14}CH_2$, C_6H_{11}) or disulfides (i.e., R–S–S–R; R = $C_{18}H_{37}$).

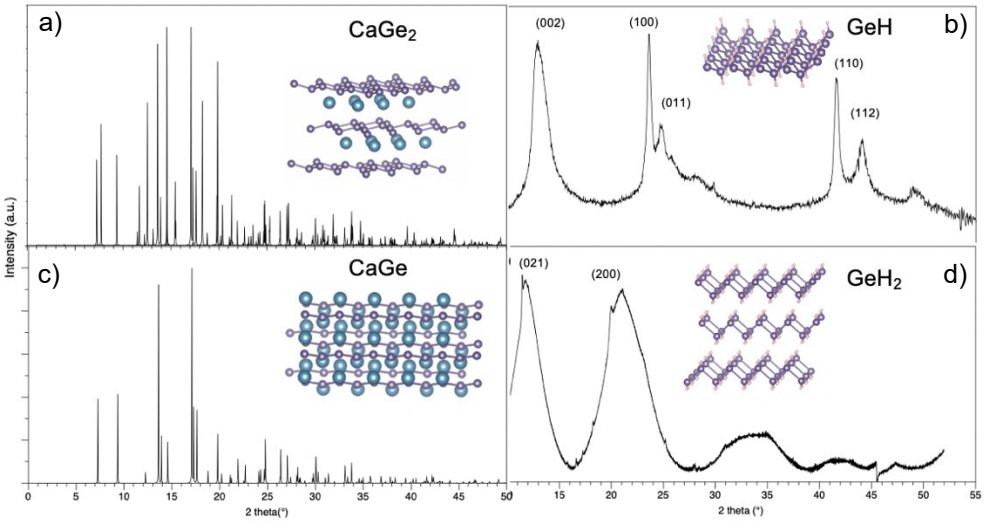

Figure 3-1. XRD patterns of a) $CaGe_2$, b) synthesized $(Ge_6H_6)_n$, c) CaGe and d) $(GeH_2)_n$. Insets show corresponding illustrations of respective crystal structures, where purple spheres represent Ge atoms, blue spheres represent Ca atoms, and pink spheres represent H atoms.

Functionalization of the resulting H-terminated Ge nanomaterials was achieved by exposing the Ge–H system in question to an excess of the chosen thiol or disulfide reagent, followed by heating at 100 °C for 15 h (Scheme 3-1). This process resulted in a qualitative change in the solvent compatibility of the Ge nanomaterials that is consistent with surface modification. For PGs, this reaction provided orange materials that readily formed dark amber suspensions in toluene, which were stable for 1–2 d (Figure 3-S4 a). In contrast, reactions with GeNSs provided black materials that were suspended in toluene for 2–3 h (Figure 3-S4 b).

FTIR spectroscopy allows identification of the chemical functional groups present in a given material, while simultaneously offering a convenient approach to evaluating nanomaterial surface modification and derivatization. A straightforward comparison of the FTIR spectra of the modified PGs (Figure 3-2 a) and GeNS (Figure 3-2 b) obtained from reactions of $(GeH_2)_n$ and (Ge_6H_6) with thiols and disulfides shows the expected features of the target functional groups.

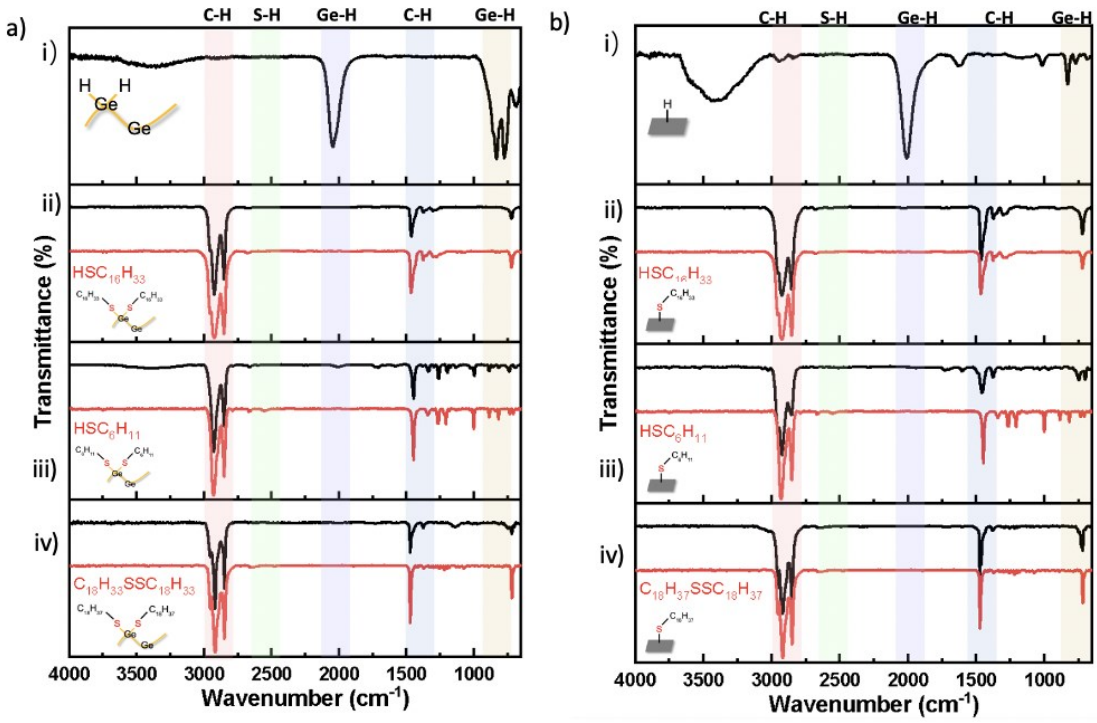

Figure 3-2. FTIR spectra of (a) polygermanes and (b) germananes functionalized with i) hydride, (ii) hexadecanethiol, (iii) cyclohexanethiol, and (iv) octadecyl disulfide, respectively. Red spectra are neat thiol ligand and back spectra are PGs and GeNSs.

We also note that residual Ge–H and Ge–O related features at 2010 and 800–960 cm^{-1}, respectively, evident in the spectra of $(GeH_2)_n$ and (Ge_6H_6) are not detected in the spectra of the functionalized systems. Furthermore, features associated with O–H stretching and bending at ~3370 and 1630 cm^{-1}, evident in the $(GeH_2)_n$ and (Ge_6H_6) spectra and attributed to absorbed water, also are diminished.[12] While one might expect features associated with S–H in the spectra of the starting thiol reagents, their absence is not surprising because these absorptions are traditionally weak. Even in the absence of this spectroscopic feature, surface modification is confirmed by the evolution of bubbles of gas that have been attributed tentatively to hydrogen formation during the coupling reaction.

To gain compositional and oxidation state information for the present functionalized PGs and GeNSs, we employed XP spectroscopy (Figure 3-3). Survey spectra (Figure 3-S1) confirmed that the materials are comprised of Ge, S, C, and O.

Turning our attention to the high-resolution spectra of the functionalized PGs and GeNSs, we note by examining the S 2p spectral region (Figure 3-3 b,d) that functionalization induces a shift of the S $2p_{3/2}$ emission to ~162.4 eV from literature values in the range of 163–164 eV for unbonded alkanethiols and disulfides (S $2p_{3/2}$ 163.5 eV BE);[38] as expected, a similar shift to ~163.5 eV from 165.0 eV is noted for the S $2p_{1/2}$ component.[38,39] These data are consistent with other reports of thiol passivation of Ge surfaces.[25,28]

Figures 3-3 a and c show the Ge 3d spectra region of the high-resolution XP spectra of functionalized PGs and GeNSs, respectively. The XPS of the Ge 3d region were fitted to the Ge $3d_{5/2}$ (higher BE) and $3d_{3/2}$ (lower BE) spin-orbit couple. As expected, the spectra of $(GeH_2)_n$ and germanane flakes show a Ge emission centered at 29.82 eV and 29.80 eV, respectively.[7, 13] After thiolation, the Ge 3d emission generally shifts to higher BE (~30.5 eV for functionalized PGs and ~30 eV for functionalized GeNSs).[29] Fitted spectra show sets of doublets: the most intense doublet (orange) is attributed to a Ge–Ge emission; a second doublet (green) centered at ~32.0 eV for functionalized PGs is typical of the 31.5 eV for functionalized GeNSs and is attributed to Ge–S (Ge^{2+}); finally, a third high energy doublet (blue), which is observed only in

the spectrum of octadecyl disulfide modified systems (Figure 3-3 c) is consistent with the presence of Ge(IV) species arising from limited surface oxidation.[42]

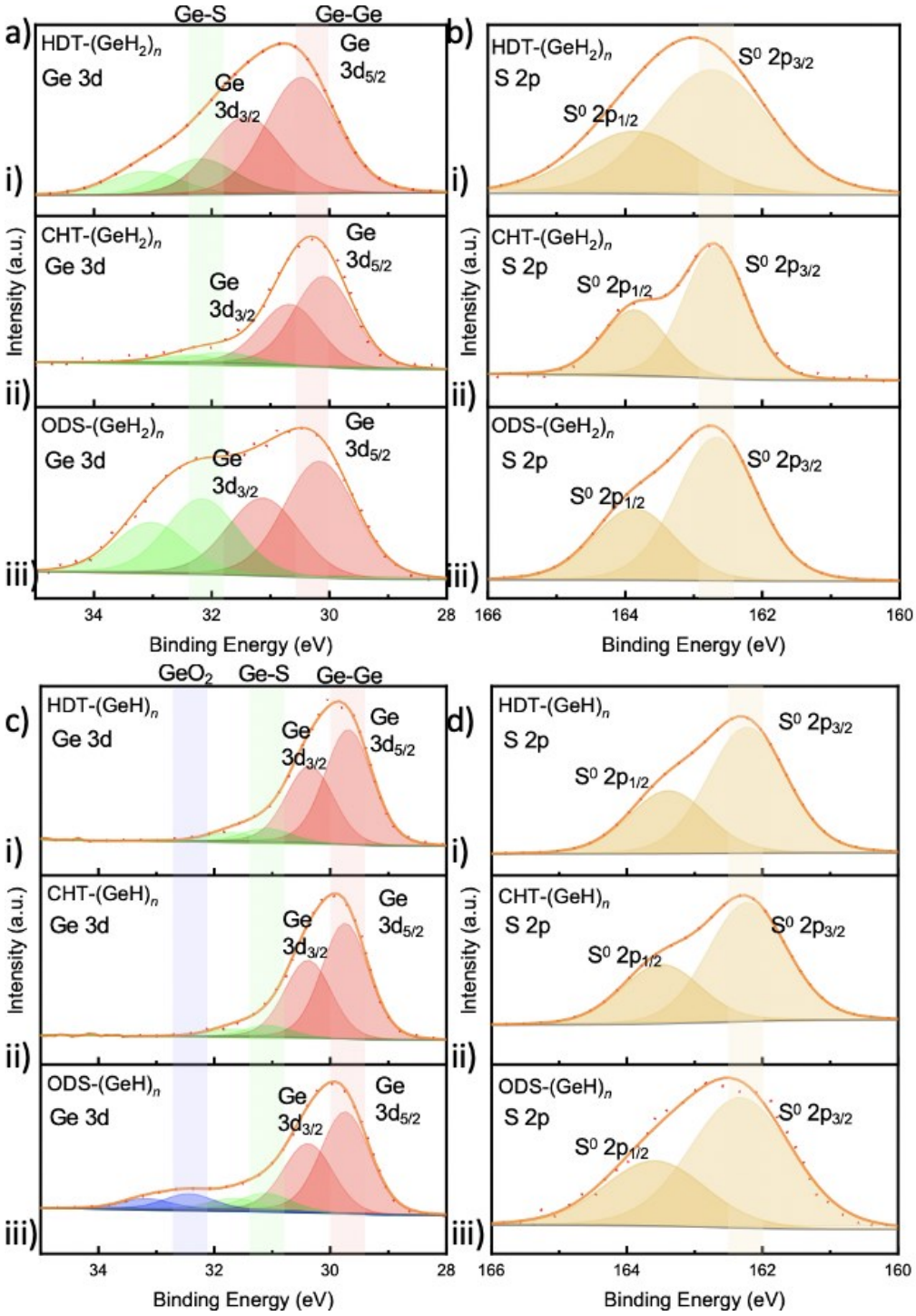

Figure 3-3. a) Ge 3d spectra and b) S 2p spectra of hexadecanethiol (i), cyclohexanethiol (ii), and octadecyl disulfide (iii) terminated PGs. c) Ge 3d spectra and d) S 2p spectra of hexadecanethiol (i), cyclohexanethiol (ii), and octadecyl disulfide (iii) terminated GeNSs.

Raman spectroscopy was used to identify the nature of the Ge–Ge bonding of the GeNSs and polygermanes after the functionalization by monitoring the Ge–Ge optical phonon vibration.[43] Raman spectra (Figure 3-4) show a Ge–Ge stretching feature, which appears at slightly lower energy (~292 cm^{-1}) than for bulk crystalline Ge (~302 cm^{-1}).[43] It is reasonable to ascribe this observation to a disorder-induced activation of phonon density.[44] The spectra also show minor tailing to lower energy that results from the increase of amorphous content.[45] Unfortunately, no obvious Ge–S peak is observed due to the lack of long-range ordering; Kauzlarich et al.[26] also did not observe a Ge–S peak.

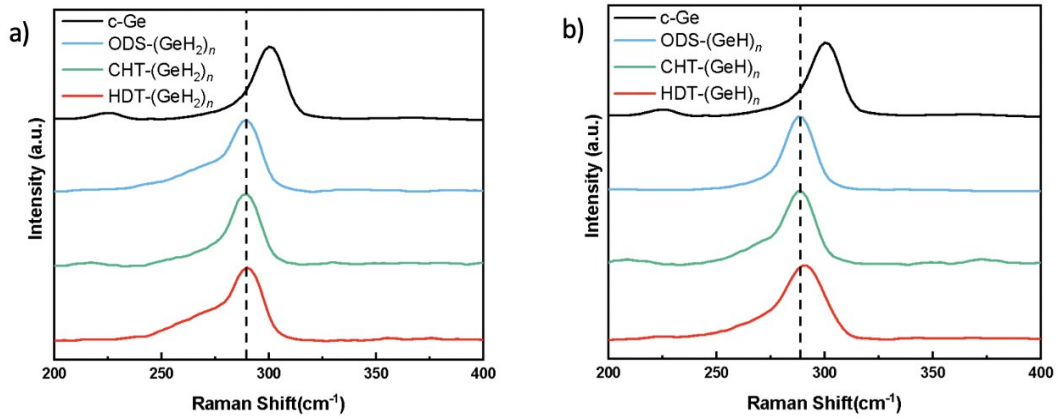

Figure 3-4. a) Raman spectra of bulk Ge (black), hexadecanethiol-terminated PGs (blue), cyclohexanethiol-terminated PGs (green), and octadecyl disulfide-terminated PGs (red). b) Raman spectra of bulk Ge (black), hexadecanethiol-terminated GeNSs (blue), cyclohexanethiol-terminated GeNSs (green), and octadecyl disulfide-terminated GeNSs (red).

Figure 3-5 shows the diffuse reflectance analysis (DRA), which provides a convenient determination of the material optical band gap energies. The DRA determined band gaps of hydride-terminated PGs and hydride-terminated GeNSs are 2.31 eV and 1.6 eV, respectively.[8,29] The DRA measurements of PGs and GeNSs reveal band gap increases in the order $C_{18}H_{36}S < C_6H_{11}S \leq C\ H_3(CH_2)_{14}CH_2S \leq$ H-terminated PGs and GeNSs. This trend can be explained by the interplay of the ligand size and electron-withdrawing nature of the surface group[45] since the ligands increase in size in the order H- > $C_6H_{11}S$- > $CH_3(CH_2)_{14}CH_2S$- > $C_{18}H_{36}S$-. Also, the Hammett constant (σ_p) increases in the order H- > $C_6H_{11}S$- > $CH_3(CH_2)_{14}CH_2S$- > $C_{18}H_{36}S$-. We note that

the band gap value decreases with increasing ligand electronegativity and size, a conclusion consistent with that of Jiang et al.[45] This is because the larger and more electronegative ligands can strain the Ge–Ge bond or framework in a tensile fashion, and thus reduce band gaps. Furthermore, the unique reaction mechanism of functionalized Ge with -$C_{18}H_{36}S$ also can expand the Ge–Ge bond and reduce band gaps.

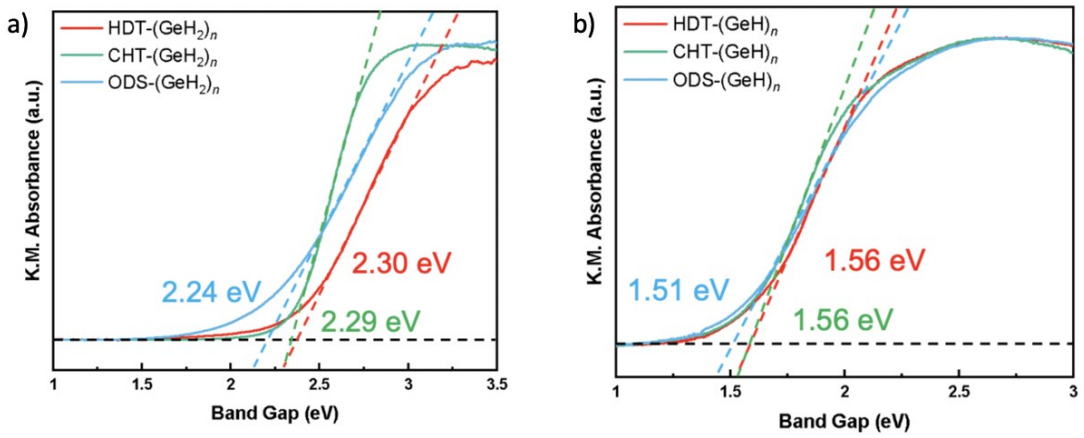

Figure 3-5. a) Diffuse reflectance spectra for (red) hexadecanethiol-terminated PGs, (green) cyclohexanethiol-terminated PGs, and (red) octadecyl disulfide-terminated PGs. b) Diffuse reflectance spectra for (red) hexadecanethiol-terminated GeNSs, (green) cyclohexanethiol-terminated GeNSs, and (red) octadecyl disulfide-terminated GeNSs.

Finally, comparing the thiolated PGs and GeNSs, both show that the lack of PL and linear slope might indicate that both PGs and GeNSs have an indirect band gap.[29] The lack of PL also can be explained by a lot of nonradiative defect states or impurities. However, the band gap energy of thiolated GeNSs is closer to H-terminated GeNSs compared to thiolated PGs, which might indicate that thiolation surface coverage on the surface of GeNSs is less than on PGs.

Conclusion

In this study, we have developed versatile methods for the thiolation surface reaction of Ge nanosystems (i.e., PGs and GeNSs). It is the first demonstration of the introduction of thiol and disulfide on PGs and GeNSs surfaces via thermally-induced heteronuclear dehydrocoupling. We also showed the relationship between the

electronic structure (i.e., band gaps) of functionalized PGs and GeNSs and the properties of surface ligands (i.e., size and electronegativity). Generally speaking, ligands that are more electron-withdrawing (more electronegative) and have greater steric bulk (larger size) can lower the band gap. This is because of the Ge–Ge bond or framework expansion, which would happen easier using disulfide instead of thiol. Furthermore, thiolated PGs get better thiolation (higher surface coverage) than thiolated GeNSs because GeNSs are hard to separate during exfoliation and stay more in the bulk GeH compared to PGs.

References

(1) Vaughn, D. D.; Schaak, R. E. Synthesis, Properties and Applications of Colloidal Germanium. Pdfnd Germanium-Based Nanomaterials. *Chem. Soc. Rev.* **2013**, *42* (7), 2861–2879.

(2) Michel, J.; Liu, J.; Kimerling, L. C. High-Performance Ge-on-Si Photodetectors. *Nat. Photonics* **2010**, *4* (8), 527–534.

(3) Henderson, E. J.; Seino, M.; Puzzo, D. P.; Ozin, G. A. Colloidally Stable Germanium Nanocrystals for Photonic Applications. *ACS Nano* **2010**, *4* (12), 7683–7691.

(4) Kennedy, T.; Brandon, M.; Ryan, K. M. Advances in the Application of Silicon and Germanium Nanowires for High-Performance Lithium-Ion Batteries. *Adv. Mater.* **2016**, *28* (27), 5696–5704.

(5) Mortazavi, B.; Dianat, A.; Cuniberti, G.; Rabczuk, T. Application of Silicene, Germanene and Stanene for Na or Li Ion Storage: A Theoretical Investigation. *Electrochim. Acta* **2016**, *213*, 865–870.

(6) Liu, N.; Bo, G.; Liu, Y.; Xu, X.; Du, Y.; Dou, S. X. Recent Progress on Germanene and Functionalized Germanene: Preparation, Characterizations, Applications, and Challenges. *Small* **2019**, *15* (32), 1–11.

(7) Rosli, N. F.; Rohaizad, N.; Sturala, J.; Fisher, A. C.; Webster, R. D.; Pumera, M. Siloxene, Germanane, and Methylgermanane: Functionalized 2D Materials of Group 14 for Electrochemical Applications. *Adv. Funct. Mater.* **2020**, *30* (21), 1–11.

(8) Nakamura, D.; Nakano, H. Liquid-Phase Exfoliation of Germanane Based on Hansen Solubility Parameters. *Chem. Mater.* **2018**, *30* (15), 5333–5338.

(9) Carolan, D. Recent Advances in Germanium Nanocrystals: Synthesis, Optical Properties and Applications. *Prog. Mater. Sci.* **2017**, *90*, 128–158.

(10) Buriak, J. M. Organometallic Chemistry on Silicon and Germanium Surfaces. *Chem. Rev.* **2002**, *102* (5), 1271–1308.

(11) Collins, G.; Holmes, J. D. Chemical Functionalisation of Silicon and Germanium Nanowires. *J. Mater. Chem.* **2011**, *21* (30), 11052–11069.

(12) Yu, H.; Thiessen, A. N.; Hossain, M. A.; Kloberg, M. J.; Rieger, B.; Veinot, J. G. C. Thermally Induced Dehydrogenative Coupling of Organosilanes and H-Terminated Silicon Quantum Dots onto Germanane Surfaces. *Chemistry of Materials*. **2020**, *32* (11), 4536–4543

(13) Yu, H.; Ni, C.; Thiessen, A. N.; Li, Z.; Veinot, J. G. C. Synthesis, Properties, and Derivatization of Poly(Dihydrogermane): A Germanium-Based Polyethylene Analogue. *ACS Nano* **2021**. *15* (6), 9368–9378

(14) Kevin A. Juarez-Ornelas, J. Oscar C. Jiminénz-Halla, Terumasa Kato, C. R. S.-A. and K. M. Supporting Information Supporting Information. *Aldenderfer, Mark S., Craig, Nathan M., Speak. Robert Jeff, Popelka-Filcoff, Rachel S.* **1997**, *2* (1), 1–5.

(15) Beekman, M.; Kauzlarich, S. M.; Doherty, L.; Nolas, G. S. Zintl Phases as Reactive Precursors for Synthesis of Novel Silicon and Germanium-Based Materials. *Materials (Basel)*. **2019**, *12* (7).

(16) Notin, M.; Mejbar, J.; Bouhajib, A.; Charles, J.; Hertz, J. The Thermodynamic Properties of Calcium Intermetallic Compounds. *J. Alloys Compd.* **1995**, *220* (1–2), 62–75.

(17) Kurylyshyn, I. M.; Fässler, T. F.; Fischer, A.; Hauf, C.; Eickerling, G.; Presnitz, M.; Scherer, W. Probing the Zintl-Klemm Concept: A Combined Experimental and Theoretical Charge Density Study of the Zintl Phase CaSi. *Angew. Chemie - Int. Ed.* **2014**, *53* (11), 3029–3032.

(18) Vogg, G.; Brandt, M. S.; Stutzmann, M.; Genchev, I.; Bergmaier, A.; Go, L.; Dollinger, G. Epitaxial CaGe " Lms on Germanium. **2000**, *212*, 148–154.

(19) Cultrara, N. D.; Wang, Y.; Arguilla, M. Q.; Scudder, M. R.; Jiang, S.; Windl, W.; Bobev, S.; Goldberger, J. E. Synthesis of 1T, 2H, and 6R Germanane Polytypes. *Chem. Mater.* **2018**, *30* (4), 1335–1343.

(20) Royen, P.; Rocktäschel, C. Zur Kenntnis Niedere Hydride Des Siliciums Und Germaniums. *ZAAC - J. Inorg. Gen. Chem.* **1966**, *346* (5–6), 279–289.

(21) Yu, H.; Helbich, T.; Scherf, L. M.; Chen, J.; Cui, K.; Fässler, T. F.; Rieger, B.; Veinot, J. G. C. Radical-Initiated and Thermally Induced Hydrogermylation of Alkenes on the Surfaces of Germanium Nanosheets. *Chem. Mater.* **2018**, *30* (7), 2274–2280.

(22) Thiessen, A. N.; Ha, M.; Hooper, R. W.; Yu, H.; Oliynyk, A. O.; Veinot, J. G. C.; Michaelis, V. K. Silicon Nanoparticles: Are They Crystalline from the Core to the Surface? *Chem. Mater.* **2019**, *31* (3), 678–688.

(23) Jiang, S.; Arguilla, M. Q.; Cultrara, N. D.; Goldberger, J. E. Improved Topotactic Reactions for Maximizing Organic Coverage of Methyl Germanane. *Chem. Mater.* **2016**, *28* (13), 4735–4740.

(24) Cai, Q.; Xu, B.; Ye, L.; Tang, T.; Huang, S.; Du, X.; Bian, X.; Zhang, J.; Di, Z.; Jin, Q.; Zhao, J. Stable Functionalization of Germanium Surface and Its Application in Biomolecules Immobilization. *Appl. Surf. Sci.* **2014**, *316* (1), 46–53.

(25) Cai, Q.; Xu, B.; Ye, L.; Di, Z.; Huang, S.; Du, X.; Zhang, J.; Jin, Q.; Zhao, J. 1-Dodecanethiol Based Highly Stable Self-Assembled Monolayers for Germanium Passivation. *Appl. Surf. Sci.* **2015**, *353*, 890–901.

(26) Muthuswamy, E.; Zhao, J.; Tabatabaei, K.; Amador, M. M.; Holmes, M. A.; Osterloh, F. E.; Kauzlarich, S. M. Thiol-Capped Germanium Nanocrystals: Preparation and Evidence for Quantum Size Effects. *Chem. Mater.* **2014**, *26* (6), 2138–2146.

(27) Wang, D.; Chang, Y. L.; Liu, Z.; Dai, H. Oxidation Resistant Germanium Nanowires: Bulk Synthesis, Long Chain Alkanethiol Functionalization, and Langmuir-Blodgett Assembly. *J. Am. Chem. Soc.* **2005**, *127* (33), 11871–11875. h

(28) Holmberg, V. C.; Korgel, B. A. Corrosion Resistance of Thiol- and Alkene-Passivated Germanium Nanowires. *Chem. Mater.* **2010**, *22* (12), 3698–3703.

(29) Bianco, E.; Butler, S.; Jiang, S.; Restrepo, O. D.; Windl, W.; Goldberger, J. E. Stability and Exfoliation of Germanane: A Germanium Graphane Analogue. *ACS Nano* **2013**, *7* (5), 4414–4421.

(30) Clark, R. J.; Aghajamali, M.; Gonzalez, C. M.; Hadidi, L.; Islam, M. A.; Javadi, M.; Mobarok, M. H.; Purkait, T. K.; Robidillo, C. J. T.; Sinelnikov, R.; Thiessen, A. N.; Washington, J.; Yu, H.; Veinot, J. G. C. From Hydrogen Silsesquioxane to Functionalized Silicon Nanocrystals. *Chem. Mater.* **2017**, *29* (1), 80–89.

(31) Yu, Y.; Rowland, C. E.; Schaller, R. D.; Korgel, B. A. Synthesis and Ligand Exchange of Thiol-Capped Silicon Nanocrystals. *Langmuir* **2015**, *31* (24), 6886–6893.

(32) Battocchio, C.; Porcaro, F.; Mukherjee, S.; Magnano, E.; Nappini, S.; Fratoddi, I.; Quintiliani, M.; Russo, M. V.; Polzonetti, G. Gold Nanoparticles Stabilized with Aromatic Thiols: Interaction at the Molecule-Metal Interface and Ligand Arrangement in the Molecular Shell Investigated by SR-XPS and NEXAFS. *J. Phys. Chem. C* **2014**, *118* (15), 8159–8168.

(33) Plymale, N. T.; Dasog, M.; Brunschwig, B. S.; Lewis, N. S. A Mechanistic Study of the Oxidative Reaction of Hydrogen- Terminated Si (111) Surfaces with Liquid Methanol. **2017**, No. 111.

(34) W.F., Sobol, P.E., Bomben, K.D. and Chastain, J. In Chastain, J., Ed., Handbook of X-Ray Photoelectron Spectroscopy, 1992

(35) Deegan, T.; Hughes, G. An X-Ray Photoelectron Spectroscopy Study of the HF Etching of Native Oxides on Ge(111) and Ge(100) Surfaces. *Appl. Surf. Sci.* **1998**, *123–124*, 66–70.

(36) Collins, G.; Aureau, D.; Holmes, J. D.; Etcheberry, A.; O'Dwyer, C. Germanium Oxide Removal by Citric Acid and Thiol Passivation from Citric Acid-Terminated Ge(100). *Langmuir* **2014**, *30* (47), 14123–14127.

(37) Bui, L. N.; Thompson, M.; Mckeown, N. B.; Romaschin, A. D.; Kalman, P. G. Surface Modification of the Biomedical Polymer Poly (Ethy1ene Terep h t h a Late). *The Analyst* **1993**, *118*, 463-474

(38) Castner, D. G.; Hinds, K.; Grainger, D. W. X-Ray Photoelectron Spectroscopy Sulfur 2p Study of Organic Thiol and Bisulfide Binding Interactions with Gold Surfaces. *Langmuir* **1996**, *12* (21), 5083–5086.

(39) Badia, A.; Cuccia, L.; Demers, L.; Morin, F.; Lennox, R. B. Structure and Dynamics in Alkanethiolate Monolayers Self-Assembled on Gold Nanoparticles: A DSC, FT-IR, and Deuterium NMR Study. *J. Am. Chem. Soc.* **1997**, *119* (11), 2682–2692.

(40) You, A.; Be, M. A. Y.; In, I. X-Ray Photoelectron Spectroscopy Characterization of Gold Nanoparticles Functionalized with Amine-Terminated Alkanethiols. **2020**, *98* (2011), 97–104.

(41) Fontana, L.; Bassetti, M.; Battocchio, C.; Venditti, I.; Fratoddi, I. Synthesis of Gold and Silver Nanoparticles Functionalized with Organic Dithiols. *Colloids Surfaces A* **2017**, *532* (May), 282–289.

(42) Prabhakaran, K.; Ogino, T. Oxidation of Ge(100) and Ge(111) Surfaces: An UPS and XPS Study. *Surf. Sci.* **1995**, *325* (3), 263–271.

(43) Ma, X.; Wu, F.; Kauzlarich, S. M. Alkyl-Terminated Crystalline Ge Nanoparticles Prepared from NaGe: Synthesis, Functionalization and Optical Properties. *J. Solid State Chem.* **2008**, *181* (7), 1628–1633.

(44) Weinstein, B.A.; Cardona, M. Second Ge Raman. *Phys. Rev. B.* **1988**, *1270* (1971).

(45) Jiang, S.; Krymowski, K.; Asel, T.; Arguilla, M. Q.; Cultrara, N. D.; Yanchenko, E.; Yang, X.; Brillson, L. J.; Windl, W.; Goldberger, J. E. Tailoring the Electronic Structure of Covalently Functionalized Germanane via the Interplay of Ligand Strain and Electronegativity. *Chem. Mater.* **2016**, *28* (21), 8071–8077.

(46) Fa, W.; Zeng, X. C. Polygermanes: Bandgap Engineering via Tensile Strain and Side-Chain Substitution. *Chem. Commun.* **2014**, *50* (65), 9126–9129.

Chapter 4

Conclusions and Future Work of Thesis

4.1 Thesis Summary

Nanomaterials based upon Group 14 elements are gaining substantial attention due to their biocompatibility, optical and electronic properties. Surface functionalization is a critical aspect of nanomaterial design because it can modify their electronic, optical, and physical properties, possibly laying a path to designer materials. In this thesis, we focus on the surface chemistry of prepared SiNCs, polygermane and Ge nanosheets and try to change some of their properties (i.e., solubility or resistance to oxidation).

In Chapter 2, we designed dissipative self-assembly of functionalized SiNCs driven by the kinetics of a dissipative reaction chemical cycle. This study builds upon Grotsch et al.'s work and examines how aspartic acid and derivatives of succinic acid can independently terminate SiNCs and produce two different types of precursors for the dissipative reaction cycle. A series of experiments conducted in this study corroborated that EDC coupling can successfully prepare the termination of SiNCs and discovered the combined effects of the two acids and SiNCs. Through analyzing the combined effects, dicarboxylic acids such as aspartic and succinic acid showcase assembly properties while SiNCs demonstrate the property of luminescence. On the condition of adding EDC to SiNCs, the type of SiNCs that aspartic acid terminated fails to show dissipative self-assembly, whereas the type of SiNCs that were terminated by succinic acid reacted partially as expected, meaning that they self-assembled only under specific conditions.

In Chapter 3, we carried out the thiolation on the hydride-terminated polygermane and Ge nanosheets to produce Ge–S bonding by simply heating the reaction with thiols and disulfide. Upon reaction, the Ge–H bonds were consumed, and C–H and C–S vibration modes were observed in FTIR spectra. After that, XPS, Raman spectra, and DRA were carried out to confirm the thiol-termination.

4.2 Outlook: Amination on the Ge Surface

Surface functionalization of the germanium nanomaterials remains an attractive area of investigation. Building on the thiolation investigation outlined in Chapter 3, amination emerges as an attractive target that has been applied to some Ge-based nanomaterials, with the formation of Ge–N bonds.[1–3] Different germanium surfaces have been functionalized previously for different purposes. Bent et al. functionalized the clean Ge (100)-2×1 surfaces with amines (i.e., ethylamine and aniline) in order to modify the material's activity and electronic properties in the semiconductors.[1] Tilley et al. prepared amine-terminated (i.e., allylamine) germanium nanocrystals to improve their stability and water solubility for cell imaging (Figure 4-1).[2] After that, Carolan and Doyle also terminated Ge nanocrystals with an amine to change their optical properties (i.e., luminescence), compared to different functional groups (CH_3, OH, COOH, C_6H_5, C_5H_4N, and C_4H_3S).[3]

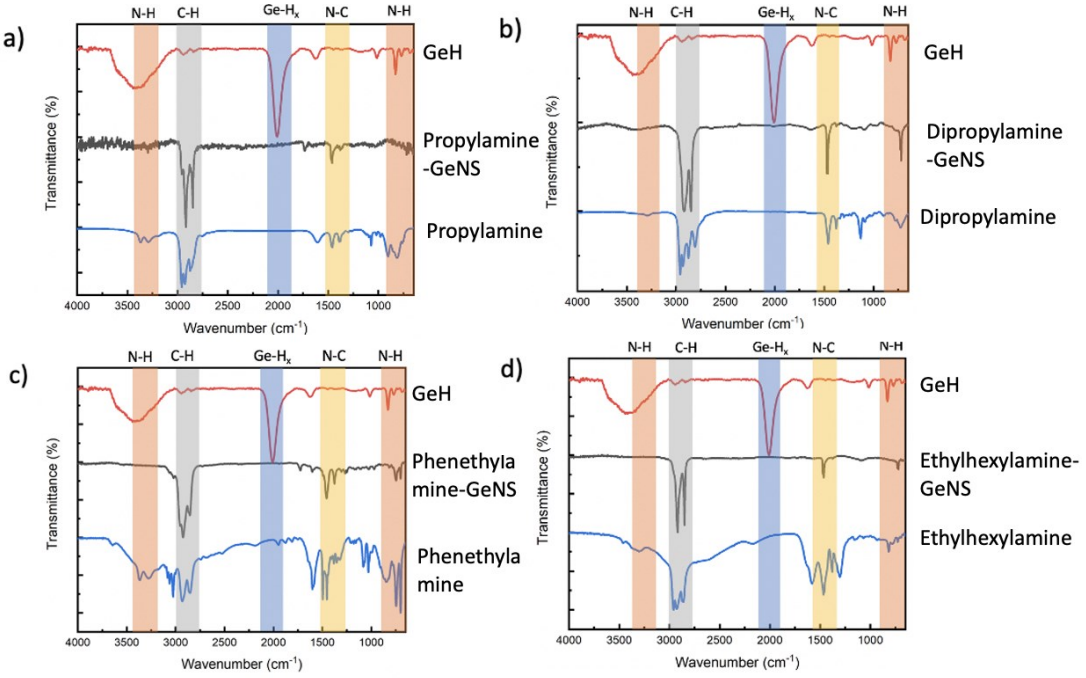

Figure 4-1. FTIR spectra of a) comparison between pure GeNS, propylamine and propylamine terminated GeNS, b) comparison between pure GeNS, dipropylamine, and dipropylamine terminated GeNS, c) comparison between pure GeNS, phenethylamine, and phyenethylamine terminated GeNS, and d) comparison between pure GeNS, ethylhexylamine, and ethylhexylamine terminated GeNS.

Herein, we present preliminary data involving reactions of GeNSs with primary ($–NH_2$), aromatic, and secondary amino groups (–NHR). These data suggest that amination reactions can occur in the temperature range of 60–150 °C. Following amination on GeNSs, the FTIR spectra of the amine-functionalized NSs show the concomitant appearance of $\nu(C–H)_{asym}$ features at 2852 cm^{-1} from both primary amine and secondary amine and the loss of ν(Ge–H) at 2001 cm^{-1} and N–H related features at 775 cm^{-1} and 3281/3410 cm^{-1}.[4] We also note that the adsorbed water ν(O–H) feature at 3400 cm^{-1} in the spectrum of GeNS is diminished substantially in the spectrum of functionalized GeNSs. This is explained, possibly, by the fact that the outer layers of the Ge–H flakes are oxidized and are removed during purification because of the limited compatibility with non-polar media.[5]

At this point, FTIR can reveal only information about the surface functional groups but cannot indicate the GeNS itself. Thus, in future experiments, further characterization is required, including XPS (Ge 3d and N 1s), Raman spectra, and DRA. Given the demonstrated reactivity of amines with GeNSs, it is also advisable to explore their reactions with polygermanes.

References

(1) Bent, S. F.; Kachian, J. S.; Rodríguez-reyes, J. C. F.; Teplyakov, A. V. Tuning the Reactivity of Semiconductor Surfaces by Functionalization with Amines of Different Basicity. **2010**, *108* (3) 956-960

(2) McVey, B. F. P.; Prabakar, S.; Gooding, J. J.; Tilley, R. D. Solution Synthesis, Surface Passivation, Optical Properties, Biomedical Applications, and Cytotoxicity of Silicon and Germanium Nanocrystals. *Chempluschem* **2017**, *82* (1), 60–73.

(3) Carolan, D.; Doyle, H. Tuning the Photoluminescence of Germanium Nanocrystals through Surface Bound Functional Groups. *Part. Part. Syst. Charact.* **2017**, *34* (2), 1–4.

(4) Yu, H.; Thiessen, A. N.; Hossain, M. A.; Kloberg, M. J.; Rieger, B.; Veinot, J. G. C. Thermally Induced Dehydrogenative Coupling of Organosilanes and H-Terminated Silicon Quantum Dots onto Germanane Surfaces. *Chem. Mater.* **2020**, *32* (11), 4536–4543.

(5) Thiessen, A. N.; Ha, M.; Hooper, R. W.; Yu, H.; Oliynyk, A. O.; Veinot, J. G. C.; Michaelis, V. K. Silicon Nanoparticles: Are They Crystalline from the Core to the Surface? *Chem. Mater.* **2019**, *31* (3), 678–688.

Bibliography

Chapter 1

(1) Eberhard, W. G.; Wcislo, W. T. Plenty of Room at the Bottom? *Am. Sci.* **2012**, *100* (3), 226–233.

(2) Bayda, S.; Adeel, M.; Tuccinardi, T.; Cordani, M.; Rizzolio, F. The History of Nanoscience and Nanotechnology: From Chemical-Physical Applications to Nanomedicine. *Molecules* **2020**, *25* (1), 1–15.

(3) Wang, G. Nanotechnology: The new features. https://arxiv.org/abs/1812.04939 (accessed Aug 30, 2021).

(4) Ramsden, J. J. What Is Nanotechnology? *Nanotechnol. Perceptions* **2005**, *1* (1), 3–17.

(5) Toné, S.; Kubo, T.; Ohyama, T.; Kusakabe, T.; Minatogawa, Y. Quantitation of MRNA Using in Vitro RNA Amplification and Northern Hybridization. *Anal. Biochem.* **2000**, *284* (2), 420–422.

(6) Radical Nanotechnology. *Introduction to Nanoscience and Nanotechnology* **2010**, 263–280.

(7) Dolez, P. I. *Nanomaterials Definitions, Classifications, and Applications*; 2015.

(8) Asha, A. B.; Narain, R. *Nanomaterials Properties*; Elsevier Inc., 2020.

(9) Suresh, S. Semiconductor Nanomaterials, Methods and Applications: A Review. *Nanosci. Nanotechnol.* **2013**, *3* (3), 62–74.

(10) de Mello Donegá, C. Synthesis and Properties of Colloidal Heteronanocrystals. *Chem. Soc. Rev.* **2011**, *40* (3), 1512–1546.

(11) Rossetti, R.; Nakahara, S.; Brus, L. E. Quantum Size Effects in the Redox Potentials, Resonance Raman Spectra, and Electronic Spectra of CdS Crystallites in Aqueous Solution. *J. Chem. Phys.* **1983**, *79* (2), 1086–1088.

(12) Ekimov, A. I.; Efros, A. L.; Onushchenko, A. A. Quantum Size Effect in Semiconductor Microcrystals. *Solid State Commun.* **1985**, *56* (11), 921–924.

(13) Weller, H.; Koch, U.; Gutierrez, M.; Henglein, A. Photochemistry of Colloidal Metal Sulfides. Absorption and Fluorescence of Extremely Small ZnS Particles (The World of the Neglected Dimensions) H.. *Berichte der Bunsengesellschaft/Physical Chem. Chem. Phys.* **1984**, *88* (7), 649–656.

(14) Weller, H. Colloidal Semiconductor Q-Particles: Chemistry in the Transition Region Between Solid State and Molecules. *Angew. Chemie Int. Ed. English* **1993**, *32* (1), 41–53.

(15) Murray, C. B.; Norris, D. J.; Bawendi, M. G. Synthesis and Characterization of Nearly Monodisperse CdE (E = S, Se, Te) Semiconductor Nanocrystallites. *J. Am. Chem. Soc.* **1993**, *115* (19), 8706–8715.

(16) Katari, J. E. B.; Colvin, V. L.; Alivisatos, A. P. X-Ray Photoelectron Spectroscopy of CdSe Nanocrystals with Applications to Studies of the Nanocrystal Surface. *J. Phys. Chem.* **1994**, *98*

(15), 4109–4117.

(17) Hines, M. A.; Guyot-Sionnest, P. Synthesis and Characterization of Strongly Luminescing ZnS-Capped CdSe Nanocrystals. *J. Phys. Chem.* **1996**, *100* (2), 468–471.

(18) Smith, A. M.; Nie, S. Semiconductor Nanocrystals: Structure, Properties, and Band Gap Engineering. *Acc. Chem. Res.* **2010**, *43* (2), 190–200.

(19) Hartman, T.; Sofer, Z. Beyond Graphene: Chemistry of Group 14 Graphene Analogues: Silicene, Germanene, and Stanene. *ACS Nano* **2019**, *13* (8), 8566–8576.

(20) Takagahara, T.; Takeda, K. Theory of the Quantum Confinement Effect on Excitons in Quantum Dots of Indirect-Gap Materials. *Phys. Rev. B* **1992**, *46* (23), 15578–15581.

(21) Mansur, H. S. Quantum Dots and Nanocomposites. *Wiley Interdiscip. Rev. Nanomedicine Nanobiotechnology* **2010**, *2* (2), 113–129.

(22) Algar, W. R.; Susumu, K.; Delehanty, J. B.; Medintz, I. L. Semiconductor Quantum Dots in Bioanalysis: Crossing the Valley of Death. *Anal. Chem.* **2011**, *83* (23), 8826–8837.

(23) Zhou, H. S.; Sasahara, H.; Honma, I.; Komiyama, H.; Haus, J. W. Coated Semiconductor Nanoparticles: The CdS/PbS System's Photoluminescence Properties. *Chem. Mater.* **1994**, *6* (9), 1534–1541.

(24) Honma, I.; Sano, T.; Komiyama, H. Surface-Enhanced Raman Scattering (SERS) for Semiconductor Microcrystallites Observed in Ag-CdS Hybrid Particles. *J. Phys. Chem.* **1993**, *97* (25), 6692–6695.

(25) Kortan, A. R.; Hull, R.; Opila, R. L.; Bawendi, M. G.; Steigerwald, M. L.; Carroll, P. J.; Brus, L. E. Nucleation and Growth of CdSe on ZnS Quantum Crystallite Seeds, and Vice Versa, in Inverse Micelle Media. *J. Am. Chem. Soc.* **1990**, *112* (4), 1327–1332.

(26) Hanifi, D. A.; Bronstein, N. D.; Koscher, B. A.; Nett, Z.; Swabeck, J. K.; Takano, K.; Schwartzberg, A. M.; Maserati, L. Threshold Quantum Yield. *Science (80-.).* **2019**, *1202* (March), 1199–1202.

(27) Pan, Z.; Zhang, H.; Cheng, K.; Hou, Y.; Hua, J.; Zhong, X. Highly E Ffi Cient Inverted Type-I CdS / CdSe Core / Shell Structure. **2012**, No. 5, 3982–3991.

(28) Kim, S.; Fisher, B.; Bawendi, M. Type-II Quantum Dots : CdTe / CdSe (Core / Shell) and CdSe / ZnTe (Core / Shell) Heterostructures. **2003**, 11466–11467.

(29) Thuy, U. T. D.; Tu, L. A.; Loan, N. T.; Chi, T. T. K.; Liem, N. Q. Comparative Photoluminescence Properties of Type-I and Type-II CdTe/CdS Core/Shell Quantum Dots. *Opt. Mater. (Amst).* **2016**, *53*, 34–38.

(30) Dasog, M.; Kehrle, J.; Rieger, B.; Veinot, J. G. C. Silicon Nanocrystals and Silicon-Polymer Hybrids: Synthesis, Surface Engineering, and Applications. *Angew. Chemie - Int. Ed.* **2016**, *55* (7), 2322–2339.

(31) Zhong, Y.; Song, B.; Peng, F.; Wu, Y.; Wu, S.; Su, Y.; He, Y. In Situ Rapid Growth of Fluorescent Silicon Nanoparticles at Room Temperature and under Atmospheric Pressure. *Chem.*

Commun. **2016**, *52* (92), 13444–13447.

(32) Park, J. H.; Gu, L.; Von Maltzahn, G.; Ruoslahti, E.; Bhatia, S. N.; Sailor, M. J. Biodegradable Luminescent Porous Silicon Nanoparticles for in Vivo Applications. *Nat. Mater.* **2009**, *8* (4), 331–336.

(33) Erogbogbo, F.; Yong, K.; Roy, I.; Xu, G.; Prasad, P. N.; Swihart, M. T. Biocompatible Luminescent Silicon. *ACS Nano* **2008**, *2* (5), 873–878.

(34) Bhattacharjee, S.; Rietjens, I. M. C. M.; Singh, M. P.; Atkins, T. M.; Purkait, T. K.; Xu, Z.; Regli, S.; Shukaliak, A.; Clark, R. J.; Mitchell, B. S.; Alink, G. M.; Marcelis, A. T. M.; Fink, M. J.; Veinot, J. G. C.; Kauzlarich, S. M.; Zuilhof, H. Cytotoxicity of Surface-Functionalized Silicon and Germanium Nanoparticles: The Dominant Role of Surface Charges. *Nanoscale* **2013**, *5* (11), 4870–4883.

(35) Exley, C. Silicon in Life:A Bioinorganic Solution to Bioorganic Essentiality1JD Birchall Memorial Lecture.1. *J. Inorg. Biochem.* **1998**, *69* (3), 139–144.

(36) Canham, L. T. Silicon Quantum Wire Array Fabrication by Electrochemical and Chemical Dissolution of Wafers. *Appl. Phys. Lett.* **1990**, *57* (10), 1046–1048.

(37) Behray, M.; Webster, C. A.; Pereira, S.; Ghosh, P.; Krishnamurthy, S.; Al-Jamal, W. T.; Chao, Y. Synthesis of Diagnostic Silicon Nanoparticles for Targeted Delivery of Thiourea to Epidermal Growth Factor Receptor-Expressing Cancer Cells. *ACS Appl. Mater. Interfaces* **2016**, *8* (14), 8908–8917.

(38) Kang, Z.; Tsang, C. H. A.; Zhang, Z.; Zhang, M.; Wong, N. B.; Zapien, J. A.; Shan, Y.; Lee, S. T. A Polyoxometalate-Assisted Electrochemical Method for Silicon Nanostructures Preparation: From Quantum Dots to Nanowires. *J. Am. Chem. Soc.* **2007**, *129* (17), 5326–5327.

(39) Bley, R. A.; Kauzlarich, S. M. A Low-Temperature Solution Phase Route for the Synthesis of Silicon Nanoclusters. *J. Am. Chem. Soc.* **1996**, *118* (49), 12461–12462.

(40) Heinrich, J. L.; Curtis, C. L.; Credo, G. M.; Kavanagh, K. L.; Sailor, M. J. Luminescent Colloidal Silicon Suspensions from Porous Silicon. *Science (80-.).* **1992**, *255* (5040), 66–68.

(41) Anglin, E. J.; Cheng, L.; Freeman, W. R.; Sailor, M. J. Porous Silicon in Drug Delivery Devices and Materials. *Adv. Drug Deliv. Rev.* **2008**, *60* (11), 1266–1277.

(42) Heath, J. R. A Liquid-Solution-Phase Synthesis of Crystalline Silicon. *Science (80-.).* **1992**, *258* (5085), 1131–1133.

(43) Zou, J.; Baldwin, R. K.; Pettigrew, K. A.; Kauzlarich, S. M. Solution Synthesis of Ultrastable Luminescent Siloxane-Coated Silicon Nanoparticles. *Nano Lett.* **2004**, *4* (7), 1181–1186.

(44) Rosso-Vasic, M.; Spruijt, E.; Van Lagen, B.; De Cola, L.; Zuilhof, H. Alkyl-Functionalized Oxide-Free Silicon Nanoparticles: Synthesis and Optical Properties. *Small* **2008**, *4* (10), 1835–1841.

(45) Li, Q.; He, Y.; Chang, J.; Wang, L.; Chen, H.; Tan, Y. W.; Wang, H.; Shao, Z. Surface-Modified Silicon Nanoparticles with Ultrabright Photoluminescence and Single-Exponential Decay for

Nanoscale Fluorescence Lifetime Imaging of Temperature. *J. Am. Chem. Soc.* **2013**, *135* (40), 14924–14927.

(46) Kanemitsu, Y.; Okamoto, S.; Otobe, M.; Oda, S. Photoluminescence Mechanism in Surface-Oxidized Silicon Nanocrystals. *Phys. Rev. B - Condens. Matter Mater. Phys.* **1997**, *55* (12), R7375–R7378.

(47) Mangolini, L.; Thimsen, E.; Kortshagen, U. HIGH-Yield Plasma Synthesis of Luminescent Silicon Quantum Dots. *2005 Proc. 4th ASME Conf. Integr. Nanosyst. Des. Synth. Appl.* **2005**, 73–74.

(48) Jurbergs, D.; Rogojina, E.; Mangolini, L.; Kortshagen, U. Silicon Nanocrystals with Ensemble Quantum Yields Exceeding 60%. *Appl. Phys. Lett.* **2006**, *88* (23), 1–3.

(49) Saitow, K. I. Silicon Nanoclusters Selectively Generated by Laser Ablation in Supercritical Fluid. *J. Phys. Chem. B* **2005**, *109* (9), 3731–3733.

(50) Hessel, C. M.; Henderson, E. J.; Veinot, J. G. C. Hydrogen Silsesquioxane: A Molecular Precursor for Nanocrystalline Si-SiO2 Composites and Freestanding Hydride-Surface-Terminated Silicon Nanoparticles. *Chem. Mater.* **2006**, *18* (26), 6139–6146.

(51) Holmberg, V. C.; Bogart, T. D.; Chockla, A. M.; Hessel, C. M.; Korgel, B. A. Optical Properties of Silicon and Germanium Nanowire Fabric. *J. Phys. Chem. C* **2012**, *116* (42), 22486–22491.

(52) Roberto, J.; Núñez, R. Photoluminescence and Patterning of Silicon Nanocrystals. **2012**, 236.

(53) Rodríguez Núñez, J. R.; Kelly, J. A.; Henderson, E. J.; Veinot, J. G. C. Wavelength-Controlled Etching of Silicon Nanocrystals. *Chem. Mater.* **2012**, *24* (2), 346–352.

(54) Dasog, M.; Bader, K.; Veinot, J. G. C. Influence of Halides on the Optical Properties of Silicon Quantum Dots. *Chem. Mater.* **2015**, *27* (4), 1153–1156.

(55) Mobarok, M. H.; Purkait, T. K.; Islam, M. A.; Miskolzie, M.; Veinot, J. G. C. Instantaneous Functionalization of Chemically Etched Silicon Nanocrystal Surfaces. *Angew. Chemie - Int. Ed.* **2017**, *56* (22), 6073–6077.

(56) Islam, M. A.; Mobarok, M. H.; Sinelnikov, R.; Purkait, T. K.; Veinot, J. G. C. Phosphorus Pentachloride Initiated Functionalization of Silicon Nanocrystals. *Langmuir* **2017**, *33* (35), 8766–8773.

(57) Yu, Y.; Fan, G.; Fermi, A.; Mazzaro, R.; Morandi, V.; Ceroni, P.; Smilgies, D. M.; Korgel, B. A. Size-Dependent Photoluminescence Efficiency of Silicon Nanocrystal Quantum Dots. *J. Phys. Chem. C* **2017**, *121* (41), 23240–23248.

(58) Clark, R. J.; Aghajamali, M.; Gonzalez, C. M.; Hadidi, L.; Islam, M. A.; Javadi, M.; Mobarok, M. H.; Purkait, T. K.; Robidillo, C. J. T.; Sinelnikov, R.; Thiessen, A. N.; Washington, J.; Yu, H.; Veinot, J. G. C. From Hydrogen Silsesquioxane to Functionalized Silicon Nanocrystals. *Chem. Mater.* **2017**, *29* (1), 80–89.

(59) Sugimoto, H.; Fujii, M.; Imakita, K. Synthesis of Boron and Phosphorus Codoped All-Inorganic Colloidal Silicon Nanocrystals from Hydrogen Silsesquioxane. *Nanoscale* **2014**, *6* (21), 12354–

12359.

(60) Geim, A. K.; Novoselov, K. S. The Rise of Graphene PROGRESS. *Nat. Mater.* **2007**, *6* (3), 183–191.

(61) Geim, A. K. Graphene Prehistory. *Physica Scripta* **2012**, *T146*, 014003.

(62) Novoselov, K. S.; Geim, A. K.; Morozov, S. V.; Jiang, D.; Katsnelson, M. I.; Grigorieva, I. V.; Dubonos, S. V.; Firsov, A. A. Two-Dimensional Gas of Massless Dirac Fermions in Graphene. *Nature* **2005**, *438* (7065), 197–200.

(63) Liu, N.; Bo, G.; Liu, Y.; Xu, X.; Du, Y.; Dou, S. X. Recent Progress on Germanene and Functionalized Germanene: Preparation, Characterizations, Applications, and Challenges. *Small* **2019**, *15* (32), 1–11.

(64) Baringhaus, J.; Ruan, M.; Edler, F.; Tejeda, A.; Sicot, M.; Taleb-Ibrahimi, A.; Li, A. P.; Jiang, Z.; Conrad, E. H.; Berger, C.; Tegenkamp, C.; De Heer, W. A. Exceptional Ballistic Transport in Epitaxial Graphene Nanoribbons. *Nature* **2014**, *506* (7488), 349–354.

(65) Fowler, J. D.; Allen, M. J.; Tung, V. C.; Yang, Y.; Kaner, R. B.; Weiller, B. H. Practical Chemical Sensors from Chemically Derived Graphene. *ACS Nano* **2009**, *3* (2), 301–306.

(66) Eda, G.; Chhowalla, M. Chemically Derived Graphene Oxide: Towards Large-Area Thin-Film Electronics and Optoelectronics. *Adv. Mater.* **2010**, *22* (22), 2392–2415.

(67) Miao, X.; Tongay, S.; Petterson, M. K.; Berke, K.; Rinzler, A. G.; Appleton, B. R.; Hebard, A. F. High Efficiency Graphene Solar Cells by Chemical Doping. *Nano Lett.* **2012**, *12* (6), 2745–2750.

(68) Qu, L.; Liu, Y.; Baek, J. B.; Dai, L. Nitrogen-Doped Graphene as Efficient Metal-Free Electrocatalyst for Oxygen Reduction in Fuel Cells. *ACS Nano* **2010**, *4* (3), 1321–1326.

(69) Ohsuna, T.; Yaokawa, R.; Nakano, H. 2D Crystal Structure Determination of Bilayer Silicene and Germanene Using Transmission Electron Microscopy. *R&D Rev. Toyota CRDL* **2019**, *50* (1), 27–37.

(70) Vogt, P.; De Padova, P.; Quaresima, C.; Avila, J.; Frantzeskakis, E.; Asensio, M. C.; Resta, A.; Ealet, B.; Le Lay, G. Silicene: Compelling Experimental Evidence for Graphenelike Two-Dimensional Silicon. *Phys. Rev. Lett.* **2012**, *108* (15), 1–5.

(71) Fleurence, A.; Friedlein, R.; Ozaki, T.; Kawai, H.; Wang, Y.; Yamada-Takamura, Y. Experimental Evidence for Epitaxial Silicene on Diboride Thin Films. *Phys. Rev. Lett.* **2012**, *108* (24), 1–5.

(72) Meng, L.; Wang, Y.; Zhang, L.; Du, S.; Wu, R.; Li, L.; Zhang, Y.; Li, G.; Zhou, H.; Hofer, W. A.; Gao, H. J. Buckled Silicene Formation on Ir(111). *Nano Lett.* **2013**, *13* (2), 685–690.

(73) Enriquez, H.; Vizzini, S.; Kara, A.; Lalmi, B.; Oughaddou, H. Silicene Structures on Silver Surfaces. *Journal of Physics: Condensed Matter* **2012**, *24* (31), 314211.

(74) Dávila, M. E.; Xian, L.; Cahangirov, S.; Rubio, A.; Le Lay, G. Germanene: A Novel Two-Dimensional Germanium Allotrope Akin to Graphene And Silicene. *New Journal of*

Physics **2014**, *16* (9), 095002.

(75) Kharadi, M. A.; Malik, G. F. A.; Khanday, F. A.; Shah, K. A.; Mittal, S.; Kaushik, B. K. Review—Silicene: From Material to Device Applications. *ECS J. Solid State Sci. Technol.* **2020**, *9* (11), 115031.

(76) Bianco, E.; Butler, S.; Jiang, S.; Restrepo, O. D.; Windl, W.; Goldberger, J. E. Stability and Exfoliation of Germanane: A Germanium Graphane Analogue. *ACS Nano* **2013**, *7* (5), 4414–4421.

(77) Butler, S. Z.; Hollen, S. M.; Cao, L.; Cui, Y.; Gupta, J. A.; Gutiérrez, H. R.; Heinz, T. F.; Hong, S. S.; Huang, J.; Ismach, A. F.; Johnston-Halperin, E.; Kuno, M.; Plashnitsa, V. V.; Robinson, R. D.; Ruoff, R. S.; Salahuddin, S.; Shan, J.; Shi, L.; Spencer, M. G.; Terrones, M.; Windl, W.; Goldberger, J. E. Progress, Challenges, and Opportunities in Two-Dimensional Materials beyond Graphene. *ACS Nano* **2013**, *7* (4), 2898–2926.

(78) Lew Yan Voon, L. C.; Sandberg, E.; Aga, R. S.; Farajian, A. A. Hydrogen Compounds of Group-IV Nanosheets. *Appl. Phys. Lett.* **2010**, *97* (16), 3–5.

(79) Houssa, M.; Dimoulas, A.; Molle, A. Silicene: A Review of Recent Experimental and Theoretical Investigations. *J. Phys. Condens. Matter* **2015**, *27* (25).

(80) Quhe, R.; Fei, R.; Liu, Q.; Zheng, J.; Li, H.; Xu, C.; Ni, Z.; Wang, Y.; Yu, D.; Gao, Z.; Lu, J. Tunable and Sizable Band Gap in Silicene by Surface Adsorption. *Scientific Reports* **2012**, *2* (1).

(81) Ding, Y.; Wang, Y. Electronic Structures of Silicene Fluoride and Hydride. *Applied Physics Letters* **2012**, *100* (8), 083102.

(82) Kaloni, T. P.; Singh, N.; Schwingenschlögl, U. Prediction of a Quantum Anomalous Hall State in Co-Decorated Silicene. *Phys. Rev. B - Condens. Matter Mater. Phys.* **2014**, *89* (3), 1–5.

(83) Jiang, S.; Butler, S.; Bianco, E.; Restrepo, O. D.; Windl, W.; Goldberger, J. E. Improving the Stability and Optical Properties of Germanane via One-Step Covalent Methyl-Termination. *Nat. Commun.* **2014**, *5*, 1–6.

(84) Li, L.; Lu, S. Z.; Pan, J.; Qin, Z.; Wang, Y. Q.; Wang, Y.; Cao, G. Y.; Du, S.; Gao, H. J. Buckled Germanene Formation on Pt(111). *Adv. Mater.* **2014**, *26* (28), 4820–4824.

(85) Xu, Y.; Tang, P.; Zhang, S. C. Large-Gap Quantum Spin Hall States in Decorated Stanene Grown on a Substrate. *Phys. Rev. B - Condens. Matter Mater. Phys.* **2015**, *92* (8), 1–5.

(86) Liu, C. C.; Feng, W.; Yao, Y. Quantum Spin Hall Effect in Silicene and Two-Dimensional Germanium. *Phys. Rev. Lett.* **2011**, *107* (7), 1–4.

(87) Georgakilas, V.; Otyepka, M.; Bourlinos, A. B.; Chandra, V.; Kim, N.; Kemp, K. C.; Hobza, P.; Zboril, R.; Kim, K. S. Functionalization of Graphene: Covalent and Non-Covalent Approaches, Derivatives and Applications. *Chem. Rev.* **2012**, *112* (11), 6156–6214.

(88) Mortazavi, B.; Dianat, A.; Cuniberti, G.; Rabczuk, T. Application of Silicene, Germanene and Stanene for Na or Li Ion Storage: A Theoretical Investigation. *Electrochim. Acta* **2016**, *213*,

865–870.

(89) Zhu, F. F.; Chen, W. J.; Xu, Y.; Gao, C. L.; Guan, D. D.; Liu, C. H.; Qian, D.; Zhang, S. C.; Jia, J. F. Epitaxial Growth of Two-Dimensional Stanene. *Nat. Mater.* **2015**, *14* (10), 1020–1025.

(90) Fang, Y.; Huang, Z. Q.; Hsu, C. H.; Li, X.; Xu, Y.; Zhou, Y.; Wu, S.; Chuang, F. C.; Zhu, Z. Z. Quantum Spin Hall States in Stanene/Ge(111). *Sci. Rep.* **2015**, *5* (111), 1–8.

(91) Schäfer, H.; Eisenmann, B.; Müller, W. Zintl Phases: Transitions between Metallic and Ionic Bonding. *Angew. Chemie Int. Ed. English* **1973**, *12* (9), 694–712.

(92) Beekman, M.; Kauzlarich, S. M.; Doherty, L.; Nolas, G. S. Zintl Phases as Reactive Precursors for Synthesis of Novel Silicon and Germanium-Based Materials. *Materials (Basel).* **2019**, *12* (7).

(93) Kauzlarich, S. M. Zintl Compounds. *Encycl. Inorg. Bioinorg. Chem.* **2011**.

(94) Nesper, R. The Zintl-Klemm Concept - A Historical Survey. *Zeitschrift fur Anorg. und Allg. Chemie* **2014**, *640* (14), 2639–2648.

(95) Nesper, R. Structure and Chemical Bonding in Zintl-Phases Containing Lithium. *Prog. Solid State Chem.* **1990**, *20* (1), 1–45.

(96) Kurylyshyn, I. M.; Fässler, T. F.; Fischer, A.; Hauf, C.; Eickerling, G.; Presnitz, M.; Scherer, W. Probing the Zintl-Klemm Concept: A Combined Experimental and Theoretical Charge Density Study of the Zintl Phase CaSi. *Angew. Chemie - Int. Ed.* **2014**, *53* (11), 3029–3032.

(97) Qiu, J.; Fu, H.; Xu, Y.; Zhou, Q.; Meng, S.; Li, H.; Chen, L.; Wu, K. From Silicene to Half-Silicane by Hydrogenation. *ACS Nano* **2015**, *9* (11), 11192–11199.

(98) Wöhler, F. Ueber Verbindungen Des Siliciums Mit Sauerstoff Und Wasserstoff. J*ustus Liebigs Ann. Chem*. **1863**, *127* (3), 257–274.

(99) Kautsky, H. Über einige ungesättigte Siliciumverbindungen. *Z. Anorg. Allg. Chem.* **1921,** 117, 209-242.

(100) Weiss, A.; Beil, G.; Meyer, H. The Topochemical Reaction of CaSi2 to a Two-Dimensional Subsiliceous Acid Si6H3(OH)3 (= Kautskys' Siloxene). *Zeitschrift fur Naturforsch. - Sect. B J. Chem. Sci.* **1980**, *35* (1), 25–30.

(101) Fraser, S. Structure R. B. *Phys. Rev. B* **1993**, *48* (24), 872–877.

(102) Yamanaka, S.; Matsu-ura, H.; Ishikawa, M. New Deintercalation Reaction of Calcium from Calcium Disilicide. *Mater. Res. Bull.* **1996**, *31* (3), 307–316.

(103) Ali, M. A.; Tchalala, M. R. Chemical Synthesis of Silicon Nanosheets from Layered Calcium Disilicide. *J. Phys. Conf. Ser.* **2014**, *491* (1).

(104) Dean, J. A. *Lange's Hendbook of CHEMISTRY*; 1999.

(105) Nakano, H.; Nakano, M.; Nakanishi, K.; Tanaka, D.; Sugiyama, Y.; Ikuno, T.; Okamoto, H.; Ohta, T. Preparation of Alkyl-Modified Silicon Nanosheets by Hydrosilylation of Layered Polysilane (Si 6H 6). *J. Am. Chem. Soc.* **2012**, *134* (12), 5452–5455.

(106) Sugiyama, Y.; Okamoto, H.; Mitsuoka, T.; Morikawa, T.; Nakanishi, K.; Ohta, T.; Nakano, H. Synthesis and Optical Properties of Monolayer Organosilicon Nanosheets. *J. Am. Chem. Soc.*

2010, *132* (17), 5946–5947.

(107) Okamoto, H.; Kumai, Y.; Sugiyama, Y.; Mitsuoka, T.; Nakanishi, K.; Ohta, T.; Nozaki, H.; Yamaguchi, S.; Shirai, S.; Nakano, H. Silicon Nanosheets and Their Self-Assembled Regular Stacking Structure. *J. Am. Chem. Soc.* **2010**, *132* (8), 2710–2718.

(108) Knapp, D.; Brunschwig, B. S.; Lewis, N. S. Chemical, Electronic, and Electrical Properties of Alkylated Ge(111) Surfaces. *J. Phys. Chem. C* **2010**, *114* (28), 12300–12307.

(109) Vogg, G. U.; Brandt, M. S.; Stutzmann, M.; Albrecht, M. From CaSi2 to Siloxene: Epitaxial Silicide and Sheet Polymer Films on Silicon. *J. Cryst. Growth* **1999**, *203* (4), 570–581.

(110) Vogg, G.; Brandt, M. S.; Stutzmann, M.; Genchev, I.; Bergmaier, A.; Go, L.; Dollinger, G. Epitaxial CaGe " Lms on Germanium. **2000**, *212*, 148–154.

(111) Vogg, G.; Miesner, C.; Brandt, M. S.; Stutzmann, M.; Abstreiter, G. Epitaxial Alloy Films of Zintl-Phase Ca(Si1-XGex)2. *J. Cryst. Growth* **2001**, *223* (4), 573–576.

(112) Vogg, G.; Meyer, L. J. P.; Miesner, C.; Brandt, M. S.; Stutzmann, M. Polygermanosilyne Calcium Hydroxide Intercalation Compounds Formed by Topotactic Transformation of Ca(Si1-XGex)2 Alloy Zintl Phases in Ambient Atmosphere. *Monatshefte fur Chemie* **2001**, *132* (10), 1125–1135.

(113) Vogg, G.; Meyer, A. J. P.; Miesner, C.; Brandt, M. S.; Stutzmann, M. Efficient Tunable Luminescence of SiGe Alloy Sheet Polymers. *Appl. Phys. Lett.* **2001**, *78* (25), 3956–3958.

(114) Jiang, S.; Arguilla, M. Q.; Cultrara, N. D.; Goldberger, J. E. Improved Topotactic Reactions for Maximizing Organic Coverage of Methyl Germanane. *Chem. Mater.* **2016**, *28* (13), 4735–4740.

(115) Nakamura, D.; Nakano, H. Liquid-Phase Exfoliation of Germanane Based on Hansen Solubility Parameters. *Chem. Mater.* **2018**, *30* (15), 5333–5338.

(116) Jiang, S.; Krymowski, K.; Asel, T.; Arguilla, M. Q.; Cultrara, N. D.; Yanchenko, E.; Yang, X.; Brillson, L. J.; Windl, W.; Goldberger, J. E. Tailoring the Electronic Structure of Covalently Functionalized Germanane via the Interplay of Ligand Strain and Electronegativity. *Chem. Mater.* **2016**, *28* (21), 8071–8077.

(117) Hartman, T.; Šturala, J.; Luxa, J.; Sofer, Z. Chemistry of Germanene: Surface Modification of Germanane Using Alkyl Halides. *ACS Nano* **2020**, *14* (6), 7319–7327.

(118) Restrepo, O. D.; Krymowski, K. E.; Goldberger, J.; Windl, W. A First Principles Method to Simulate Electron Mobilities in 2D Materials. *New Journal of Physics* **2014**, *16* (10), 105009.

(119) Rosli, N. F.; Rohaizad, N.; Sturala, J.; Fisher, A. C.; Webster, R. D.; Pumera, M. Siloxene, Germanane, and Methylgermanane: Functionalized 2D Materials of Group 14 for Electrochemical Applications. *Adv. Funct. Mater.* **2020**, *30* (21), 1–11.

(120) Amamou, W.; Odenthal, P. M.; Bushong, E. J.; O'Hara, D. J.; Luo, Y. K.; Van Baren, J.; Pinchuk, I.; Wu, Y.; Ahmed, A. S.; Katoch, J.; Bockrath, M. W.; Tom, H. W. K.; Goldberger, J. E.; Kawakami, R. K. Large Area Epitaxial Germanane for Electronic Devices. *2D Mater.* **2015**, *2* (3).

(121) Liu, Z.; Wang, Z.; Sun, Q.; Dai, Y.; Huang, B. Methyl-Terminated Germanane GeCH 3 Synthesized by Solvothermal Method with Improved Photocatalytic Properties. *Appl. Surf. Sci.* **2019**, *467–468* (June 2018), 881–888.

(122) Yu, H.; Helbich, T.; Scherf, L. M.; Chen, J.; Cui, K.; Fässler, T. F.; Rieger, B.; Veinot, J. G. C. Radical-Initiated and Thermally Induced Hydrogermylation of Alkenes on the Surfaces of Germanium Nanosheets. *Chem. Mater.* **2018**, *30* (7), 2274–2280.

(123) Yu, H.; Thiessen, A. N.; Hossain, M. A.; Kloberg, M. J.; Rieger, B.; Veinot, J. G. C. Thermally-Induced Dehydrogenative Coupling of Organosilanes and H-Terminated Silicon Quantum Dots onto Germanane Surfaces. *Chem. Mater.* **2020**. *32* (11), 4536–4543

(124) Clark, T. J.; Lee, K.; Manners, I. Transition-Metal-Catalyzed Dehydrocoupling: A Convenient Route to Bonds between Main-Group Elements. *Chem. - A Eur. J.* **2006**, *12* (34), 8634–8648.

(125) Su, B.; Wu, Y.; Jiang, L. The Art of Aligning One-Dimensional (1D) Nanostructures. *Chem. Soc. Rev.* **2012**, *41* (23), 7832–7856.

(126) Tsuji, H.; Michl, J.; Tamao, K. Recent Experimental and Theoretical Aspects of the Conformational Dependence of UV Absorption of Short Chain Peralkylated Oligosilanes. *J. Organomet. Chem.* **2003**, *685* (1–2), 9–14.

(127) Schepers, T.; Michl, J. Optimized Ladder C and Ladder H Models for Sigma Conjugation: Chain Segmentation in Polysilanes. *J. Phys. Org. Chem.* **2002**, *15* (8), 490–498.

(128) Miller, R. D.; Michl, J. Polysilane High Polymers. *Chem. Rev.* **1989**, *89* (6), 1359–1410.

(129) Fukazawa, A.; Tsuji, H.; Tamao, K. All-Anti-Octasilane: Conformation Control of Silicon Chains Using the Bicyclic Trisilane as a Building Block. *J. Am. Chem. Soc.* **2006**, *128* (21), 6800–6801.

(130) Tsuji, H.; Toshimitsu, A.; Tamao, K. Unique Reactivity of a Diphenyldisilane Unit Incorporated in a Bicyclic Ring System: Generation of a Disilanyllithium via the Silicon-Phenyl Bond Cleavage with Lithium. *Khimiya Geterotsiklicheskikh Soedin.* **2001**, *37* (11), 1500–1505.

(131) Tamao, K.; Tsuji, H.; Terada, M.; Asahara, M.; Yamaguchi, S.; Toshimitsu, A. Conformation Control of Oligosilanes Based on Configurationally Constrained Bicyclic Disilane Units. *Angew. Chemie - Int. Ed.* **2000**, *39* (18), 3287–3290.

(132) Tsuji, H.; Fukazawa, A.; Yamaguchi, S.; Toshimitsu, A.; Tamao, K. All-Anti-Pentasilane: Conformation Control of Oligosilanes Based on the Bis(Tetramethylene)-Tethered Trisilane Unit. *Organometallics* **2004**, *23* (14), 3375–3377.

(133) Sato, K.; Tsuji, H.; Hirakuri, K.; Fukata, N.; Yamauchi, Y. Controlled Chemical Etching for Silicon Nanocrystals with Wavelength-Tunable Photoluminescence. *Chem. Commun.* **2009**, No. 25, 3759–3761.

(134) West, R.; Miller, R. D. Organometallics 1985, 4, 1318-1319 Registry. **1985**, No. 266, 1318–1319.

(135) Kipping, F. S.; Sands, J. E. XCIV.—Organic derivatives of silicon. Part XXVI. Piperidine as an

analytical reagent. **1921**, No. 848, 848–850.

(136) Kashimura, S.; Ishifune, M.; Yamashita, N.; Bu, H. B.; Takebayashi, M.; Kitajima, S.; Yoshiwara, D.; Kataoka, Y.; Nishida, R.; Kawasaki, S. I.; Murase, H.; Shono, T. Electroreductive Synthesis of Polysilanes, Polygermanes, and Related Polymers with Magnesium Electrodes. *J. Org. Chem.* **1999**, *64* (18), 6615–6621.

(137) Koe, J. Contemporary Polysilane Synthesis and Functionalisation. *Polym. Int.* **2009**, *58* (3), 255–260.

(138) Marro, E. A.; Klausen, R. S. Conjugated Polymers Inspired by Crystalline Silicon †. *Chem. Mater.* **2019**, *31* (7), 2202–2211.

(139) Amadoruge, M. L.; Weinert, C. S. Singly Bonded Catenated Germanes: Eighty Years of Progress. *Chem. Rev.* **2008**, *108* (10), 4253–4294.

(140) Mochida, K.; Chiba, H. Synthesis, Absorption Characteristics and Some Reactions of Polygermanes. *J. Organomet. Chem.* **1994**, *473* (1–2), 45–54.

(141) Shono, T.; Kashimura, S.; Murase, H. Electroreductive Synthesis of Polygermane and Germane-Silane Copolymer. *J. Chem. Soc. Chem. Commun.* **1992**, *19900* (12), 896–897.

(142) Aitken, C.; Harrod, J. F.; Malek, A.; Samuel, E. Oligomerization of Phenylgermanes by Catalytic Dehydrocoupling. *J. Organomet. Chem.* **1988**, *349* (3), 285–291.

(143) Choi, N.; Tanaka, M. Zirconocene-Catalyzed Dehydrogenative Coupling of Phenylgermane and Properties of the Resulting Partially Network Polyphenylgermanes. *J. Organomet. Chem.* **1998**, *564* (1–2), 81–84.

(144) Baumgartner, T.; Jäkle, F. *Main Group Strategies towards Functional Hybrid Materials*; 2017.

(145) Katz, S. M.; Reichl, J. A.; Berry, D. H. Catalytic Synthesis of Poly(Arylmethylgermanes) by Demethanative Coupling: A Mild Route to σ-Conjugated Polymers. *J. Am. Chem. Soc.* **1998**, *120* (38), 9844–9849.

(146) Reichl, J. A.; Popoff, C. M.; Gallagher, L. A.; Remsen, E. E.; Berry, D. H. Ruthenium-Catalyzed Demethanative Coupling of HGeMe3: A High Yield Route to Polygermanes. *J. Am. Chem. Soc.* **1996**, *118* (39), 9430–9431.

(147) Royen, P.; Rocktäschel, C. Zur Kenntnis Niedere Hydride Des Siliciums Und Germaniums. *ZAAC - J. Inorg. Gen. Chem.* **1966**, *346* (5–6), 279–289.

(148) Yu, H.; Ni, C.; Thiessen, A. N.; Li, Z.; Veinot, J. G. C. Synthesis, Properties, and Derivatization of Poly(Dihydrogermane): A Germanium-Based Polyethylene Analogue. *ACS Nano* **2021**. *15* (6), 9368–9378

(149) Palenzona, A.; Manfrinetti, P.; Fornasini, M. L. The Phase Diagram of the Ca-Ge System. *J. Alloys Compd.* **2002**, *345* (1–2), 144–147.

(150) Leon-Escamilla, E. A.; Corbett, J. D. Hydrogen Impurity Effects. A5Tt3 Intermetallic Compounds between A = Ca, Sr, Ba, Eu and Tt = Si, Ge, Sn with Cr5B3-like Structures That Are Stable Both as Binary and as Ternary Hydride and Fluoride Phases. *J. Solid State Chem.*

2001, *159* (1), 149–162.

(151) Borchardt-Ott, W. Die Kristallstruktur. **1990**, *319* (1926), 21–26.

(152) Alloy, B.; Diagrams, P.; Okamoto, H.; Subramanian, P. R.; Kacprzak, L. Ca (Calcium) Binary Alloy Phase Diagrams. *Alloy Phase Diagrams* **2018**, *3*, 228–238.

(153) Djaballah, Y.; Pasturel, A.; Belgacem-Bouzida, A. Thermodynamic Assessment of the Calcium-Germanium System. *J. Alloys Compd.* **2010**, *497* (1–2), 74–79.

(154) Schafer, H. Work for the Modern Chemistry of Intermetallics. *Annu. Rev. Mater. Sci.* **1985**, *15*, 1–41.

(155) Arguilla, M. Q.; Cultrara, N. D.; Scudder, M. R.; Jiang, S.; Ross, R. D.; Goldberger, J. E. Optical Properties and Raman-Active Phonon Modes of Two-Dimensional Honeycomb Zintl Phases. *J. Mater. Chem. C* **2017**, *5* (43),

(156) Cultrara, N. D.; Wang, Y.; Arguilla, M. Q.; Scudder, M. R.; Jiang, S.; Windl, W.; Bobev, S.; Goldberger, J. E. Synthesis of 1T, 2H, and 6R Germanane Polytypes. *Chem. Mater.* **2018**, *30* (4), 1335–1343.

(157) Tobash, P. H.; Bobev, S. Synthesis, Structure and Electronic Structure of a New Polymorph of CaGe2. *J. Solid State Chem.* **2007**, *180* (5), 1575–1581.

(158) Ambrosi, A.; Pumera, M. Exfoliation of Layered Materials Using Electrochemistry. *Chem. Soc. Rev.* **2018**, *47* (19), 7213–7224.

(159) Halim, U.; Zheng, C. R.; Chen, Y.; Lin, Z.; Jiang, S.; Cheng, R.; Huang, Y.; Duan, X. A Rational Design of Cosolvent Exfoliation of Layered Materials by Directly Probing Liquid-Solid Interaction. *Nat. Commun.* **2013**, *4*, 1–7.

(160) Wu, W.; Xu, J.; Tang, X.; Xie, P.; Liu, X.; Xu, J.; Zhou, H.; Zhang, D.; Fan, T. Two-Dimensional Nanosheets by Rapid and Efficient Microwave Exfoliation of Layered Materials. *Chem. Mater.* **2018**, *30* (17), 5932–5940.

(161) Cardon, M. The Devil and the Surfaces. *Physics (College. Park. Md).* **1945**, 1945–1945.

(162) Kovacs, G. T. A.; Maluf, N. I.; Petersen, K. E. Bulk Micromachining of Silicon. *Proc. IEEE* **1998**, *86* (8), 1536–1551.

(163) K.E. Jensen.; D. Pennachio.; D. Recht.; D.A. Weitz.; F. Spaepen, "Rapid growth of large, defect-free colloidal crystals", **2013**, Soft Matter 9: 320-328.

(164) Buriak, J. M. Organometallic Chemistry on Silicon and Germanium Surfaces. *Chem. Rev.* **2002**, *102* (5), 1271–1308.

(165) Loscutoff, P. W.; Bent, S. F. Reactivity of the Germanium Surface: Chemical Passivation and Functionalization. *Annu. Rev. Phys. Chem.* **2006**, *57*, 467–495.

(166) Maeda, Y. Visible Photoluminescence from Nanocrystallite Ge Embedded in a Glassy SiO2 Matrix: Evidence in Support of the Quantum-Confinement Mechanism. *Phys. Rev. B* **1995**, *51* (3), 1658–1670.

(167) Maeda, Y.; Tsukamoto, N.; Yazawa, Y.; Kanemitsu, Y.; Masumoto, Y. Visible

Photoluminescence of Ge Microcrystals Embedded in SiO2 Glassy Matrices. *Appl. Phys. Lett.* **1991**, *59* (24), 3168–3170.

(168) Cho, S.; Man Kang, I.; Rok Kim, K.; Park, B.-G.; Harris, J. S. Silicon-Compatible High-Hole-Mobility Transistor with an Undoped Germanium Channel for Low-Power Application. *Applied Physics Letters* **2013**, *103* (22), 222102.

(169) Higashi, G. S.; Chabal, Y. J.; Trucks, G. W.; Raghavachari, K. Ideal Hydrogen Termination of the Si (111) Surface. *Appl. Phys. Lett.* **1990**, *56* (7), 656–658.

(170) Deegan, T.; Hughes, G. An X-Ray Photoelectron Spectroscopy Study of the HF Etching of Native Oxides on Ge(111) and Ge(100) Surfaces. *Appl. Surf. Sci.* **1998**, *123–124*, 66–70.

(171) He, J.; Patitsas, S. N.; Preston, K. F.; Wolkow, R. A.; Wayner, D. D. M. Covalent Bonding of Thiophenes to Si(111) by a Halogenation/Thienylation Route. *Chemical Physics Letters*. **1998**, pp 508–514.

(172) Okubo, T.; Tsuchiya, H.; Sadakata, M.; Yasuda, T.; Tanaka, K. Organic Functional Group Introduced to Si(1 1 1) via Silicon-Carbon Bond: A Liquid-Phase Approach. *Appl. Surf. Sci.* **2001**, *171* (3–4), 252–256.

(173) Bansal, A.; Li, X.; Lauermann, I.; Lewis, N. S.; Yi, S. I.; Weinberg, W. H. Alkylation of Si Surfaces Using a Two-Step Halogenation/Grignard Route. *J. Am. Chem. Soc.* **1996**, *118* (30), 7225–7226.

(174) Wong, K. T.; Kim, Y. G.; Soriaga, M. P.; Brunschwig, B. S.; Lewis, N. S. Synthesis and Characterization of Atomically Flat Methyl-Terminated Ge(111) Surfaces. *J. Am. Chem. Soc.* **2015**, *137* (28), 9006–9014.

(175) Warner, J. H.; Hoshino, A.; Yamamoto, K.; Tilley, R. D. Water-Soluble Photoluminescent Silicon Quantum Dots. *Angew. Chemie - Int. Ed.* **2005**, *44* (29), 4550–4554.

(176) Sieval, A. B.; Linke, R.; Zuilhof, H.; Sudhölter, E. J. R. High-Quality Alkyl Monolayers on Silicon Surfaces. *Adv. Mater.* **2000**, *12* (19), 1457–1460.

(177) Purkait, T. K.; Iqbal, M.; Wahl, M. H.; Gottschling, K.; Gonzalez, C. M.; Islam, M. A.; Veinot, J. G. C. Borane-Catalyzed Room-Temperature Hydrosilylation of Alkenes/Alkynes on Silicon Nanocrystal Surfaces. *J. Am. Chem. Soc.* **2014**, *136* (52), 17914–17917.

(178) Ciampi, S.; Harper, J. B.; Gooding, J. J. Wet Chemical Routes to the Assembly of Organic Monolayers on Silicon Surfaces via the Formation of Si-C Bonds: Surface Preparation, Passivation and Functionalization. *Chem. Soc. Rev.* **2010**, *39* (6), 2158–2183.

(179) Wang, D.; Buriak, J. M. Trapping Silicon Surface-Based Radicals. *Langmuir* **2006**, *22* (14), 6214–6221.

(180) Liu, F.; Luber, E. J.; Huck, L. A.; Olsen, B. C.; Buriak, J. M. Nanoscale Plasmonic Stamp Lithography on Silicon. *ACS Nano* **2015**, *9* (2), 2184–2193.

(181) Yang, L.; Lua, Y. Y.; Lee, M. V.; Linford, M. R. Chemomechanical Functionalization and Patterning of Silicon. *Acc. Chem. Res.* **2005**, *38* (12), 933–942.

(182) Shirahata, N.; Linford, M. R.; Furumi, S.; Pei, L.; Sakka, Y.; Gates, R. J.; Asplund, M. C. Laser-Derived One-Pot Synthesis of Silicon Nanocrystals Terminated with Organic Monolayers. *Chem. Commun.* **2009**, No. 31, 4684–4686.

(183) Linford, M. R.; Chidsey, C. E. D.; Fenter, P.; Eisenberger, P. M. Alkyl Monolayers on Silicon Prepared from 1-Alkenes and Hydrogen-Terminated Silicon. *J. Am. Chem. Soc.* **1995**, *117* (11), 3145–3155.

(184) Wagner, P.; Nock, S.; Spudich, J. A.; Volkmuth, W. D.; Chu, S.; Cicero, R. L.; Wade, C. P.; Linford, M. R.; Chidsey, C. E. D. Bioreactive Self-Assembled Monolayers on Hydrogen-Passivated Si(111) as a New Class of Atomically Flat Substrates for Biological Scanning Probe Microscopy. *J. Struct. Biol.* **1997**, *119* (2), 189–201.

(185) Boukherroub, R.; Petit, A.; Loupy, A.; Chazalviel, J. N.; Ozanam, F. Microwave-Assisted Chemical Functionalization of Hydrogen-Terminated Porous Silicon Surfaces. *J. Phys. Chem. B* **2003**, *107* (48), 13459–13462.

(186) Boukherroub, R.; Morin, S.; Bensebaa, F.; Wayner, D. D. M. New Synthetic Routes to Alkyl Monolayers on the Si(111) Surface. *Langmuir* **1999**, *15* (11), 3831–3835.

(187) Gerlich, D.; Cullen, G. W.; Amick, J. A. The Stabilization of Germanium Surfaces by Ethylation. *J. Electrochem. Soc.* **1962**, *109* (2), 133.

(188) Truong, K. D.; Rowntree, P. A. Formation of Self-Assembled Butanethiol Monolayers on Au Substrates: Spectroscopic Evidence for Highly Ordered Island Formation in Sub-Monolayer Films. *J. Phys. Chem.* **1996**, *100* (51), 19917–19926.

(189) Yu, H.; Webb, L. J.; Heath, J. R.; Lewis, N. S. Scanning Tunneling Spectroscopy of Methyl- and Ethyl-Terminated Si(111) Surfaces. *Appl. Phys. Lett.* **2006**, *88* (25), 2–4.

(190) Han, S. M.; Ashurst, W. R.; Carraro, C.; Maboudian, R. Formation of Alkanethiol Monolayer on Ge(111). *J. Am. Chem. Soc.* **2001**, *123* (10), 2422–2425.

(191) Choi, K.; Buriak, J. M. Hydrogermylation of Alkenes and Alkynes on Hydride-Terminated Ge(100) Surfaces. *Langmuir* **2000**, *16* (20), 7737–7741.

(192) Li, Y. H.; Wang, D.; Buriak, J. M. Molecular Layer Deposition of Thiol - Ene Multilayers on Semiconductor Surfaces. *Langmuir* **2010**, *26* (2), 1232–1238.

(193) Li, Y. H.; Buriak, J. M. Dehydrogenative Silane Coupling on Silicon Surfaces via Early Transition Metal Catalysis. *Inorg. Chem.* **2006**, *45* (3), 1096–1102.

(194) Chuah, L. S.; Hassan, Z.; Hassan, H. A. Visible-Light Emission Due to Quantum Size Effects in Porous Crystalline Silicon. *AIP Conf. Proc.* **2010**, *1250* (September), 385–388.

(195) Bodlaki, D.; Yamamoto, H.; Waldeck, D. H.; Borguet, E. Ambient Stability of Chemically Passivated Germanium Interfaces. *Surf. Sci.* **2003**, *543* (1–3), 63–74.

(196) Kluth, G. J.; Sung, M. M.; Maboudian, R. Thermal Behavior of Alkylsiloxane Self-Assembled Monolayers on the Oxidized Si(100) Surface. *Langmuir* **1997**, *13* (14), 3775–3780.

(197) Höhlein, I. M. D.; Angi, A.; Sinelnikov, R.; Veinot, J. G. C.; Rieger, B. Functionalization of

Hydride-Terminated Photoluminescent Silicon Nanocrystals with Organolithium Reagents. *Chem. - A Eur. J.* **2015**, *21* (7), 2755–2758.

(198) Fok, E.; Shih, M.; Meldrum, A.; Veinot, J. G. C. Preparation of Alkyl-Surface Functionalized Germanium Quantum Dots via Thermally Initiated Hydrogermylation. *Chem. Commun.* **2004**, *4* (4), 386–387.

(199) Yu, Y.; Rowland, C. E.; Schaller, R. D.; Korgel, B. A. Synthesis and Ligand Exchange of Thiol-Capped Silicon Nanocrystals. *Langmuir* **2015**, *31* (24), 6886–6893.

(200) Holmberg, V. C.; Korgel, B. A. Corrosion Resistance of Thiol- and Alkene-Passivated Germanium Nanowires. *Chem. Mater.* **2010**, *22* (12), 3698–3703.

(201) Cheng, X.; Lowe, S. B.; Ciampi, S.; Magenau, A.; Gaus, K.; Reece, P. J.; Gooding, J. J. Versatile "Click Chemistry" Approach to Functionalizing Silicon Quantum Dots: Applications toward Fluorescent Cellular Imaging. *Langmuir* **2014**, *30* (18), 5209–5216.

(202) Veinot, J. G. C. Synthesis, Surface Functionalization, and Properties of Freestanding Silicon Nanocrystals. *Chem. Commun.* **2006**, No. 40, 4160–4168.

(203) Thiessen, A. N.; Zhang, L.; Oliynyk, A. O.; Yu, H.; O'Connor, K. M.; Meldrum, A.; Veinot, J. G. C. A Tale of Seemingly "Identical" Silicon Quantum Dot Families: Structural Insight into Silicon Quantum Dot Photoluminescence. *Chem. Mater.***2020**, *32* (16), 6838–6846

(204) Yang, Z.; Iqbal, M.; Dobbie, A. R.; Veinot, J. G. C. Surface-Induced Alkene Oligomerization: Does Thermal Hydrosilylation Really Lead to Monolayer Protected Silicon Nanocrystals? *J. Am. Chem. Soc.* **2013**, *135* (46), 17595–17601.

(205) Tilley, R. D.; Warner, J. H.; Yamamoto, K.; Matsui, I.; Fujimori, H. Micro-Emulsion Synthesis of Monodisperse Surface Stabilized Silicon Nanocrystals. *Chem. Commun.* **2005**, No. 14, 1833–1835.

(206) Höhlein, I. M. D.; Kehrle, J.; Helbich, T.; Yang, Z.; Veinot, J. G. C.; Rieger, B. Diazonium Salts as Grafting Agents and Efficient Radical-Hydrosilylation Initiators for Freestanding Photoluminescent Silicon Nanocrystals. *Chem. - A Eur. J.* **2014**, *20* (15), 4212–4216.

(207) Yu, Y.; Hessel, C. M.; Bogart, T. D.; Panthani, M. G.; Rasch, M. R.; Korgel, B. A. Room Temperature Hydrosilylation of Silicon Nanocrystals with Bifunctional Terminal Alkenes. *Langmuir* **2013**, *29* (5), 1533–1540.

(208) Yang, Z.; Gonzalez, C. M.; Purkait, T. K.; Iqbal, M.; Meldrum, A.; Veinot, J. G. C. Radical Initiated Hydrosilylation on Silicon Nanocrystal Surfaces: An Evaluation of Functional Group Tolerance and Mechanistic Study. *Langmuir* **2015**, *31* (38), 10540–10548.

(209) Dasog, M.; De Los Reyes, G. B.; Titova, L. V.; Hegmann, F. A.; Veinot, J. G. C. Size vs Surface: Tuning the Photoluminescence of Freestanding Silicon Nanocrystals Across the Visible Spectrum via Surface Groups. *ACS Nano* **2014**, *8* (9), 9636–9648.

(210) Dasog, M.; Yang, Z.; Regli, S.; Atkins, T. M.; Faramus, A.; Singh, M. P.; Muthuswamy, E.; Kauzlarich, S. M.; Tilley, R. D.; Veinot, J. G. C. Chemical Insight into the Origin of Red and

Blue Photoluminescence Arising from Freestanding Silicon Nanocrystals. *ACS Nano* **2013**, *7* (3), 2676–2685.

(211) Dasog, M.; Veinot, J. G. C. Size Independent Blue Luminescence in Nitrogen Passivated Silicon Nanocrystals. *Phys. Status Solidi Appl. Mater. Sci.* **2012**, *209* (10), 1844–1846.

(212) Wilcoxon, J. P.; Provencio, P. P.; Samara, G. A. Synthesis and Optical Properties of Colloidal Germanium Nanocrystals. *Phys. Rev. B - Condens. Matter Mater. Phys.* **2001**, *64* (3), 1–9.

(213) Tanke, R. S.; Kauzlarich, S. M.; Patten, T. E.; Pettigrew, K. A.; Murphy, D. L.; Thompson, M. E.; Lee, H. W. H. Synthesis of Germanium Nanoclusters with Irreversibly Attached Functional Groups : Acetals , Alcohols , Esters , and Polymers. **2003**, No. 15, 1682–1689.

(214) Lambert, T. N.; Andrews, N. L.; Gerung, H.; Boyle, T. J.; Oliver, J. M.; Wilson, B. S.; Han, S. M. Water-Soluble Germanium (0) Nanocrystals : Cell Recognition and Near-Infrared Photothermal Conversion Properties. **2007**, *87131*, 691–699.

(215) Ruddy, D. A.; Erslev, P. T.; Habas, S. E.; Seabold, J. A.; Neale, N. R. Surface Chemistry Exchange of Alloyed Germanium Nanocrystals: A Pathway Toward Conductive Group IV Nanocrystal Films. **2013**. *4* (3), 416–421

(216) Near-, S. S.; Ruddy, D. A.; Johnson, J. C.; Smith, E. R.; Neale, N. R. Size and Bandgap Control in The. **2010**, *4* (12), 7459–7466.

(217) Iqbal, M.; Purkait, T. K.; Goss, G. G.; Bolton, J. R.; Gamal El-Din, M.; Veinot, J. G. C. Application of Engineered Si Nanoparticles in Light-Induced Advanced Oxidation Remediation of a Water-Borne Model Contaminant. *ACS Nano* **2016**, *10* (5), 5405–5412.

(218) Holmes, A. L.; Hütges, J.; Reckmann, A.; Muthuswamy, E.; Meerholz, K.; Kauzlarich, S. M. Probing Electronics as a Function of Size and Surface of Colloidal GERMANIUM NANOCRYSTALS. *The Journal of Physical Chemistry C* **2015**, *119* (10), 5671–5678.

(219) Wheeler, L. M.; Nichols, A. W.; Chernomordik, B. D.; Anderson, N. C.; Beard, M. C.; Neale, N. R. All-Inorganic Germanium Nanocrystal Films By Cationic LIGAND EXCHANGE. *Nano Letters* **2016**, *16* (3), 1949–1954.

(220) Carolan, D. Recent Advances in Germanium Nanocrystals: Synthesis, Optical Properties and Applications. *Prog. Mater. Sci.* **2017**, *90*, 128–158.

(221) Helbich, T.; Lyuleeva, A.; Ludwig, T.; Scherf, L. M.; Fässler, T. F.; Lugli, P.; Rieger, B. One-Step Synthesis of Photoluminescent Covalent Polymeric Nanocomposites from 2D Silicon Nanosheets. *Adv. Funct. Mater.* **2016**, *26* (37), 6711–6718.

(222) Helbich, T.; Lyuleeva, A.; Höhlein, I. M. D.; Marx, P.; Scherf, L. M.; Kehrle, J.; Fässler, T. F.; Lugli, P.; Rieger, B. Radical-Induced Hydrosilylation Reactions for the Functionalization of Two-Dimensional Hydride Terminated Silicon Nanosheets. *Chem. - A Eur. J.* **2016**, *22* (18), 6194–6198.

(223) Lyuleeva, A.; Holzmüller, P.; Helbich, T.; Stutzmann, M.; Brandt, M. S.; Becherer, M.; Lugli, P.; Rieger, B. Charge Transfer Doping in Functionalized Silicon Nanosheets/P3HT Hybrid

Material for Applications in Electrolyte-Gated Field-Effect Transistors. *J. Mater. Chem. C* **2018**, *6* (27), 7343–7352.

(224) Lyuleeva, A.; Helbich, T.; Rieger, B.; Lugli, P. Polymer-Silicon Nanosheet Composites: Bridging the Way to Optoelectronic Applications. *J. Phys. D. Appl. Phys.* **2017**, *50* (13).

(225) Helbich, T.; Lyuleeva, A.; Marx, P.; Scherf, L. M.; Purkait, T. K.; Fässler, T. F.; Lugli, P.; Veinot, J. G. C.; Rieger, B. Lewis Acid Induced Functionalization of Photoluminescent 2D Silicon Nanosheets for the Fabrication of Functional Hybrid Films. *Adv. Funct. Mater.* **2017**, *27* (21).

(226) Okamoto, H.; Sugiyama, Y.; Nakanishi, K.; Ohta, T.; Mitsuoka, T.; Nakano, H. Surface Modification of Layered Polysilane with n -Alkylamines, α,ω-Diaminoalkanes, and ω-Aminocarboxylic Acids. *Chem. Mater.* **2015**, *27* (4), 1292–1298.

(227) Ohshita, J.; Yamamoto, K.; Tanaka, D.; Nakashima, M.; Kunugi, Y.; Ohashi, M.; Nakano, H. Preparation and Photocurrent Generation of Silicon Nanosheets with Aromatic Substituents on the Surface. *J. Phys. Chem. C* **2016**, *120* (20), 10991–10996.

(228) Ohashi, M.; Shirai, S.; Nakano, H. Direct Chemical Synthesis of Benzyl-Modified Silicane from Calcium Disilicide. *Chem. Mater.* **2019**, *31* (13), 4720–4725.

Chapter 2

(1) Grötsch, R. K.; Boekhoven, J. *Unique Properties of Supramolecular Biomaterials through Nonequilibrium Self-Assembly*; Elsevier Ltd., 2018.

(2) Mitchison, T. J.; Biol, J. C.; Kelleher, J. F.; Atkinson, S. J.; Pollard, T. D.; Biol, J. C.; Hartgerink, J. D.; Beniash, E.; Stupp, S. I. Self-Assembly and Mineralization of Peptide-Amphiphile Nanofibers. **2001**, *294* (November), 1684–1689.

(3) Israelachvili, J. N.; Mitchell, D. J.; Ninham, B. W. Theory of Self-Assembly of Hydrocarbon Amphiphiles into Micelles and Bilayers. *J. Chem. Soc. Faraday Trans. 2 Mol. Chem. Phys.* **1976**, *72*, 1525–1568.

(4) Van Rossum, S. A. P.; Tena-Solsona, M.; Van Esch, J. H.; Eelkema, R.; Boekhoven, J. Dissipative Out-of-Equilibrium Assembly of Man-Made Supramolecular Materials. *Chem. Soc. Rev.* **2017**, *46* (18), 5519–5535.

(5) Silva, G. A.; Czeisler, C.; Niece, K. L.; Beniash, E.; Harrington, D. A.; Kessler, J. A.; Stupp, S. I. Selective Differentiation of Neural Progenitor Cells by High-Epitope Density Nanofibers. *Science (80-.).* **2004**, *303* (5662), 1352–1355.

(6) Zhang, S. Fabrication of Novel Biomaterials through Molecular Self-Assembly. *Nat. Biotechnol.* **2003**, *21* (10), 1171–1178.

(7) Erogbogbo, F.; Yong, K.; Roy, I.; Xu, G.; Prasad, P. N.; Swihart, M. T. Biocompatible Luminescent Silicon. *ACS Nano* **2008**, *2* (5), 873–878.

(8) Hessel, C. M.; Rasch, M. R.; Hueso, J. L.; Goodfellow, B. W.; Akhavan, V. A.; Puvanakrishnan, P.; Tunnel, J. W.; Korgel, B. A. Alkyl Passivation and Amphiphilic Polymer Coating of Silicon

Nanocrystals for Diagnostic Imaging. *Small* **2010**, *6* (18), 2026–2034.

(9) Dasog, M.; Veinot, J. G. C. Size Independent Blue Luminescence in Nitrogen Passivated Silicon Nanocrystals. *Phys. Status Solidi Appl. Mater. Sci.* **2012**, *209* (10), 1844–1846.

(10) Cheng, X.; Lowe, S. B.; Ciampi, S.; Magenau, A.; Gaus, K.; Reece, P. J.; Gooding, J. J. Versatile "Click Chemistry" Approach to Functionalizing Silicon Quantum Dots: Applications toward Fluorescent Cellular Imaging. *Langmuir* **2014**, *30* (18), 5209–5216.

(11) Sorrenti, A.; Leira-Iglesias, J.; Markvoort, A. J.; De Greef, T. F. A.; Hermans, T. M. Non-Equilibrium Supramolecular Polymerization. *Chem. Soc. Rev.* **2017**, *46* (18), 5476–5490.

(12) Heinen, L.; Heuser, T.; Steinschulte, A.; Walther, A. Antagonistic Enzymes in a Biocatalytic Ph Feedback System Program Autonomous DNA Hydrogel Life Cycles. *Nano Lett.* **2017**, *17* (8), 4989–4995.

(13) della Sala, F.; Neri, S.; Maiti, S.; Chen, J. L. Y.; Prins, L. J. Transient Self-Assembly of Molecular Nanostructures Driven by Chemical Fuels. *Curr. Opin. Biotechnol.* **2017**, *46*, 27–33.

(14) Merindol, R.; Walther, A. Materials Learning from Life: Concepts for Active, Adaptive and Autonomous Molecular Systems. *Chem. Soc. Rev.* **2017**, *46* (18), 5588–5619.

(15) Whitesides, G. M.; Boncheva, M. Beyond Molecules: Self-Assembly of Mesoscopic and Macroscopic Components. *Proc. Natl. Acad. Sci. U. S. A.* **2002**, *99* (8), 4769–4774.

(16) Patist, A.; Oh, S. G.; Leung, R.; Shah, D. O. Kinetics of Micellization: Its Significance to Technological Processes. *Colloids Surfaces A Physicochem. Eng. Asp.* **2001**, *176* (1), 3–16.

(17) Van Ravensteijn, B. G. P.; Hendriksen, W. E.; Eelkema, R.; Van Esch, J. H.; Kegel, W. K. Fuel-Mediated Transient Clustering of Colloidal Building Blocks. *J. Am. Chem. Soc.* **2017**, *139* (29), 9763–9766.

(18) Tena-Solsona, M.; Rieß, B.; Grötsch, R. K.; Löhrer, F. C.; Wanzke, C.; Käsdorf, B.; Bausch, A. R.; Müller-Buschbaum, P.; Lieleg, O.; Boekhoven, J. Non-Equilibrium Dissipative Supramolecular Materials with a Tunable Lifetime. *Nat. Commun.* **2017**, *8* (May), 1–8.

(19) Kundu, P. K.; Das, S.; Ahrens, J.; Klajn, R. Controlling the Lifetimes of Dynamic Nanoparticle Aggregates by Spiropyran Functionalization. *Nanoscale* **2016**, *8* (46), 19280–19286.

(20) Klajn, R.; Wesson, P. J.; Bishop, K. J. M.; Grzybowski, B. A. Writing Self-Erasing Images Using Metastable Nanoparticle "Inks." *Angew. Chemie - Int. Ed.* **2009**, *48* (38), 7035–7039.

(21) Grötsch, R. K.; Angı, A.; Mideksa, Y. G.; Wanzke, C.; Tena-Solsona, M.; Feige, M. J.; Rieger, B.; Boekhoven, J. Dissipative Self-Assembly of Photoluminescent Silicon Nanocrystals. *Angew. Chemie - Int. Ed.* **2018**, *57* (44), 14608–14612.

(22) Rieß, B.; Grötsch, R. K.; Boekhoven, J. The Design of Dissipative Molecular Assemblies Driven by Chemical Reaction Cycles. *Chem* **2020**, *6* (3), 552–578.

(23) Thiessen, A. N.; Zhang, L.; Oliynyk, A. O.; Yu, H.; O'Connor, K. M.; Meldrum, A.; Veinot, J. G. C. A Tale of Seemingly "Identical" Silicon Quantum Dot Families: Structural Insight into Silicon Quantum Dot Photoluminescence. *Chem. Mater.***2020**, 32, 16, 6838–6846

(24) Robidillo, C. J. T.; Islam, M. A.; Aghajamali, M.; Faramus, A.; Sinelnikov, R.; Zhang, X.; Boekhoven, J.; Veinot, J. G. C. Functional Bioinorganic Hybrids from Enzymes and Luminescent Silicon-Based Nanoparticles. *Langmuir* **2018**, *34* (22), 6556–6569.

(25) Clark, R. J.; Dang, M. K. M.; Veinot, J. G. C. Exploration of Organic Acid Chain Length on Water-Soluble Silicon Quantum Dot Surfaces. *Langmuir* **2010**, *26* (19), 15657–15664.

(26) Zacharie, B.; Abbott, S. D.; Baigent, C. B.; Doyle, C.; Yalagala, R. S. An Efficient Two-Step Preparation of α-, β-, γ- or δ-Amino Acids from 2-Pyrazinones, 2-Hydroxypyrimidines or 2-Pyridones Respectively. *European J. Org. Chem.* **2018**, *2018* (46), 6486–6493.

(27) Kariyawasam, L. S.; Hartley, C. S. Dissipative Assembly of Aqueous Carboxylic Acid Anhydrides Fueled by Carbodiimides. *J. Am. Chem. Soc.* **2017**, *139* (34), 11949–11955.

(28) Boekhoven, J.; Brizard, A. M.; Kowlgi, K. N. K.; Koper, G. J. M.; Eelkema, R.; Van Esch, J. H. Dissipative Self-Assembly of a Molecular Gelator by Using a Chemical Fuel. *Angew. Chemie - Int. Ed.* **2010**, *49* (28), 4825–4828.

(29) Grötsch, R. K.; Wanzke, C.; Speckbacher, M.; Angl, A.; Rieger, B.; Boekhoven, J. Pathway Dependence in the Fuel-Driven Dissipative Self-Assembly of Nanoparticles. *J. Am. Chem. Soc.* **2019**. *141* (25), 9872–9878

(30) Hessel, C. M.; Henderson, E. J.; Veinot, J. G. C. Hydrogen Silsesquioxane: A Molecular Precursor for Nanocrystalline Si-SiO2 Composites and Freestanding Hydride-Surface-Terminated Silicon Nanoparticles. *Chem. Mater.* **2006**, *18* (26), 6139–6146.

(31) Tamm, L. K.; Tatulian, S. A. Infrared Spectroscopy of Proteins and Peptides in Lipid Bilayers. *Q. Rev. Biophys.* **1997**, *30* (4), 365–429.

(32) Jedlovszky-Hajdú, A.; Bombelli, F. B.; Monopoli, M. P.; Tombácz, E.; Dawson, K. A. Surface Coatings Shape the Protein Corona of SPIONs with Relevance to Their Application in Vivo. *Langmuir* **2012**, *28* (42), 14983–14991.

(33) Damodaran, V. B.; Fee, C. J.; Ruckh, T.; Popat, K. C. Conformational Studies of Covalently Grafted Poly(Ethylene Glycol) on Modified Solid Matrices Using X-Ray Photoelectron Spectroscopy. *Langmuir* **2010**, *26* (10), 7299–7306.

(34) Briggs, D.; Beamson, G. Primary and Secondary Oxygen-Induced C1s Binding Energy Shifts in X-Ray Photoelectron Spectroscopy of Polymers. *Anal. Chem.* **1992**, *64* (15), 1729–1736.

(35) Buhl, M.; Vonhören, B.; Ravoo, B. J. Immobilization of Enzymes via Microcontact Printing and Thiol-Ene Click Chemistry. *Bioconjug. Chem.* **2015**, *26* (6), 1017–1020.

Chapter 3

(1) Vaughn, D. D.; Schaak, R. E. Synthesis, Properties and Applications of Colloidal Germanium. Pdfnd Germanium-Based Nanomaterials. *Chem. Soc. Rev.* **2013**, *42* (7), 2861–2879.

(2) Michel, J.; Liu, J.; Kimerling, L. C. High-Performance Ge-on-Si Photodetectors. *Nat. Photonics*

2010, *4* (8), 527–534.

(3) Henderson, E. J.; Seino, M.; Puzzo, D. P.; Ozin, G. A. Colloidally Stable Germanium Nanocrystals for Photonic Applications. *ACS Nano* **2010**, *4* (12), 7683–7691.

(4) Kennedy, T.; Brandon, M.; Ryan, K. M. Advances in the Application of Silicon and Germanium Nanowires for High-Performance Lithium-Ion Batteries. *Adv. Mater.* **2016**, *28* (27), 5696–5704.

(5) Mortazavi, B.; Dianat, A.; Cuniberti, G.; Rabczuk, T. Application of Silicene, Germanene and Stanene for Na or Li Ion Storage: A Theoretical Investigation. *Electrochim. Acta* **2016**, *213*, 865–870.

(6) Liu, N.; Bo, G.; Liu, Y.; Xu, X.; Du, Y.; Dou, S. X. Recent Progress on Germanene and Functionalized Germanene: Preparation, Characterizations, Applications, and Challenges. *Small* **2019**, *15* (32), 1–11.

(7) Rosli, N. F.; Rohaizad, N.; Sturala, J.; Fisher, A. C.; Webster, R. D.; Pumera, M. Siloxene, Germanane, and Methylgermanane: Functionalized 2D Materials of Group 14 for Electrochemical Applications. *Adv. Funct. Mater.* **2020**, *30* (21), 1–11.

(8) Nakamura, D.; Nakano, H. Liquid-Phase Exfoliation of Germanane Based on Hansen Solubility Parameters. *Chem. Mater.* **2018**, *30* (15), 5333–5338.

(9) Carolan, D. Recent Advances in Germanium Nanocrystals: Synthesis, Optical Properties and Applications. *Prog. Mater. Sci.* **2017**, *90*, 128–158.

(10) Buriak, J. M. Organometallic Chemistry on Silicon and Germanium Surfaces. *Chem. Rev.* **2002**, *102* (5), 1271–1308.

(11) Collins, G.; Holmes, J. D. Chemical Functionalisation of Silicon and Germanium Nanowires. *J. Mater. Chem.* **2011**, *21* (30), 11052–11069.

(12) Yu, H.; Thiessen, A. N.; Hossain, M. A.; Kloberg, M. J.; Rieger, B.; Veinot, J. G. C. Thermally Induced Dehydrogenative Coupling of Organosilanes and H-Terminated Silicon Quantum Dots onto Germanane Surfaces. *Chemistry of Materials*. **2020**, *32* (11), 4536–4543

(13) Yu, H.; Ni, C.; Thiessen, A. N.; Li, Z.; Veinot, J. G. C. Synthesis, Properties, and Derivatization of Poly(Dihydrogermane): A Germanium-Based Polyethylene Analogue. *ACS Nano* **2021**. *15* (6), 9368–9378

(14) Kevin A. Juarez-Ornelas, J. Oscar C. Jiminénz-Halla, Terumasa Kato, C. R. S.-A. and K. M. Supporting Information Supporting Information. *Aldenderfer, Mark S., Craig, Nathan M., Speak. Robert Jeff, Popelka-Filcoff, Rachel S.* **1997**, *2* (1), 1–5.

(15) Beekman, M.; Kauzlarich, S. M.; Doherty, L.; Nolas, G. S. Zintl Phases as Reactive Precursors for Synthesis of Novel Silicon and Germanium-Based Materials. *Materials (Basel)*. **2019**, *12* (7).

(16) Notin, M.; Mejbar, J.; Bouhajib, A.; Charles, J.; Hertz, J. The Thermodynamic Properties of Calcium Intermetallic Compounds. *J. Alloys Compd.* **1995**, *220* (1–2), 62–75.

(17) Kurylyshyn, I. M.; Fässler, T. F.; Fischer, A.; Hauf, C.; Eickerling, G.; Presnitz, M.; Scherer, W. Probing the Zintl-Klemm Concept: A Combined Experimental and Theoretical Charge Density

Study of the Zintl Phase CaSi. *Angew. Chemie - Int. Ed.* **2014**, *53* (11), 3029–3032.

(18) Vogg, G.; Brandt, M. S.; Stutzmann, M.; Genchev, I.; Bergmaier, A.; Go, L.; Dollinger, G. Epitaxial CaGe " Lms on Germanium. **2000**, *212*, 148–154.

(19) Cultrara, N. D.; Wang, Y.; Arguilla, M. Q.; Scudder, M. R.; Jiang, S.; Windl, W.; Bobev, S.; Goldberger, J. E. Synthesis of 1T, 2H, and 6R Germanane Polytypes. *Chem. Mater.* **2018**, *30* (4), 1335–1343.

(20) Royen, P.; Rocktäschel, C. Zur Kenntnis Niedere Hydride Des Siliciums Und Germaniums. *ZAAC - J. Inorg. Gen. Chem.* **1966**, *346* (5–6), 279–289.

(21) Yu, H.; Helbich, T.; Scherf, L. M.; Chen, J.; Cui, K.; Fässler, T. F.; Rieger, B.; Veinot, J. G. C. Radical-Initiated and Thermally Induced Hydrogermylation of Alkenes on the Surfaces of Germanium Nanosheets. *Chem. Mater.* **2018**, *30* (7), 2274–2280.

(22) Thiessen, A. N.; Ha, M.; Hooper, R. W.; Yu, H.; Oliynyk, A. O.; Veinot, J. G. C.; Michaelis, V. K. Silicon Nanoparticles: Are They Crystalline from the Core to the Surface? *Chem. Mater.* **2019**, *31* (3), 678–688.

(23) Jiang, S.; Arguilla, M. Q.; Cultrara, N. D.; Goldberger, J. E. Improved Topotactic Reactions for Maximizing Organic Coverage of Methyl Germanane. *Chem. Mater.* **2016**, *28* (13), 4735–4740.

(24) Cai, Q.; Xu, B.; Ye, L.; Tang, T.; Huang, S.; Du, X.; Bian, X.; Zhang, J.; Di, Z.; Jin, Q.; Zhao, J. Stable Functionalization of Germanium Surface and Its Application in Biomolecules Immobilization. *Appl. Surf. Sci.* **2014**, *316* (1), 46–53.

(25) Cai, Q.; Xu, B.; Ye, L.; Di, Z.; Huang, S.; Du, X.; Zhang, J.; Jin, Q.; Zhao, J. 1-Dodecanethiol Based Highly Stable Self-Assembled Monolayers for Germanium Passivation. *Appl. Surf. Sci.* **2015**, *353*, 890–901.

(26) Muthuswamy, E.; Zhao, J.; Tabatabaei, K.; Amador, M. M.; Holmes, M. A.; Osterloh, F. E.; Kauzlarich, S. M. Thiol-Capped Germanium Nanocrystals: Preparation and Evidence for Quantum Size Effects. *Chem. Mater.* **2014**, *26* (6), 2138–2146.

(27) Wang, D.; Chang, Y. L.; Liu, Z.; Dai, H. Oxidation Resistant Germanium Nanowires: Bulk Synthesis, Long Chain Alkanethiol Functionalization, and Langmuir-Blodgett Assembly. *J. Am. Chem. Soc.* **2005**, *127* (33), 11871–11875.

(28) Holmberg, V. C.; Korgel, B. A. Corrosion Resistance of Thiol- and Alkene-Passivated Germanium Nanowires. *Chem. Mater.* **2010**, *22* (12), 3698–3703. \

(29) Bianco, E.; Butler, S.; Jiang, S.; Restrepo, O. D.; Windl, W.; Goldberger, J. E. Stability and Exfoliation of Germanane: A Germanium Graphane Analogue. *ACS Nano* **2013**, *7* (5), 4414–4421.

(30) Clark, R. J.; Aghajamali, M.; Gonzalez, C. M.; Hadidi, L.; Islam, M. A.; Javadi, M.; Mobarok, M. H.; Purkait, T. K.; Robidillo, C. J. T.; Sinelnikov, R.; Thiessen, A. N.; Washington, J.; Yu, H.; Veinot, J. G. C. From Hydrogen Silsesquioxane to Functionalized Silicon Nanocrystals. *Chem. Mater.* **2017**, *29* (1), 80–89.

(31) Yu, Y.; Rowland, C. E.; Schaller, R. D.; Korgel, B. A. Synthesis and Ligand Exchange of Thiol-Capped Silicon Nanocrystals. *Langmuir* **2015**, *31* (24), 6886–6893.

(32) Battocchio, C.; Porcaro, F.; Mukherjee, S.; Magnano, E.; Nappini, S.; Fratoddi, I.; Quintiliani, M.; Russo, M. V.; Polzonetti, G. Gold Nanoparticles Stabilized with Aromatic Thiols: Interaction at the Molecule-Metal Interface and Ligand Arrangement in the Molecular Shell Investigated by SR-XPS and NEXAFS. *J. Phys. Chem. C* **2014**, *118* (15), 8159–8168.

(33) Plymale, N. T.; Dasog, M.; Brunschwig, B. S.; Lewis, N. S. A Mechanistic Study of the Oxidative Reaction of Hydrogen- Terminated Si (111) Surfaces with Liquid Methanol. **2017**, No. 111.

(34) W.F., Sobol, P.E., Bomben, K.D. and Chastain, J. In Chastain, J., Ed., Handbook of X-Ray Photoelectron Spectroscopy, 1992

(35) Deegan, T.; Hughes, G. An X-Ray Photoelectron Spectroscopy Study of the HF Etching of Native Oxides on Ge(111) and Ge(100) Surfaces. *Appl. Surf. Sci.* **1998**, *123–124*, 66–70.

(36) Collins, G.; Aureau, D.; Holmes, J. D.; Etcheberry, A.; O'Dwyer, C. Germanium Oxide Removal by Citric Acid and Thiol Passivation from Citric Acid-Terminated Ge(100). *Langmuir* **2014**, *30* (47), 14123–14127.

(37) Bui, L. N.; Thompson, M.; Mckeown, N. B.; Romaschin, A. D.; Kalman, P. G. Surface Modification of the Biomedical Polymer Poly (Ethy1ene Terep h t h a Late). *The Analyst* **1993**, *118*, 463-474

(38) Castner, D. G.; Hinds, K.; Grainger, D. W. X-Ray Photoelectron Spectroscopy Sulfur 2p Study of Organic Thiol and Bisulfide Binding Interactions with Gold Surfaces. *Langmuir* **1996**, *12* (21), 5083–5086.

(39) Badia, A.; Cuccia, L.; Demers, L.; Morin, F.; Lennox, R. B. Structure and Dynamics in Alkanethiolate Monolayers Self-Assembled on Gold Nanoparticles: A DSC, FT-IR, and Deuterium NMR Study. *J. Am. Chem. Soc.* **1997**, *119* (11), 2682–2692.

(40) You, A.; Be, M. A. Y.; In, I. X-Ray Photoelectron Spectroscopy Characterization of Gold Nanoparticles Functionalized with Amine-Terminated Alkanethiols. **2020**, *98* (2011), 97–104.

(41) Fontana, L.; Bassetti, M.; Battocchio, C.; Venditti, I.; Fratoddi, I. Synthesis of Gold and Silver Nanoparticles Functionalized with Organic Dithiols. *Colloids Surfaces A* **2017**, *532* (May), 282–289.

(42) Prabhakaran, K.; Ogino, T. Oxidation of Ge(100) and Ge(111) Surfaces: An UPS and XPS Study. *Surf. Sci.* **1995**, *325* (3), 263–271.

(43) Ma, X.; Wu, F.; Kauzlarich, S. M. Alkyl-Terminated Crystalline Ge Nanoparticles Prepared from NaGe: Synthesis, Functionalization and Optical Properties. *J. Solid State Chem.* **2008**, *181* (7), 1628–1633.

(44) SWeinstein, B.A.; Cardona, M. Second Ge Raman. *Phys. Rev. B.* **1988**, *1270* (1971).

(45) Jiang, S.; Krymowski, K.; Asel, T.; Arguilla, M. Q.; Cultrara, N. D.; Yanchenko, E.; Yang, X.;

Brillson, L. J.; Windl, W.; Goldberger, J. E. Tailoring the Electronic Structure of Covalently Functionalized Germanane via the Interplay of Ligand Strain and Electronegativity. *Chem. Mater.* **2016**, *28* (21), 8071–8077.

(46) Fa, W.; Zeng, X. C. Polygermanes: Bandgap Engineering via Tensile Strain and Side-Chain Substitution. *Chem. Commun.* **2014**, *50* (65), 9126–9129.

Chapter 4

(1) Bent, S. F.; Kachian, J. S.; Rodríguez-reyes, J. C. F.; Teplyakov, A. V. Tuning the Reactivity of Semiconductor Surfaces by Functionalization with Amines of Different Basicity. **2010**, *108* (3) 956-960

(2) McVey, B. F. P.; Prabakar, S.; Gooding, J. J.; Tilley, R. D. Solution Synthesis, Surface Passivation, Optical Properties, Biomedical Applications, and Cytotoxicity of Silicon and Germanium Nanocrystals. *Chempluschem* **2017**, *82* (1), 60–73.

(3) Carolan, D.; Doyle, H. Tuning the Photoluminescence of Germanium Nanocrystals through Surface Bound Functional Groups. *Part. Part. Syst. Charact.* **2017**, *34* (2), 1–4.

(4) Yu, H.; Thiessen, A. N.; Hossain, M. A.; Kloberg, M. J.; Rieger, B.; Veinot, J. G. C. Thermally Induced Dehydrogenative Coupling of Organosilanes and H-Terminated Silicon Quantum Dots onto Germanane Surfaces. *Chem. Mater.* **2020**, *32* (11), 4536–4543.

(5) Thiessen, A. N.; Ha, M.; Hooper, R. W.; Yu, H.; Oliynyk, A. O.; Veinot, J. G. C.; Michaelis, V. K. Silicon Nanoparticles: Are They Crystalline from the Core to the Surface? *Chem. Mater.* **2019**, *31* (3), 678–688.

Appendix A : Dissipative Self-assembly of Dicarboxylic Acid Functionalized SiNCs

Figure 2-S1. The apparatus for HSQ synthesis.

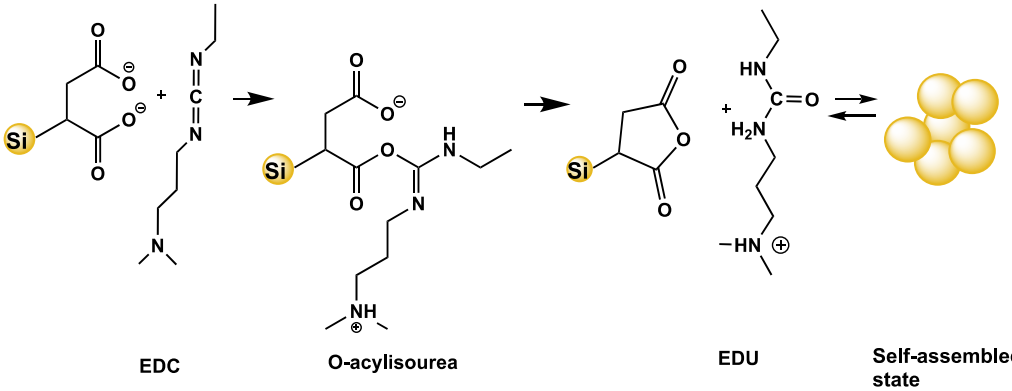

Figure 2-S2. Ideal activation and self-assembly pathway of dicarboxylic acid functionalized SiNCs in aqueous solution.

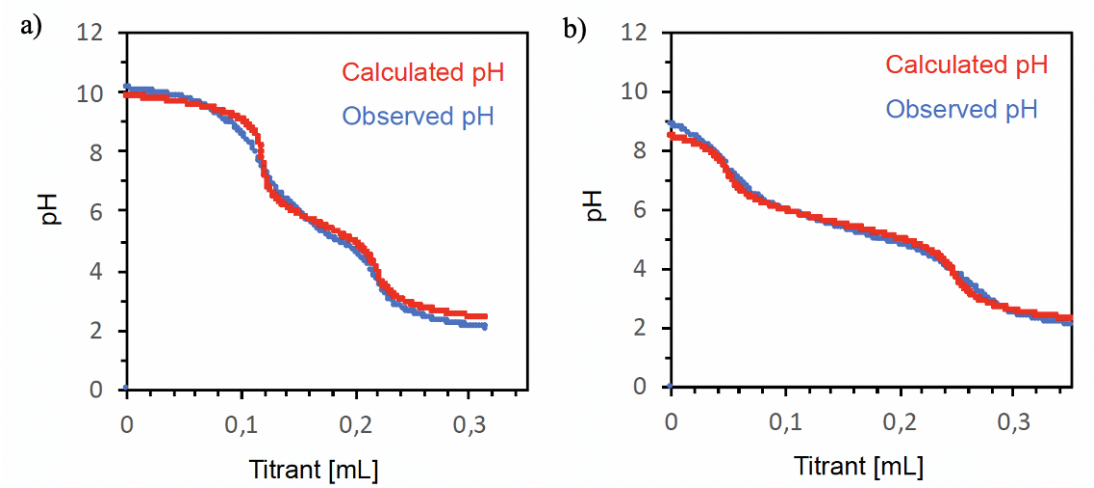

Figure 2-S3. Plot of the pH value vs. volume of titrant (0.01 M HCl) for a) asp-SiNCs and b) suc-SiNCs. The blue curves represent the observed values, the red markers represent the calculated values by HySS 2009. Upon the fit, pK_a of the asp-SiNCs is a) 5.5 suc-SiNCs is and b) 5.5.

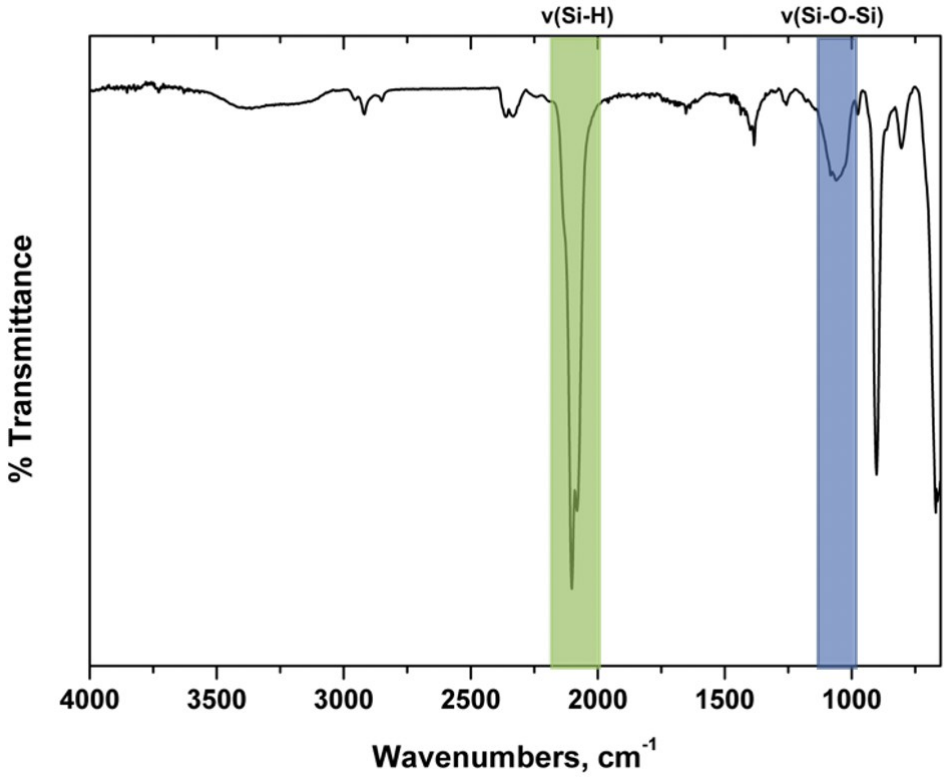

Figure 2-S4. FTIR spectrum of hydride-terminated SiNCs.

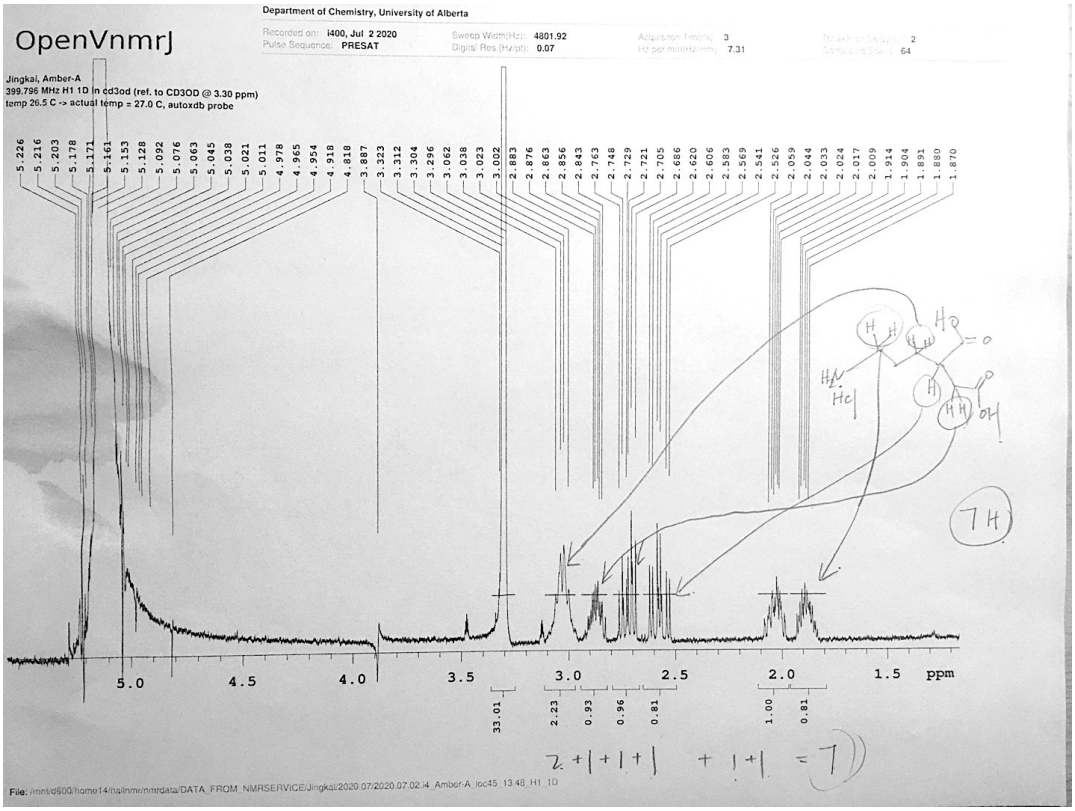

Figure 2-S5. ^{1}H NMR spectrum of (RS)-2-[2-aminoethyl] butandioic acid, hydrochloride. δ(ppm) = 2.97–3.09 (m, 2 H), 2.83–2.91 (m, 1 H), 2.71 (A of ABX, J = 17.2, 7.8 Hz, 1 H), 2.56 (B of ABX, J = 16.8, 5.8 Hz, 1 H), 1.99– 2.08 (m, 1 H), 1.84–1.93 (m, 1 H). This result is consistent with Zacharie et al.[19]

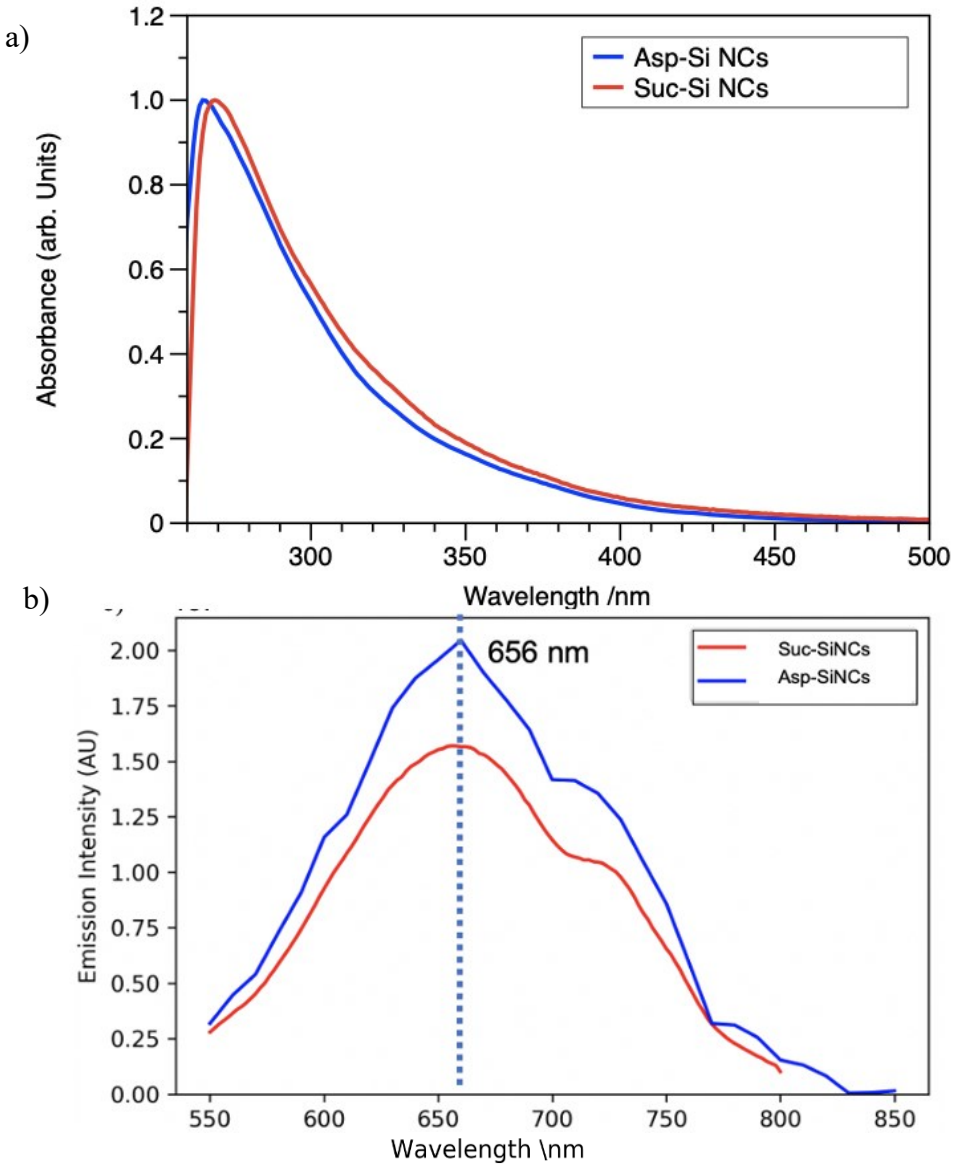

Figure 2-S6. (a) UV Absorption and (b) PL of the aspartic acid and succinic acid-terminated SiNCs.

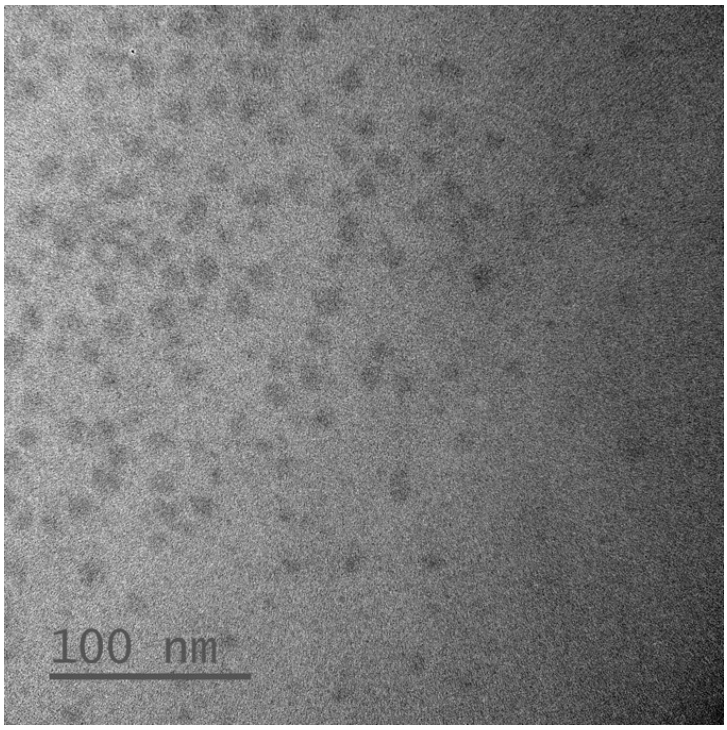

Figure 2-S7. Bright-field TEM of undecanoic acid and allyloxy poly(ethylene oxide)methyl ether terminated water-soluble SiNCs. The mean diameter in the images is 4.18 ± 1.1 nm. Unfortunately, attempts to image the asp-SiNCs and suc-SiNCs were unsuccessful, which can be explained by the surface dicarboxylic acid crosslinking.[17]

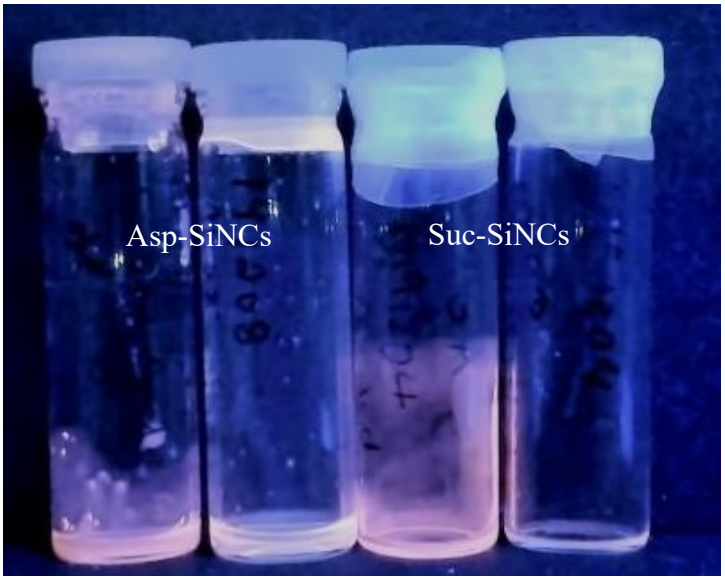

Figure 2-S8. Typical PL-emission (λ_{ex} = 365 nm) of freeze-dried asp-SiNCs and suc-SiNCs in a vial.

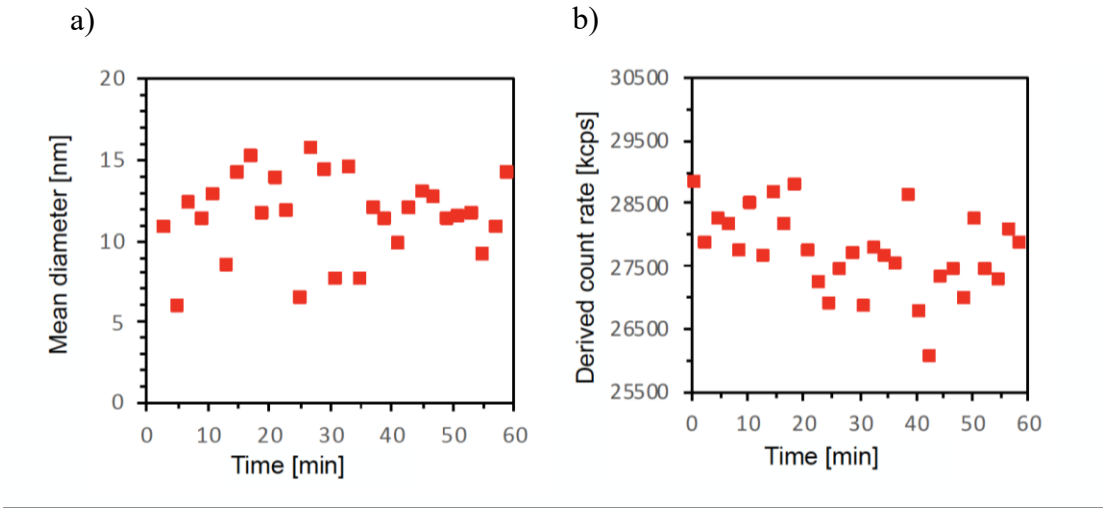

Figure 2-S9. (a) Hydrodynamic diameter and (b) count rate of suc-SiNCs in MES buffered aqueous solution obtained by DLS.

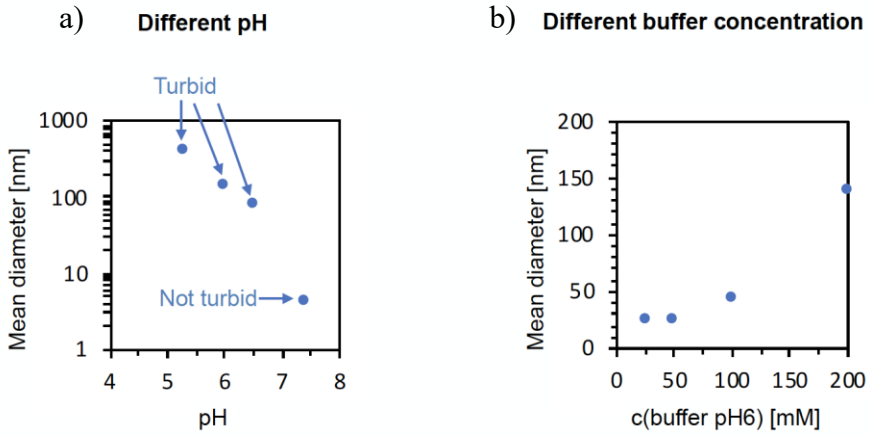

Figure 2-S10. (a) Hydrodynamic diameter and (b) count rate of suc-SiNCs in MES buffered aqueous solution with different pH values and concentrations obtained by DLS.

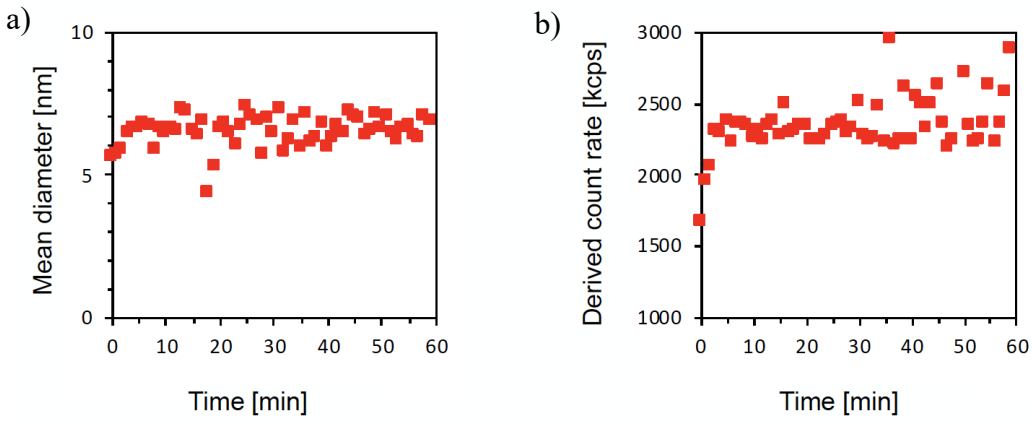

Figure 2-S11. (a) Hydrodynamic diameter and (b) count rate of 10 mM suc-SiNCs in 25 mM, pH 7 MES buffered aqueous solution obtained by DLS.

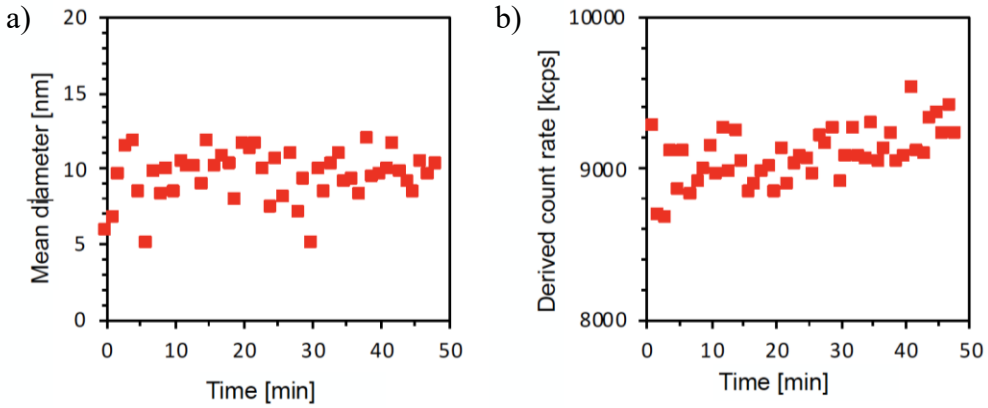

Figure 2-S12. (a) Hydrodynamic diameter and (b) count rate of 5 mM suc-SiNCs in 25 mM, pH 7 MES buffered aqueous solution obtained by DLS.

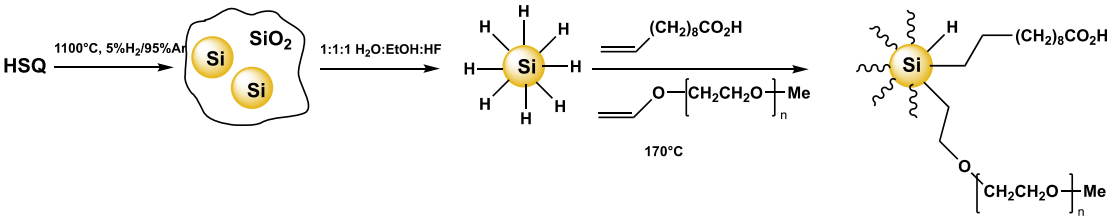

Figure 2-S13. Synthesis of SiNCs via thermal disproportionation of hydrogen silsesquioxane (HSQ), and one-step synthesis of water-soluble SiNCs.[25]

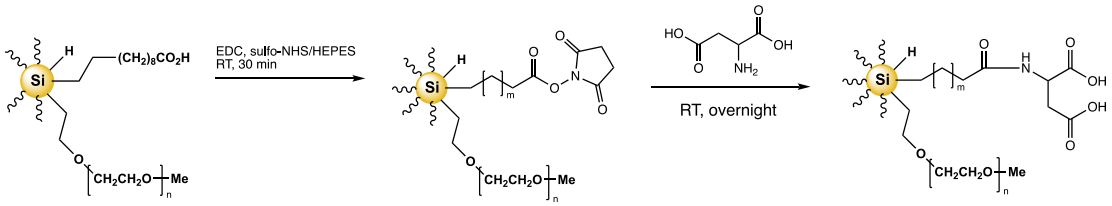

Figure 2-S14. Synthesis of asp-SiNCs EDC coupling with water-soluble SiNCs.

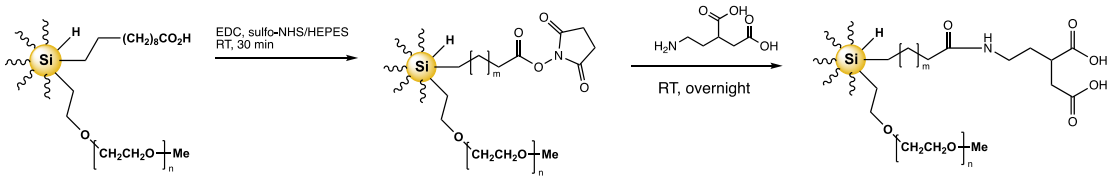

Figure 2-S15. Synthesis of suc-SiNCs EDC coupling with water-soluble SiNCs.

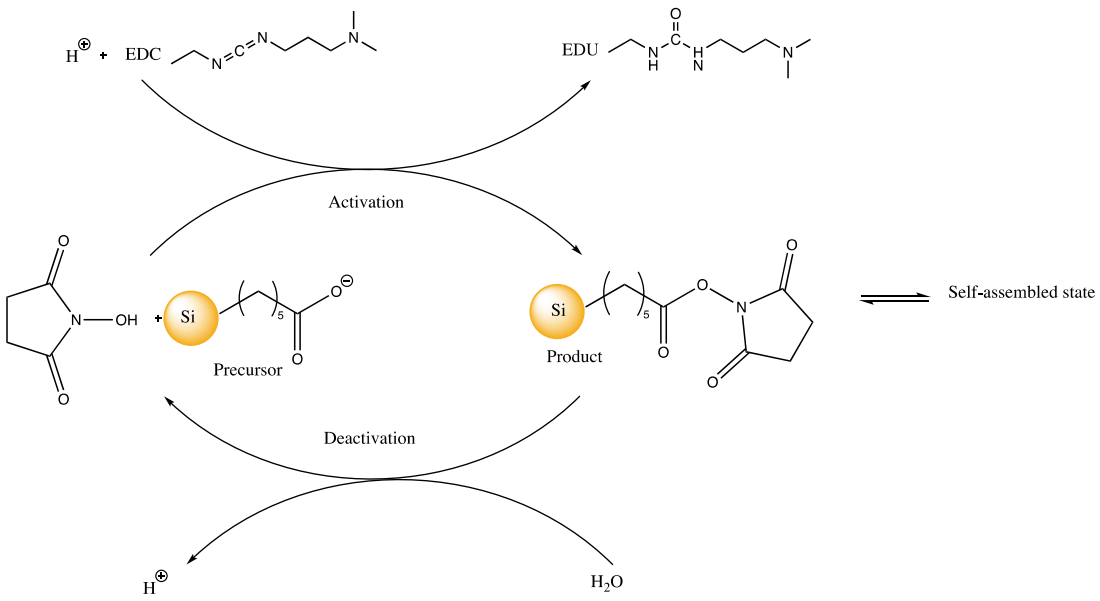

Figure 2-S16. Scheme of the chemical reaction cycle developed by Grötsch et al. Carboxylate functionalized SiNCs reacted with EDC and NHS to convert to a transient NHS ester.[14]

The surface coverage of functionalized SiNCs based on TGA weight loss calculation:

$$\%\,Surface\ coverage = \frac{\%\,Experimental\ weight\ loss}{\%\,Theoritical\ weight\ loss} \times 100 \cdots\cdots\cdots\cdots\cdots\cdots (2-S1)$$

$$\%\ Theoritical\ weight\ loss = \frac{Ligands\ theoretical\ weight}{Lignads\ and\ SiNCs\ theoretical\ weight} \times 100 \cdots\cdots (2-S2)$$

$$SiNCs\ theoretical\ weight = \frac{N(Si) \times M(Si)}{N_A} \cdots\cdots\cdots\cdots\cdots\cdots\cdots\cdots\cdots\cdots\cdots\cdots\cdots\cdots (2-S3)$$

$$Ligands\ theoretical\ weight = \frac{N(L) \times M(L)}{N_A} \cdots\cdots\cdots\cdots\cdots\cdots\cdots\cdots\cdots\cdots\cdots\cdots\cdots\cdots (2-S4)$$

Where, N (Si) = Total number of silicon atoms per NC

N (L) = Total number of ligands per NC surface

M (Si) = Molar mass of Si

M (L) = Molar mass of ligand

N_A = Avogadro number

Thus,

$$\%Theoretical\ weight\ loss = \frac{N(L) \times M(L)}{N(L) \times M(L) + N(Si) \times M(Si)} \times 100 \cdots\cdots\cdots\cdots\cdots\cdots (2-S5)$$

Appendix B: Thermally-Induced Dehydrocoupling of Thiol and Disulfide on the Surfaces of Polygermanes and Germanium Nanosheets

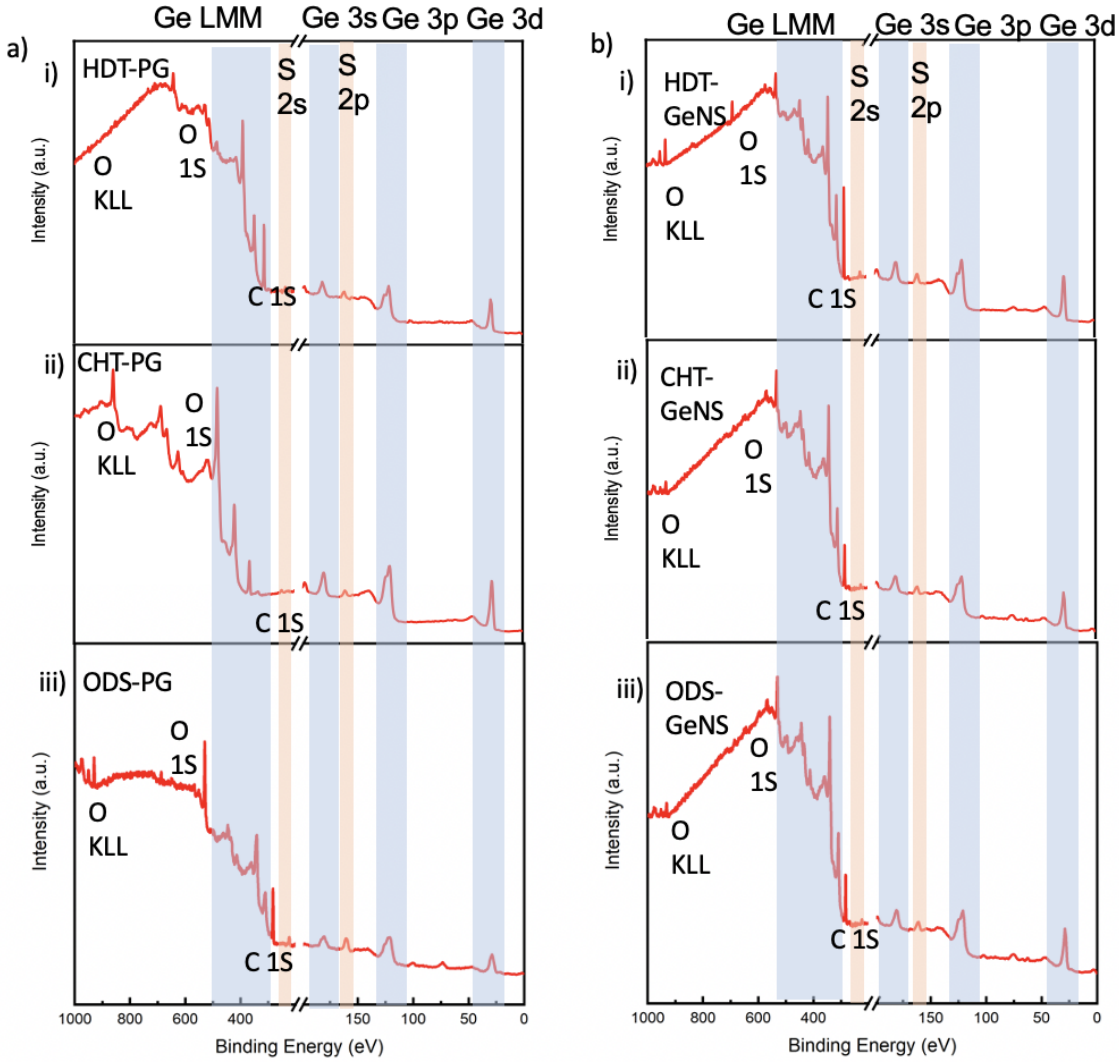

Figure 3-S1. Survey XP spectra of (a) polygermanes and (b) germananes functionalized with (i) hexadecanethiol, (ii) cyclohexanethiol, and (iii) octadecyl disulfide, respectively.

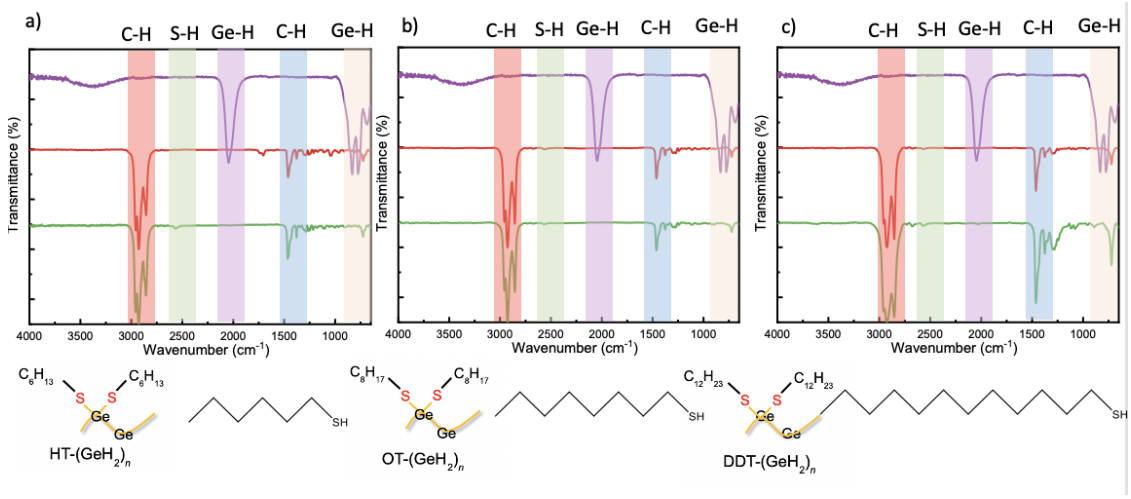

Figure 3-S2. FTIR spectra of (a) hexanethiol, (b) octanethiol and (c) dodecanethiol functionalized PGs. Red spectra are neat thiol ligand, purple spectra are PGs, and green spectra are functionalized PGs.

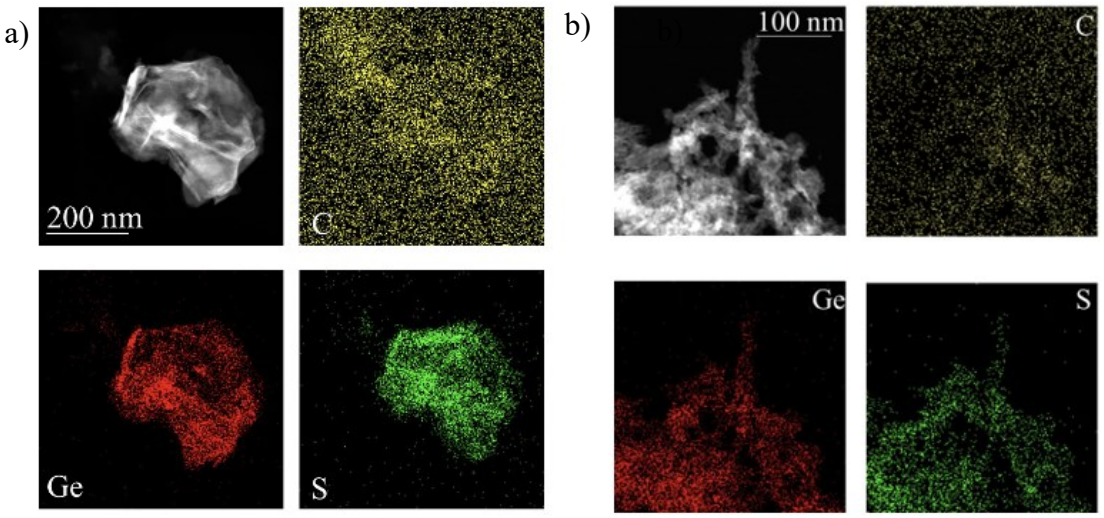

Figure 3-S3. HAADF-STEM images with mapping of cyclohexanethiol functionalized a) GeNSs and b) PGs.

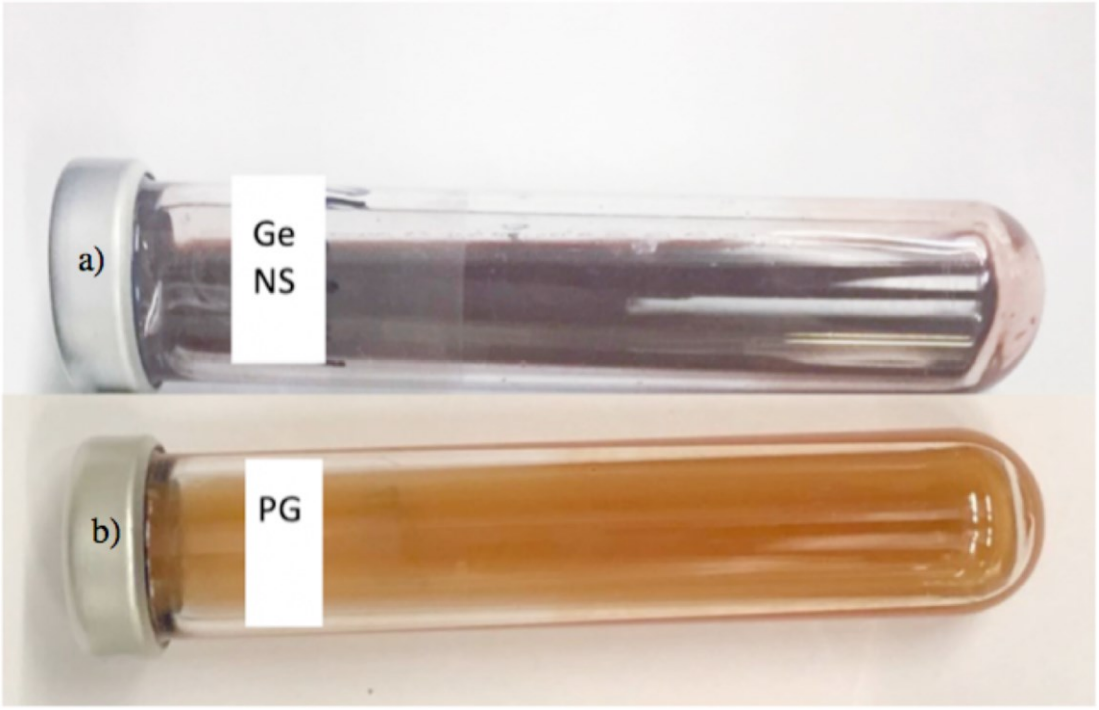

Figure 3-S4. Photograph of (a) GeNSs and (b) PGs in toluene.

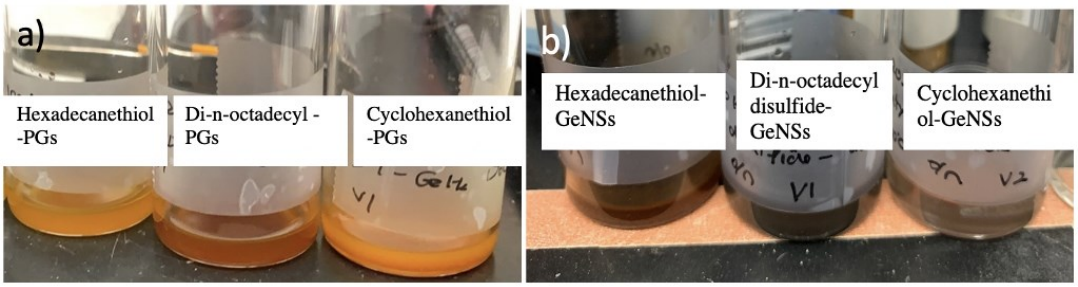

Figure 3-S5. Photograph of functionalized (a) GeNSs and (b) PGs in toluene.